Climate controlled mechanisms of subpolar North Atlantic carbon uptake

Friederike Fröb

Thesis for the degree of philosophiae doctor (PhD)
at the University of Bergen

2017

Date of defence: 27.06.2017

Acknowledgements

First and foremost I would like to thank my supervisor Are Olsen for giving me the opportunity to come to Bergen. Thank you for your generous help, constant good advice and your dedication. I would not have been able to learn that much without your guidance. I am also very grateful to Emil Jeansson, for his support, encouragement and the best soundtrack during a cruise ever.

I would like to thank all my co-authors for the great collaboration and the excellent discussions, especially Kjetil Våge, Abdir Omar, Meike Becker, Léon Chavik, Igor Yashayaev, Kent Moore, and Siv Lauvset. Thanks also to those who gave last minute input to this thesis!

I would also like to thank Fiz F Pérez and the colleagues at IIM-CSIC for giving me the opportunity to spend some time abroad. Thank you, Maribel, for showing me around Vigo and Galicia, without you, it would not have been such a great experience.

I would like to thank all my colleagues and friends at GFI and at the Bjerknes Center, especially everyone at SKD, including the coffee maker. Thanks for all the scientific discussions, after work beers, sailing trips, hiking trips and dance parties. The PhD community in Bergen is truly great and I am glad to have met so many amazing people here. Thank you Mari, Lea, and especially Marie, go team carbon!

A very special thank goes to all Züri houmies for always reminding me of the world outside academia. Wiebke and Sophia, thanks for coming to Bergen in January and for promising to return anyways. And last, thanks to my family for being always there for me.

The work of this thesis was funded by the SNACS project (229752) through the KLIMAFORSK program of the Norwegian Research Council.

Abstract

The North Atlantic is a key region for global climate variability. Earlier studies have shown changes in the large-scale circulation, air-sea heat and freshwater fluxes and the carbon cycle in the North Atlantic in relation to anthropogenic forcing, but changes attributed to natural variability are less certain. However, in order to fully comprehend the ocean carbon sink and its variability, both, anthropogenic and non-anthropogenic driving mechanisms need to be evaluated.

The results of this thesis are presented in four papers. In the first paper, the impact of atmospheric forcing on convection in the subpolar North Atlantic, in particular with regard to ocean ventilation and carbon sequestration is presented based on a unique dataset collected during a winter cruise to the Irminger Sea. In the second paper, a long term perspective on inorganic carbon inventory changes and its natural and anthropogenic components is given. Inventory changes were decomposed into their main driving mechanisms and related to the evolution and distribution of the main water masses in the Irminger Sea. The third paper discusses surface fCO_2 and pH trends across the Irminger Sea and Iceland Basin and their main driving mechanisms. The North Atlantic shows large decadal freshening and cooling signal, which produce a large non-anthropogenic driving mechanism on surface ocean fCO_2 trends. The fourth paper discusses pH changes in the interior Irminger Sea and the Iceland Basin as well as the driving mechanisms for the observed variability.

Combined, the four papers in this thesis increase our understanding of fundamental interactions between atmospheric, hydrographic and biogeochemical processes in the subpolar North Atlantic. In particular, trends associated to natural variability and anthropogenic climate change are distinguished, which contribute to a better understanding of the variability of carbon cycle processes in the modern ocean.

List of publications

I Fröb, F., A. Olsen, K. Våge, G.W.K. Moore, I. Yashayaev, E. Jeansson, and B. Rajasakaren (2016), Irminger Sea deep convection injects oxygen and anthropogenic carbon to the ocean interior, *Nature Communications* **7**, 13244.

II Fröb, F., A. Olsen, F.F. Pérez, M.I. García-Ibáñez, E. Jeansson, A. Omar, and S.K. Lauvset (2017), Inorganic Carbon and Water Masses in the Irminger Sea since 1991, *Biogeosciences Discussions*, **27**.

III Fröb, F., A. Olsen, M. Becker, L. Chafik, T. Johanessen, G. Reverdin, and A. Omar, Impact of recent North Atlantic freshening and cooling on the carbon cycle, *prepared for submission to GRL*.

IV García-Ibáñez, M. I., P. Zunino, F. Fröb, L.I. Carracedo, A. Ríos, H. Mercier, A. Olsen, and F.F. Pérez (2016), Ocean Acidification in the Subpolar North Atlantic: mechanisms controlling pH changes, *Biogeosciences*, **13**, 3701-3715.

Contents

1 Introduction

"As in most scientific problems, no substitute exists for adequate observations. Without sufficient observations, useful prediction will likely never be possible. Models will evolve and improve, but, without data, will be untestable, and observations not taken today are lost forever. The great difficulty facing scientists trying to understand and predict the system is the extremely limited duration over which even marginally adequate observations of the climate system exist" (Wunsch et al., 2013, p. 4435).

Since the beginning of the industrial revolution in the mid 18th century, atmospheric CO_2 concentrations have increased almost exponentially from approximately 277 ppm in 1750 to 402 ppm in 2016 (NOAA-ESRL, 2015). Emitted via fossil fuel burning, cement production and land use changes, particularly agriculture, human-induced CO_2 has perturbed the natural carbon cycle. After the 2015 Paris Climate Conference, more than 190 countries agreed to limit their carbon emissions so global warming will not exceed 2°C above preindustrial levels (UNFCCC, 2015). One challenge will be to monitor the fate of anthropogenic carbon in the relevant reservoirs of the earth system in order to verify that the measures put in place to reduce the carbon emissions are effective. Estimates of the human perturbation of the global carbon budget in the atmosphere, the ocean and on land as well as the fluxes between these reservoirs, shown in Figure 1.1, reveal that the oceans play a crucial role in the global carbon cycle (Ciais et al., 2013). The oceans are a vast reservoir of carbon and because they contain approximately 50 times more carbon than the atmosphere, small changes in the oceanic reservoir might impact atmospheric CO_2 concentrations significantly. Currently, the oceans take up approximately 25 % of the annual emissions (Mikaloff Fletcher et al., 2006, Takahashi et al., 2009). While the oceanic uptake of CO_2 mitigates climate change, it also affects the CO_2 system in seawater, which is most visible in the decline of pH (Gattuso and Hansson, 2011). Ecosystems will have difficulties to adapt to these pH changes and the ongoing ocean acidification, which ultimately will impact societies that depend on ocean resources for food and recreation.

On timescales of decades, the rate at which CO_2 is transported from the atmosphere into the ocean is limited by the physical mixing time between the surface and interior (Sarmiento et al., 1992). The uptake rate is likely to decrease in the future because the surface ocean will become even more stratified than it is today due to surface warming and an increased input of freshwater, largely related to changes in the hydrological cycle and ice sheet melt. Until the end of the 21st century, Earth System Models project this decline in oceanic anthropogenic CO_2 uptake efficiency (Arora et al., 2013, Friedlingstein

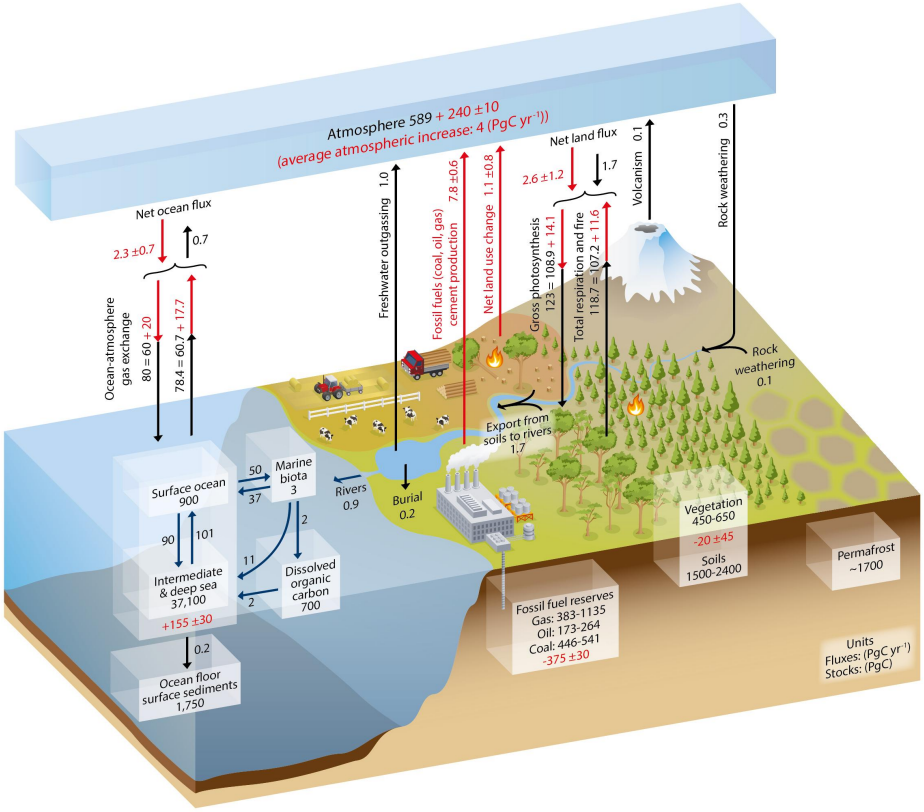

Figure 1.1: Schematic of the global CO_2 reservoirs and fluxes. The black numbers indicate preindustrial values and the red numbers the anthropogenic perturbation averaged over the years 2000-2009. The arrows indicate annual fluxes between the reservoirs. Figure from Ciais et al. (2013).

et al., 2006, Schwinger et al., 2014), however, the magnitude of carbon cycle climate feedbacks vary significantly among models. In order to improve projections of the future ocean carbon cycle, a range of ocean carbon observation systems will help to better understand the spatio-temporal variability of the oceanic carbon sink on global and regional scales. While mooring stations and Argo (Array for Real-time Geostrophic Oceanography) floats carry sensors that mainly report hydrographic parameters, shipboard measurements are required to monitor the CO_2 system in seawater. Dedicated research cruises and autonomous measuring systems installed on board of Voluntary Observing Ships (VOS) cover the main ocean basins and the data are synthesized in global data products such as SOCAT and GLODAPv2 (Bakker et al., 2016, Olsen et al., 2016). As observations in remote areas, particularly during the harsh winter season, are often scarce, the detection of long term trends from limited observational records is challenging (Gruber, 2009). However, as the observational records extend in time, direct evidence of the climate sensitivity of the marine carbon cycle emerges.

The focus region of this study is the subpolar North Atlantic with particular emphasis on the Irminger Sea. The subpolar North Atlantic plays a dominant role in the global climate system, because relative to the area size, large amounts of carbon are taken up due to strong meridional overturning circulation and the formation of North Atlantic Deep Water. In the subpolar region, deep convection provides a direct pathway into the deep ocean. Over the past decades, changes in the large-scale circulation, air-sea heat and freshwater fluxes and the carbon cycle were observed in relation to anthropogenic forcing and natural variability. Only if the understanding of the mechanisms of natural climate variability can be improved, the climate sensitivity of the subpolar North Atlantic in relation to anthropogenic forcing can be determined, particularly on decadal time scales.

2 Scientific background

2.1 Hydrographic setting

The Irminger Sea, Labrador Sea and the Iceland Basin are part of the subpolar North Atlantic. Towards the north, the area is limited by the Greenland-Iceland Rise and the Iceland-Faroe Ridge. The Denmark Strait connects the Greenland Sea and the Irminger Sea and the Labrador Sea is connected to the Baffin Bay via the Davis Strait. The Faroe-Shetland Channel and the Faroe Bank Channel connect the Norwegian Basin and the Iceland Basin. The Irminger Sea and the Iceland Basin are divided by the Reykjanes Ridge. Cape Farewell, located at the southern tip of Greenland, marks the boundary between the Irminger Sea and the Labrador Sea. The southern boundary of the subpolar North Atlantic is at approximately 50° N.

The large-scale circulation of the subpolar North Atlantic has been widely described in the literature (e.g. Lavender et al., 2005, Våge et al., 2011, Yashayaev and Clarke, 2008). The upper ocean in this region is dominated by a cyclonic circulation feature with strong boundary currents between 50° and 65° N - the subpolar gyre (see Fig. 2.1). The strength and shape of the subpolar gyre varies on decadal timescales, and affects the salinity and temperature of northward advecting water masses from the subtropical gyre (Häkkinen and Rhines, 2004, Hátún et al., 2005). The North Atlantic Current (NAC) carries warm and salty water masses from southwest to northeast, where they largely recirculate to the south. As these water masses move cyclonically around the northern and western boundaries of the Iceland Basin, Irminger Basin and the Labrador Sea, they lose heat to the atmosphere and become fresher as freshwater is added to the water column via precipitation and river runoff (Hátún et al., 2005, Yashayaev and Clarke, 2008). Therefore, the subpolar North Atlantic shows strong east-west gradients in temperature and salinity. The surface currents in the Irminger Sea and Iceland Basin are mostly oriented parallel to the Reykjanes Ridge (Knutsen et al., 2005). In the Irminger Sea, the East Greenland Current carries cold and fresh water of Arctic origin southwards and turns into the West Greenland Current as it passes Cape Farewell. The Labrador Current, a continuation of the West Greenland Current and the Baffin Island Current, flows southwards along the western side of the Labrador Sea. The narrow cyclonic recirculation feature in the southwest Irminger Basin is referred to as the Irminger Gyre (Våge et al., 2011). At depth, the dense overflows across the Greenland-Scotland Ridge interact with water masses formed via convective activity in the subpolar North Atlantic, which ultimately leads to decadal variations in the Atlantic Meridional Overturning Circulation (e.g. Hansen and Østerhus, 2000).

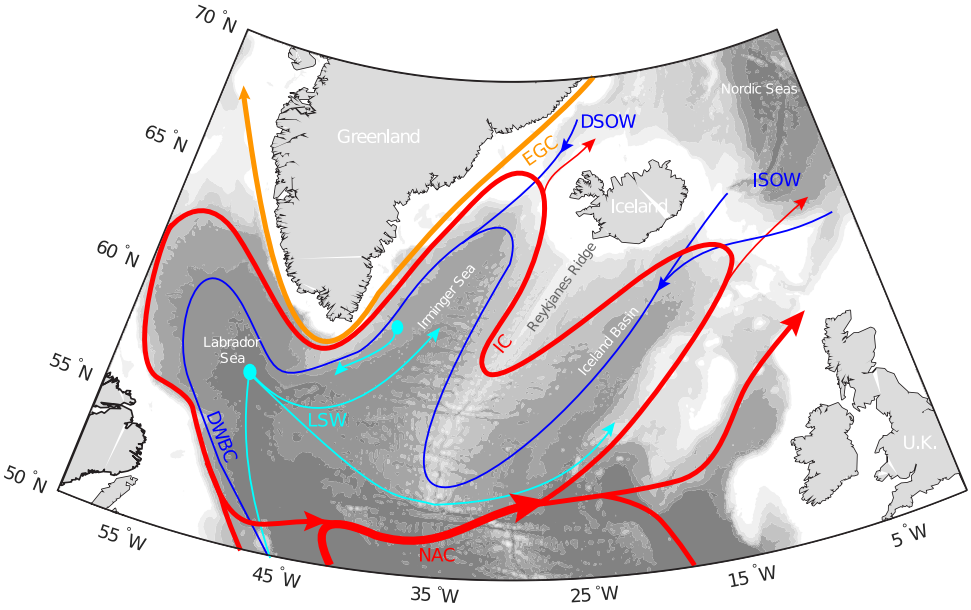

Figure 2.1: Schematic subpolar North Atlantic circulation. The branches of the North Atlantic Current (NAC) turning into the Irminger Current (IC) are shown in red and the East Greenland Current (EGC) is plotted in orange. The Iceland-Scotland Overflow Water (ISOW) and the Denmark Strait Overflow Water (DSOW), in dark blue, jointly with the Labrador Sea Water (LSW), in cyan, contribute to the Deep Western Boundary Current (DWBC). The filled contours show the bathymetry at 500 m steps. Adapted from Lherminier et al. (2010) and Pérez et al. (2013), taken from paper II.

2.1.1 Atmospheric forcing

The leading mode of interannual atmospheric variability over the mid-North Atlantic is the North Atlantic Oscillation (NAO) (Curry et al., 1998, Hurrell and Deser, 2009). The NAO describes a large-scale oscillation between a low pressure system located near Iceland and a high pressure system located near the Azores. The NAO index is calculated as the sea level pressure difference between Stykkisholmur, Iceland and Lisbon, Portugal (Hurrell, 1996). The NAO fluctuates between a weaker than normal and stronger than normal state, affecting thereby the strength of westerly winds and storm tracks over the Atlantic, which themselves induce changes in surface temperature and precipitation patterns (Hurrell, 1996). The index is positive if the sea-level pressure near Iceland is anomalously low, while that near the Azores is anomalously high. During this positive phase of the NAO westerly winds are stronger than normal and storm tracks are more meridionally oriented. Vice versa, the index is negative if the sea-level pressure gradient across the North Atlantic is small and as a consequence the westerlies are more zonal. Variations in the NAO have been linked to air-sea fluxes of heat and freshwater in the North Atlantic, large-scale circulation changes and the extent and strength of convective processes (e.g. Curry et al., 1998, Hurrell, 1996).

The Irminger Sea is located beneath the North Atlantic storm track and thus strongly affected by the passing of low pressure systems (Våge et al., 2011). Tip jets, which are intense, periodic westerly winds, are formed more frequently during the positive phase of the NAO (Moore, 2003) as a result of the interaction of passing extra-tropical cyclones with the high topography of southern Greenland (Doyle and Shapiro, 1999, Moore and Renfrew, 2005). Tip jets are associated with high wind speeds and lead to strong sea-air heat fluxes over the Irminger Sea (Moore and Renfrew, 2005, Våge et al., 2008). While these small scale wind events can potentially induce ocean convection, global scale atmospheric models fail to accurately represent the magnitude of tip jet events around Greenland due to their coarse resolution (DuVivier et al., 2016).

2.1.2 Dense water formation

A direct connection between the surface ocean and the deep ocean, as a result of open-ocean convection, occurs only in a few regions across the global ocean: the Greenland and the Iceland Seas, the Labrador and Irminger Seas, the Mediterranean and the Weddell Sea. Mostly throughout the year, the ocean is stably stratified and only during winter in regions with strong surface forcing, the thermocline can be locally erased and deep mixing occurs (Bacon et al., 2003). Prior to the onset of convection, it is believed that the water column needs to be preconditioned (Marshall and Schott, 1999). In late fall to early winter, a cyclonic circulation brings weakly stratified water in its center towards the surface due to a doming of the isopycnals. This surface cooling during winter causes the weak stratification of the surface ocean to erode. If sufficient buoyancy loss occurs, the dense surface water begins to sink down in plume-like features. As soon as the surface begins to restratify during spring, these plumes collapse and the convection ceases (Marshall and Schott, 1999).

In the early 20th century, Nansen (1912) argued that the deep water of the North Atlantic is formed in an area south of the Greenland-Scotland Ridge, most likely the Irminger Sea. Although follow-on winter cruises to the south and southeast of Cape Farewell confirmed this hypothesis, evidence of deep convection also occurring in the Labrador Sea emerged (Wüst, 1943). The idea of the Irminger Sea as a location of deep convection fell out of favor and the Labrador Sea became the main area of interest for subsequent convection studies. The Labrador Sea is indeed most important for North Atlantic mode water formation, the so called Labrador Sea Water (e.g. Rhein et al., 2002, Talley and McCartney, 1982). Once Labrador Sea Water is formed, it spreads southwards in the Deep Western Boundary Current, into the Irminger Sea and towards the Iceland Basin (Straneo et al., 2003). In the center of the cyclonic circulation of the Irminger Gyre, preconditioning conditions for convection are in fact fulfilled (Bacon et al., 2003, Marshall and Schott, 1999) and under favorable oceanic and atmospheric conditions, high buoyancy loss also leads to deep convection in the Irminger Sea and Labrador Sea Water formation (de Jong et al., 2012, Falina et al., 2007, Pickart et al., 2003a,b, Straneo et al., 2003, Våge et al., 2011, 2008).

2.1.3 Water mass composition

In the subpolar gyre, substantial deep and mode water formation takes place. At depth, North Atlantic Deep Water is formed, the key component of the lower limb of the Atlantic Meridional Overturning Circulation that is composed of Denmark Strait Overflow Water, Iceland-Scotland Overflow Water and Labrador Sea Water (Dickson and Brown, 1994). Denmark Strait Overflow Water originates from the Arctic Ocean and the Nordic Seas (Jeansson et al., 2008, Tanhua et al., 2005). This water mass is relatively recently ventilated, enriched in oxygen, CO_2 and other dissolved atmospheric gases such as freons. Iceland-Scotland Overflow Water originates most likely from intermediate waters of the Nordic Seas (Hansen and Østerhus, 2000). The properties of Iceland-Scotland Overflow Water are modified while it flows through the Iceland Basin to the Irminger Sea. As mentioned in section 2.1.2, Labrador Sea Water is formed via recurring deep convection in the subpolar North Atlantic, as a consequence of high heat loss during winter (Lazier et al., 2002, Pickart et al., 2003a, Yashayaev et al., 2007b). Labrador Sea Water is a cold, dense water mass with high concentrations of dissolved atmospheric gases, with a minimum in potential vorticity. This water masses show high spatial and temporal variability. For example, from 1987 to 1994 an extremely dense Labrador Sea Water class build up in the subpolar North Atlantic, as a consequence of intense recurring winter convection forced by a strong positive state of the NAO. As the NAO index shifted towards a more neutral state in the mid 1990s, the Labrador Sea Water was not renewed and started to decay, i.e. it accumulated heat and salt. After 2000, a shallower and less dense Labrador Sea Water class build up, which was slightly warmer and saltier than the LSW class of the early 1990s (Yashayaev et al., 2007a).

2.2 Biogeochemistry and carbon cycle processes

As a consequence of global climate change, not only the physical state of the ocean will be affected, but also biogeochemical cycles and ecosystems will be altered by increased temperatures, ocean acidification and ocean deoxygenation. However, on small spatial and temporal scales, natural variability is likely to mask the anthropogenic perturbation. This thesis focuses on the most recent impact climate had on the carbon cycle in the subpolar North Atlantic.

2.2.1 The CO_2 system in seawater

In the ocean, inorganic carbon occurs in different forms. When CO_2 dissolved in sea water, it first forms aqueous CO_2 (CO_2, aq), which reacts with water to carbonic acid (H_2CO_3). Both forms are electrically neutral and can not be analytically distinguished from each other. The CO_2^* dissociates stepwise to bicarbonate (HCO_3^-) and carbonate (CO_3^{2-}) ions. The CO_2 system in seawater can be described by three equilibrium equations:

$$CO_{2,g} \overset{K_0}{\rightleftharpoons} CO_2 \tag{2.1}$$

$$CO_2 + 2\,H_2O \overset{K_1}{\rightleftharpoons} HCO_3^- + H_3O^+ \tag{2.2}$$

$$HCO_3^- + H_2O \overset{K_2}{\rightleftharpoons} CO_3^{2-} + H_3O^+ \tag{2.3}$$

Here, K_0 is the Henry constant for CO_2 in seawater and K_1 and K_2 are the first and second dissociation constants of carbonic acid. All constants depend on temperature, salinity and pressure of seawater (Lueker et al., 2000, Mehrbach et al., 1973). The dominant species in seawater is bicarbonate, which constitute 88.6 % for global ocean mean surface water properties, followed by carbonate (10.9 %) and carbonic acid (0.5 %) (Sarmiento and Gruber, 2006). When CO_2 is added to seawater, the carbonate acts as a buffer:

$$CO_2 + CO_3^{2-} + H_2O \rightleftharpoons 2HCO_3^- \tag{2.4}$$

This leads to a net decrease in carbonate ions, which in turn lowers the saturation state of $CaCO_3$. The increase in surface ocean CO_2 perturbs the CO_2 buffer system in seawater, as the bicarbonate partly dissociates again, which lowers the pH (Zeebe and Wolf-Gladrow, 2001).

The CO_2 system in seawater can be fully described if at least two of the following four parameters are known: total dissolved inorganic carbon (DIC), total alkalinity (A_t), pH and the fugacity of CO_2 in seawater (fCO_2).

Both DIC and A_t are conservative with respect to changes in temperature or pressure. DIC is the sum of all dissolved inorganic carbon species:

$$DIC = [CO_2, aq] + [H_2CO_3] + [HCO_3^-] + [CO_3^{2-}]. \tag{2.5}$$

A_t can be understood as the access of proton acceptors over proton donors relative to a pKa of 4.5 (Dickson, 1981, Wolf-Gladrow et al., 2007). The contributions of minor bases

such as borate, phosphate, silicate or ammonia, are generally low.

$$A_t = [HCO_3^-] + 2[CO_3^{2-}] + [B(OH)_4^-] + [OH^-] - [H^+] + \text{minor bases} \quad (2.6)$$

The thermodynamic state of all acid-base-systems in seawater is represented by pH:

$$pH = -\log [H^+]. \quad (2.7)$$

The amount of CO_2 in seawater can be expressed as fugacity fCO_2 in a gas phase that is equilibrated with sea water. fCO_2 accounts for the non-ideal behaviour of CO_2 in air (Zeebe and Wolf-Gladrow, 2001):

$$fCO_2 = xCO_2 \times p \exp\left(p \frac{B + 2\delta}{RT}\right) \quad (2.8)$$

Here, xCO_2 is the mole fraction of CO_2, p is the total pressure, T the temperature and R the ideal gas constant. B is the first virial coefficient of CO_2 and δ is the cross virial coefficient, which are coefficients of the virial equation (representation of the equation of state) to approxiamte real gases (Weiss, 1974).

The capacity of the ocean to absorb CO_2 can be quantified with the Revelle factor:

$$\gamma = \frac{\Delta fCO_2}{\Delta DIC} \frac{DIC}{fCO_2} \quad (2.9)$$

Typical surface ocean values result in a Revelle factor of 12, which means that a 1 % change in DIC will result in a 12 % change in surface ocean fCO_2 (Sarmiento and Gruber, 2006). Increasing surface ocean CO_2 concentrations lead to higher Revelle factors, therefore the ocean becomes less efficient in absorbing CO_2. The oceans Revelle factor has already increased by approximately 1 unit since the industrial revolution (Sabine et al., 2004). The warmer sea surface in low latitudes has generally lower Revelle factors than the colder waters of the subpolar gyre in the high latitudes.

2.2.2 Anthropogenic carbon

Anthropogenic CO_2 (C_{ant}) in the ocean can not be measured directly, but can be derived from in situ observations. Different approaches have been made to quantify C_{ant} against the high oceanic DIC background concentration. Vázquez-Rodríguez et al. (2009) compared different methods to estimate C_{ant} in the Atlantic. In general, the spatial distribution of estimated C_{ant} for the different methods agrees well, except in the Nordic Seas and the Southern Ocean. All methods have their advantages and disadvantages (basically all assume a circulation in steady state), which shall be presented here in more detail for three methods.

Based on the works of Brewer (1978) and Chen and Millero (1979), Gruber et al. (1996) proposed the ΔC^* method to estimate C_{ant}. This back-calculation method corrects the preformed DIC in the modern ocean against preindustrial preformed values (π): $C_{ant} = DIC^{\circ,t} - DIC^{\circ,\pi}$. Measured DIC is back-calculated to $DIC^{\circ t}$, i.e. the

DIC concentration of a water parcel that is in direct contact with the atmosphere before subduction, by taking changes in temperature, salinity, remineralisation of organic matter and $CaCO_3$ dissolution into account. $DIC^{\circ,\pi}$ is quantified as the sum of the saturated DIC concentration with respect to the preindustrial atmosphere and the air-sea CO_2 disequilibrium (ΔC_{dis}). Two main assumptions need to be made to apply the ΔC^* method: first, preindustrial and present day preformed alkalinity values do not need to be differentiated and second, the air-sea CO_2 disequilibrium has remained constant over time.

The φC_T° method (Pérez et al., 2008, Vázquez-Rodríguez et al., 2009, 2012) follows the same principles as the ΔC^* method. However, preformed alkalinity and the disequilibrium term are determined using data of the subsurface layer (100-200 m), which has been shown to represent and preserve winter conditions during water mass formation (Vázquez-Rodríguez et al., 2012). The φC_T° method corrects any spatial and temporal variability of ΔC_{dis} and takes the effects of both, $CaCO_3$ dissolution changes and the sea surface temperature increase since preindustrial times on parametrized preformed alkalinity into account. The main advantage of the φC_T° method over other back-calculation methods is that no data of age tracers, such as chlorofluorocarbons (CFCs), are needed.

The 'short cut' version of the ΔC^* method uses transient tracer data to compute C_{ant}, which is basically a transit time distribution (TTD) approach. The TTD is a tracer-based method to estimate C_{ant} (Hall et al., 2002, Waugh et al., 2006), which relies on the assumption that C_{ant} acts as a passive and inert tracer. Combining the source function of the tracer at sea surface and the transit time distribution, the concentration of any passive, inert tracer is determined at any place and time in the ocean. The TTDs can be approximated by inverse Gaussian functions at each location in the interior ocean based on measurements of transient tracers such as chlorofluorocarbons (CFCs) or sulfur hexafluoride (SF_6). C_{ant} can be estimated, assuming that (1) the biological pump is not affected by the increasing concentration of C_{ant} in the ocean, because CO_2 is not a limiting nutrient for marine ecosystems, (2) circulation is in steady state and (3) there is no spatial dependence for the surface source function (Waugh et al., 2006). Uncertainty arises due to the need of assuming the saturation degree of the tracers in sea water, which probably also changes in time, but ultimately effects surface history of the tracer (Tanhua et al., 2008). In order to constrain the TTD, a ratio between the mean age and the width of the TTD needs to be assumed, which affects the shape of the TTD. The main advantages of the TTD method are that no direct measurements of DIC in the ocean are needed and that the method is insensitive to biological processes in the surface ocean.

2.2.3 Carbon uptake in the subpolar North Atlantic

The net transfer of CO_2 across the air-sea interface is controlled by the fugacity difference between the ocean and the overlying atmosphere ($\Delta fCO_2 = fCO_2^{oc} - fCO_2^{atm}$), the solubility of CO_2 in seawater and the gas transfer velocity. The gas transfer velocity is limited by the turbulence at the air-water interface, which can be influenced by friction velocity, breaking waves, bubble formation, temperature and humidity gradients. Mostly, these parameters can be linked to wind speed, therefore gas transfer rates are often

expressed as a function of wind speed (Nightingale et al., 2000, Wanninkhof, 1992). The growth rate of fCO_2^{oc} relative to fCO_2^{atm} determines whether the oceanic sink strength of CO_2 increases or decreases with time.

The global annual mean air-sea CO_2 flux is -1.42 Gt C yr^{-1} (Takahashi et al., 2009), but when riverine input is taken into account, the net ocean uptake is close to -2 Gt C yr^{-1}. The North Atlantic, north of 50° N, contributes to the global flux with roughly 20 %. A global sea-air flux map is shown in Figure 2.2 a, for the reference year 2000. The subpolar North Atlantic is a strong sink for CO_2 with high interannual variability compared to other ocean areas (Figure 2.2 b). During winter, the surface ocean is saturated or slightly supersaturated with respect to atmospheric values (Olsen et al., 2008) and to some extent, outgassing of CO_2 occurs. During spring and summer, the water column becomes highly undersaturated as a result of biological drawdown of CO_2. The seasonal variability of fCO_2^{oc} depends not only on intra-annual temperature and salinity changes but also the timing and magnitude of phytoplankton blooms (Henson et al., 2006, 2013). On interannual to decadal timescales, a combination of physical and biological drivers leads to the observed high variability of the North Atlantic carbon sink.

Based on carbon measurements between 1982 and 2002 at the Bermuda time-series station, Gruber et al. (2002) found substantial variability in air-sea CO_2 fluxes. Most likely, temperature changes and winter mixed layer depth variability, associated with the state of the NAO, drove air-sea CO_2 flux anomalies in the subtropical gyre. If scaled to the entire North Atlantic, the variability of the carbon sink strength would be as large as ±50 %. Several studies report a decline of North Atlantic CO_2 uptake in the 1990s and early 2000s, driven by surface warming in the western subpolar gyre (Corbière et al., 2007), local and advected changes in the ΔfCO_2 (Omar and Olsen, 2006), or declining wintertime mixing and ventilation (Schuster and Watson, 2007). According to Metzl et al. (2010), the sea surface fCO_2 growth rates in the western subpolar gyre accelerated after 2003, explained by changes in the CO_2 seawater chemistry and increased deep mixing. The historic hindcast simulations between 1979 and 2004 by citetThomas2008 largely reproduce the observed trends by Corbière et al. (2007), Omar and Olsen (2006), Schuster and Watson (2007). Thomas et al. (2008) show that beyond the observational records, the North Atlantic carbon sink shows large multiannual variability linked to NAO-driven circulation changes, as well as surface warming and cooling patterns. Beside the state of the NAO, a reduction in the vertical supply of DIC, as a result of weaker convection in the subpolar gyre in the early 2000s, has also been shown to lead to a modeled decline in fCO_2 (Ullman et al., 2009). On longer timescales, however, the fCO_2^{oc} trends in the North Atlantic are mainly driven by the increase in DIC associated with the uptake of anthropogenic carbon, but limited by the buffer capacity (McKinley et al., 2011, Tjiputra et al., 2012). By year 2100, more than 40 % of the ocean surface could have higher fCO_2^{oc} than fCO_2^{atm} growth rates, assuming an RCP8.5 scenario Tjiputra et al. (2012), leading to a substantial reduction in oceanic CO_2 uptake.

The magnitude of ocean acidification is proportional to the amount of CO_2 taken up through air-sea gas exchange (Doney et al., 2009, Gattuso and Hansson, 2011). Since the mid 18th century, global ocean average pH has dropped approximately 0.1 units and it is predicted to decline further unless CO_2 emissions are curbed. Over the past two decades, the pH in North Atlantic surface waters has declined at a similar rate as global

ocean pH ($0.0018\,\mathrm{yr}^{-1}$) (Lauvset et al., 2015). In the high latitudes, the surface waters are naturally low in carbonate as they have high DIC concentrations because of higher CO_2 solubility at low temperatures. Due to a lower buffer capacity against the uptake of CO_2, ocean acidification will be strong. Lauvset et al. (2015) argue that changing DIC in the ocean and its impact on the buffer capacity need to be quantified in order to fully determine the important drivers for observed trends in surface ocean pH.

2.2.4 Carbon inventories in the subpolar North Atlantic

In general, CO_2 uptake does not equal CO_2 storage. For example, in equatorial upwelling regions, old water masses are brought to contact with the atmosphere and take up C_{ant}. However, the water is transported towards the subtropical gyres, where is is eventually brought to the deep ocean so that the C_{ant} is actually stored (Sarmiento et al., 1992). The cumulated amount of C_{ant} stored in the ocean between 1750 and 2014 is $170\pm20\,\mathrm{Pg\,C}$, which is approximately 30 % of the cumulative emissions (Le Quéré et al., 2016). Because of deep water formation, the subpolar North Atlantic is a key region for the storage and transport of CO_2 in the global ocean although the area covers only 14% of the global ocean area (Sabine et al., 2004).

The anthropogenic CO_2 storage rate is related to the extent and intensity of ventilation processes, primarily driven by the NAO (section 2.1.1) (Levine et al., 2011, McKinley et al., 2011, Pérez et al., 2008, 2010, Steinfeldt et al., 2009, Wanninkhof et al., 2010, Woosley et al., 2016). In 1996, the NAO shifted from a positive to a negative phase, leading to strong reductions in surface heat fluxes in the subpolar North Atlantic and only weak formation of C_{ant}-enriched LSW. Pérez et al. (2008) find a decline in C_{ant} storage rates after 1997 as a result of enhanced surface stratification and weakened deep convection. Confirming results by (Pérez et al., 2008) Steinfeldt et al. (2009) show that large reductions in C_{ant} storage occurred between 1997 and 2003 in the subpolar gyre, as a consequence of absent deep ventilation and aging of the remnant water masses. However, they also reveal that a part of the variability of C_{ant} storage rates is related to volume changes of water masses, particularly the Labrador Sea Water layer, which decreased east of the Reykjanes Ridge, while it increased west of it. Based on deep repeat hydrographic measurements Pérez et al. (2013) estimate fluxes and storage rates in the North Atlantic and show, how a reduction in the Atlantic Meridional Overturning Circulation has weakened the North Atlantic sink for C_{ant} between 1990 and 2006. After 2010, the NAO index has shifted again towards more positive values, leading to overall higher storage rates of C_{ant} in the early 2000s than in the 1990s (Woosley et al., 2016).

While a response of anthropogenic CO_2 storage to atmospheric forcing in the North Atlantic has been largely determined, less is known about variations in natural DIC, its relation to atmospheric forcing and relevance for total DIC inventories (Tanhua and Keeling, 2012). For the atmospheric CO_2 concentrations, changes in DIC are most important, however, the overall processes that lead to the observed changes remain unclear. A first approach was done by Tanhua and Keeling (2012), who evaluated DIC, abiotic DIC as a approxiamtion of C_{ant}, and oxygen trends in the North Atlantic, but large uncertainties remain.

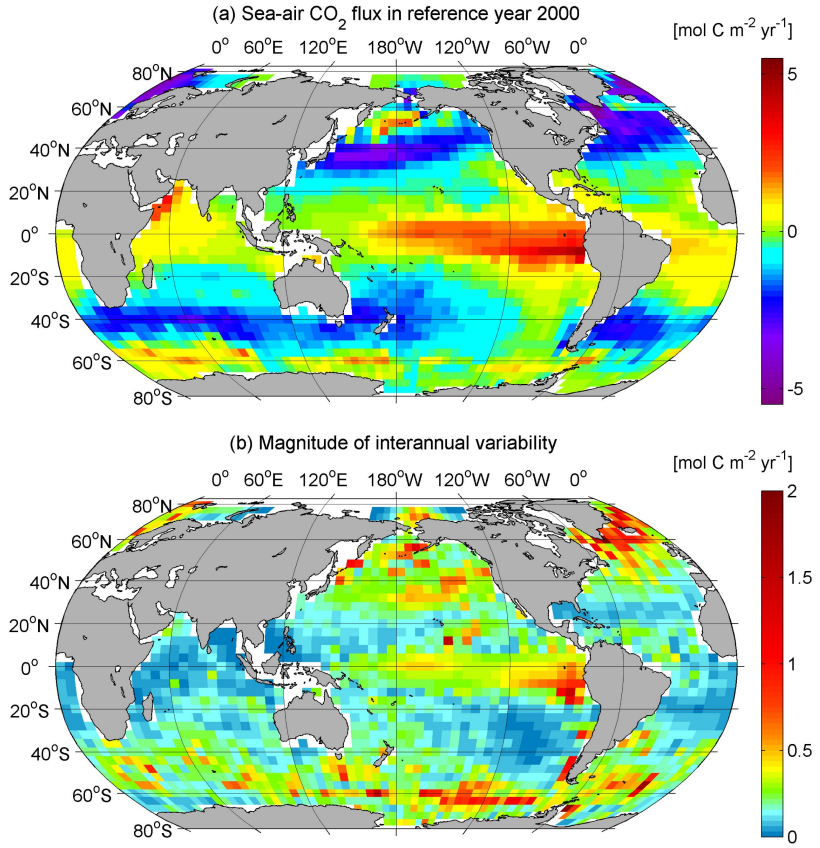

Figure 2.2: (a) Sea-air CO_2 flux based on empirical approaches relating in situ measurements with satellite observations of wind and sea surface temperature for the reference year 2000 and validated against the ΔpCO_2 climatology of Takahashi et al. (2009). (b) Magnitude of interannual variability of the sea-air CO_2 flux from a diagnostic model using empirical subannual relationships between climatological pCO_2 in surface seawater and sea surface temperature, along with interannual changes in SST and wind speed. Figure from http://www.pmel.noaa.gov/co2/story/Surface+CO2+Flux+maps after Feely et al. (2006) and Park et al. (2010).

3 Objectives

The overall goal of this study is to gain better understanding of fundamental interactions between atmospheric, hydrographic and biogeochemical processes in a small but highly dynamic key region for global climate variability. The results will document and help to understand the mechanisms behind climate related changes on the biogeochemistry and the carbon cycle in the subpolar North Atlantic through the 1990s and 2000s, with particular emphasis on the Irminger Sea.

The main objectives of this thesis are divided into four topics, each covered by a separate publication:

1. While deep convection has been shown to occur in the Irminger Sea under a specific set of oceanic and atmospheric conditions, the imprint of winter mixing in the Irminger Sea on biogeochemistry remains unclear. Moreover, direct observations of deep convection are scarce due to the harsh wintertime conditions in the subpolar gyre and only indirect evidence of the impact of atmospheric forcing on mixed layer depth and anthropogenic CO_2 and oxygen saturation concentration has been presented. **Paper I** aims to better understand the process of convection in the Irminger Sea, how it is linked to atmospheric forcing, and how it affects carbon sequestration and ventilation based on a unique wintertime dataset.

2. The response of anthropogenic CO_2 storage to atmospheric forcing in the subpolar North Atlantic has been determined, however, less is known about the natural carbon cycle. The variability of the strength of the ocean carbon sink can only be fully understood if natural variability is separated from anthropogenically driven trends. **Paper II** determines, how interior DIC inventories, and their natural and anthropogenic components, have changed over the past decades and how these changes are related to the distribution and evolution of water masses in the Irminger Sea.

3. While large scale changes in salinity and temperature have been observed on decadal timescales in the North Atlantic, the impact on surface fCO_2 and pH remains unclear. The aim of **Paper III** is to determine spatial trends of surface fCO_2 measurements across the Irminger Sea and the Iceland Basin based on data collected by the VOS *Nuka Arctica*. A decomposition of the trends allows to identify the main drivers of the observed changes.

4. While the surface ocean tends to track the atmospheric perturbation, the acidification at depth depends on the amount of anthropogenic CO_2 that is brought to the deep ocean through mixing processes and convection. However, in order to moni-

tor pH changes through the water column, the trends and drivers of the observed changes need to be determined, which is the aim of the analysis in the Irminger Sea and the Iceland Basin performed in **Paper IV**.

4 Summary

The four papers combined in this thesis show that the carbon cycle in the subpolar North Atlantic undergoes significant spatial and temporal variability. The main driver for observed changes is the increasing input of anthropogenic CO_2 into all depths of the ocean. The natural carbon cycle is largely linked to changes in local water mass composition, driven by large scale circulation changes and subpolar mode water formation as well as the state of the atmosphere. In particular on shorter timescales, the non-anthropogenic drivers become more import than the input of anthropogenic CO_2.

Paper I: **Irminger Sea deep convection injects oxygen and anthropogenic carbon to the ocean interior,**
Fröb, F., A. Olsen, K. Våge, G.W.K. Moore, I. Yashayaev, E. Jeansson, and B. Rajasakaren (2016), *Nature Communications*, **7**, 13244.

The aim of **Paper I** was to describe the impact of atmospheric forcing on convection in the subpolar gyre, in particular with regard to ocean ventilation and carbon sequestration. Based on an unique dataset, collected during a winter cruise to the Irminger Sea in 2015, these processes are directly linked to each other. First, the origin, extent and chemical properties of the winter mixed layer is described. While the mixing typically does not exceed 500 m in the Irminger Sea, in the winter 2014/15 mixed layers were as deep as 1400 m, driven by exceptional heat loss, which was enhanced by a large number of tip jet events associated with a high North Atlantic Oscillation index. Preconditioning of the water column was of secondary importance for the onset of convection. As a result of the deep convection, oxygen and anthropogenic CO_2 concentrations were close to saturation concentrations with respect to the atmosphere in the winter mixed layer. Compared to historic data, depleted oxygen levels at mid-depth were replenished and large amounts of carbon being sequestered to the deep ocean. The observations show that local deep convection driven by strong atmospheric forcing leads to efficient ocean ventilation and anthropogenic carbon uptake in the Irminger Sea.

Paper II: **Inorganic Carbon and Water Masses in the Irminger Sea since 1991,**
Fröb, F., A. Olsen, F.F. Pérez, M.I. García-Ibáñez, E. Jeansson, A. Omar, and S.K. Lauvset (2017), *Biogeosciences Discussions*, **27**.

In **Paper II**, a long term perspective on inorganic carbon inventory changes in the interior Irminger Sea is given. Based on repeated hydrographic depth profiles between 1991 and 2015, the inventories of total dissolved inorganic carbon and its natural and anthropogenic components are estimated. An extended Optimum MultiParameter method is used to quantify the distribution and evolution of the main water masses in the Irminger Sea. The overall inventory in DIC is driven by an increase in anthropogenic carbon, while the natural component decreases over the entire period. As changes in the carbon storage rate can be driven by concentration changes in the water column, for example due to aging of water masses, or by changes in the distribution of water masses with different concentrations, either by local formation or advection, the trends can be decomposed into their main drivers. Variations of natural DIC inventories are mainly driven by changes in the layer thickness of the main water masses, particularly of the Labrador Sea Water classes and surface water masses, while anthropogenic carbon is most affected by concentration changes. The DIC inventory changes show a clear response to the NAO and associated changes in the strength of convection, but for anthropogenic carbon the signal is less robust. While the oxygen inventory has declined over the entire period in all water masses, the deep convection event in 2015 was strong enough to replenish oxygen at depth to levels of the early 1990s.

Paper III: **Impact of recent North Atlantic freshening and cooling on the carbon cycle,**
Fröb, F., A. Olsen, M. Becker, L. Chafik, T. Johanessen, G. Reverdin, and A. Omar, *prepared for submission to GRL.*

In **Paper III**, a long term perspective on surface fCO_2 trends across the Irminger Sea and Iceland Basin is given and the main driving mechanisms for the observed changes are discussed. While the North Atlantic has undergone large changes in sea surface temperature and salinity over the past decades, the impact on surface fCO_2 and pH are less certain. Surface fCO_2 data were collected on the VOS M/V *Nuka Arctica* in the subpolar North Atlantic between 2004 and 2014. Due to recurring deep convection, surface fCO_2 trends are slightly lower in the Irminger Sea, while towards the east, the surface fCO_2 trends largely track the atmosphere. Ocean acidification is weaker in the west than in the east. The fCO_2 and pH trends are decomposed into their main drivers, i.e. sea surface temperature, salinity, dissolved inorganic carbon and alkalinity. Over the entire time period, the subpolar North Atlantic surface ocean significantly cooled and freshened. While the fCO_2 trends maintain equilibrium, trends in DIC are significantly decreased in the Iceland Basin, where alkalinity becomes a more important driver as a consequence of the decrease in salinity. This effect is only partly compensated by the increase in CO_2 solubility due to the cooling. The freshening is not large enough to induce a strong decline in pH, as pH trends in the surface ocean are ultimately limited by the atmospheric fCO_2 growth rate. The large freshening is not a local feature, but has been linked to decadal large scale circulation changes, which impact the DIC growth

rates in the North Atlantic. Surface ocean observations of carbon properties are highly valuable in order to better understand the role regional internal climate variability has on the oceanic uptake efficiency of atmospheric CO_2.

Paper IV: **Ocean Acidification in the Subpolar North Atlantic: mechanisms controlling pH changes,**
García-Ibáñez, M. I., P. Zunino, F. Fröb, L.I. Carracedo, A. Ríos, H. Mercier, A. Olsen, and F.F. Pérez (2016), *Biogeosciences*, **13**, 3701-3715.

The aim of **Paper IV** was to give a long term perspective on pH changes in the interior Irminger Sea and the Iceland Basin and to discuss the main drivers for the observed variability. Based on deep repeat hydrographic measurements between 1991 and 2015, basin-wide ocean CO_2 chemistry changes and ocean acidification in the main water masses are discussed. Over the entire time period, pH has declined, in particular in surface and intermediate water masses. A decomposition of the trends into their main drivers revealed that the increase in anthropogenic CO_2 dominated the decline in pH, partially offset by increased alkalinity. In the upper ocean, pH declines at a lower rate than expected from the rising atmospheric CO_2 concentration due to large scale circulation changes in the subpolar North Atlantic that transport saline and alkaline waters northwards and hence, increase the buffer capacity. As LSW was not reventilated until 2015, a strong decline in pH is associated to the aging of this water mass. Overall, the acidification trends in the Irminger Sea are stronger than in the Iceland Basin due to the presence of younger water masses.

5 Future perspectives

The results of this thesis raise a number of open questions and possibilities for future work, some might be of pure academic interest, others of more societal relevance.

The results of **Paper I** show that deep convection clearly occurs in the Irminger Sea, however, it remains uncertain, how much CO_2 is actually stores. If the production rates of Labrador Sea Water in the subpolar North Atlantic would be known, the actual amount of CO_2 transported to depth could be calculated. Another question that could then be addressed is how much the Labrador Sea Water formed by deep convection in the Irminger Sea contributes to North Atlantic Deep Water. This could given an indication of how important the Irminger Sea is in a global sense with respect to carbon storage. It would also be interesting to analyze hydrographic and biogeochemical parameters before, during and after deep convection. As preformed conditions for water masses are set during water mass formation, assumptions that are made for e.g. saturation concentrations of newly formed water masses could be compared to actual measurements. This could also result in a more complete mechanistic description of the convection process itself (more than what has been done in **Paper I**).

The OMP analysis used in **Paper II** does not take temporal changes of source water type properties into account. This could be solved by using a technique for tracing ocean water masses (Gebbie and Huybers, 2010). The evolution of different Labrador Sea Water classes could then be better resolved, but also water masses that have similar source water type parameters could be better distinguished from each other. It would be interesting to combine the results of **Paper II** with velocity fields in the ocean in order to resolve volume transports of the different water masses and their respective concentration changes. Taking the horizontal and vertical advection of carbon into account, the magnitude and the variability of the carbon budget in the Irminger Sea could be better described in order to describe the horizontal and vertical advection of carbon.

The observational basis for assessing carbon cycle variability is limited in the subpolar North Atlantic, particularly in the challenging winter season. Higher spatial and temporal resolution of the observational data might reveal more robust trends and drivers and resolve intra-annual to interannual to decadal variability better. As shown in **Paper II and Paper III**, the use of a salinity-alkalinity relationships to approximate alkalinity in the surface and deep ocean is subject to uncertainty. Any impacts on alkalinity of $CaCO_3$ dissolution changes are disregarded. Therefore, at least two of the four parameters of the CO_2 system in seawater should be reported either during dedicated cruises or via autonomous measurement systems installed on VOS lines. In this way, a more complete picture of surface carbon cycle processes could arise. If this is not possible, a more

complex alkalinity relationship needs to be developed that does not only rely on salinity.

In **Paper III** only winter trends were analyzed, but it would be interesting to include all seasons to investigate spatial and seasonal variabilities of the subpolar North Atlantic carbon cycle. This could only be achieved, if biological processes are considered. In order to account for variability related to biological processes, which were not discussed throughout this thesis, nutrients need to be systematically observed as well. Additionally, measurements of δ^{13}C(DIC) across the surface ocean have the potential to help to estimate future anthropogenic carbon uptake, however, this needs further investigation.

Another issue raised throughout this thesis, is that the connection between the surface ocean and the deep ocean remains unsolved. It is not quite clear how signals attributed to surface ocean variability affect processes at greater depths and vice versa. For example, in **Paper III** lower fCO_2 trends in the Irminger Sea were attributed to deep convection, however, in the actual fCO_2 surface data are no clear signals from the known events. Moreover, it is not clear how these signals would actually look like, because the water masses that are brought up from greater depths to the surface have lower anthropogenic carbon concentrations, but might be enriched with DIC - depending on their age.

While in **Paper IV** the trends in pH in the interior ocean are larger in the Irminger Sea than in the Iceland Basin, the results of **Paper III** show the opposite for surface pH trends. This might be related to the different time periods that were considered, however, the reasons are not entirely clear. Further investigation of the trends and drivers on subdecadal scales are necessary to improve our understanding of the ongoing ocean acidification.

Last, it is uncertain how changes in the interior and surface ocean uptake efficiency of CO_2 feed back to the atmosphere. High precision CO_2 measurements could resolve the imprint that interannual to subdecadal changes in the surface and interior ocean have on the atmospheric CO_2 concentrations.

Bibliography

Arora, V. K., G. J. Boer, P. Friedlingstein, M. Eby, C. D. Jones, J. R. Christian, G. Bonan, L. Bopp, V. Brovkin, P. Cadule, T. Hajima, T. Ilyina, K. Lindsay, J. F. Tjiputra, and T. Wu. 2013. Carbon-Concentration and Carbon-Climate Feedbacks in CMIP5 Earth System Models. *Journal of Climate* **26**, 5289–5314.

Bacon, S., W. Gould, and Y. Jia. 2003. Open-ocean convection in the Irminger Sea. *Geophysical Research Letters*.

Bakker, D. C. E., B. Pfeil, K. M. O'Brien, K. I. Currie, S. D. Jones, C. S. Landa, S. K. Lauvset, N. Metzl, D. R. Munro, S.-I. Nakaoka, A. Olsen, D. Pierrot, S. Saito, K. Smith, C. Sweeney, T. Takahashi, C. Wada, R. Wanninkhof, S. R. Alin, M. Becker, R. G. Bellerby, A. V. Borges, J. Boutin, Y. Bozec, E. Burger, W.-J. Cai, R. D. Castle, C. E. Cosca, M. D. DeGrandpre, M. Donnelly, G. Eischeid, R. A. Feely, T. Gkritzalis, M. González-Dávila, C. Goyet, A. Guillot, N. Hardman-Mountford, J. Hauck, M. Hoppema, M. P. Humphreys, C. W. Hunt, J. S. P. Ibánhez, T. Ichikawa, M. Ishii, L. W. Juranek, V. Kitidis, A. Körtzinger, U. K. Koffi, A. Kozyr, A. Kuwata, N. Lefèvre, C. Lo Monaco, A. Manke, P. Marrec, J. T. Mathis, F. J. Millero, N. Monacci, P. M. S. Monteiro, A. Murata, T. Newberger, Y. Nojiri, I. Nonaka, A. M. Omar, T. Ono, X. A. Padín, G. Rehder, A. Rutgersson, C. L. Sabine, J. Salisbury, J. M. Santana-Casiano, D. Sasano, U. Schuster, R. Sieger, I. Skjelvan, T. Steinhoff, K. Sullivan, S. C. Sutherland, A. Sutton, K. Tadokoro, M. Telszewski, H. Thomas, B. Tilbrook, S. van Heuven, D. Vandemark, D. W. Wallace, and R. Woosley. 2016. Surface Ocean CO_2 Atlas (SOCAT) V4.

Brewer, P. G. 1978. Direct observation of the oceanic CO_2 increase. *Geophysical Research Letters* **5**, 997–1000.

Chen, G., and F. Millero. 1979. Gradual increase of oceanic CO_2. *Nature* **277**, 205–206.

Ciais, P., C. Sabine, G. Bala, L. Bopp, V. Brovkin, J. Canadell, A. Chhabra, R. DeFries, J. Galloway, M. Heimann, C. Jones, C. L. Quéré, R. Myneni, S. Piao, and P. Thornton. 2013. *Climate Change 2013: The Physical Science Basis. Contribution of Working Group I to the Fifth Assessment Report of the Intergovernmental Panel on Climate Change*. In: Carbon and Other Biogeochemical Cycles. Cambridge University Press, Cambridge, United Kingdom and New York, NY, USA.

Corbière, A., N. Metzl, G. Reverdin, C. Brunet, and T. Takahashi. 2007. Interannual and decadal variability of the oceanic carbon sink in the North Atlantic subpolar gyre. *Tellus B* **59**, 168–178.

Curry, R., M. McCartney, and T. Joyce. 1998. Oceanic transport of subpolar climate signals to mid-depth subtropical waters. *Nature* **391**, 575–577.

de Jong, M. F., H. M. van Aken, K. Våge, and R. S. Pickart. 2012. Convective mixing in the central Irminger Sea: 2002-2010. *Deep-Sea Research Part I-Oceanographic Research Papers* **63**, 36–51.

Dickson, A. G. 1981. An exact definition of total alkalinity and a procedure for the estimation of alkalinity and total inorganic carbon from titration data. *Deep-Sea Research Part A-Oceanographic Research Papers* **28**, 609–623.

Dickson, R., and J. Brown. 1994. The Production of North-Atlantic Deep-Water - Sources, Rates and Pathways. *Journal of Geophysical Research - Oceans* **99**, 12319–12341.

Doney, S. C., V. Fabry, R. Feely, and J. A. Kleypas. 2009. Ocean Acidification: The Other CO_2 Problem. *Annual Review of Marine Science* **1**, 169–192.

Doyle, J., and M. Shapiro. 1999. Flow response to large-scale topography: the Greenland tip jet. *Tellus Series A-Dynamic Meteorology and Oceanography* **51**, 728–748. Rossby-100 Symposium, Stockholm, Sweden, Jun 08-12, 1998.

DuVivier, A. K., J. J. Cassano, A. Craig, J. Hamman, W. Maslowski, B. Nijssen, R. Osinski, and A. Roberts. 2016. Winter atmospheric buoyancy forcing and oceanic response during strong wind events around southeastern greenland in the regional arctic system model (rasm) for 1990–2010. *Journal of Climate* **29**, 975–994.

Falina, A., A. Sarafanov, and A. Sokov. 2007. Variability and renewal of Labrador Sea Water in the Irminger Basin in 1991-2004. *Journal of Geophysical Research - Oceans*.

Feely, R., T. Takahashi, R. Wanninkhof, M. McPhaden, C. Cosca, S. Sutherland, and M.-E. Carr. 2006. Decadal variability of the air-sea CO_2 fluxes in the equatorial Pacific Ocean. *Journal of Geophysical Research: Oceans* **111(C08)**, C08S90.

Friedlingstein, P., P. Cox, R. Betts, L. Bopp, W. Von Bloh, V. Brovkin, P. Cadule, S. Doney, M. Eby, I. Fung, G. Bala, J. John, C. Jones, F. Joos, T. Kato, M. Kawamiya, W. Knorr, K. Lindsay, H. D. Matthews, T. Raddatz, P. Rayner, C. Reick, E. Roeckner, K. G. Schnitzler, R. Schnur, K. Strassmann, A. J. Weaver, C. Yoshikawa, and N. Zeng. 2006. Climate-carbon cycle feedback analysis: Results from the C^4MIP model intercomparison. *Journal of Climate* **19**, 3337–3353.

Gattuso, J.-P., and L. Hansson. 2011. *Ocean Acidification*. Oxford University Press, New York.

Gebbie, G., and P. Huybers. 2010. Total Matrix Intercomparison: A Method for Determining the Geometry of Water-Mass Pathways. *Journal of Physical Oceanography* **40**, 1710–1728.

Gruber, N. 2009. Carbon cycle: Fickle trends in the ocean. *Nature* **458**, 155–156.

Gruber, N., C. Keeling, and N. Bates. 2002. Interannual variability in the North Atlantic Ocean carbon sink. *Science* **298**, 2374–2378.

Gruber, N., J. Sarmiento, and T. Stocker. 1996. An improved method for detecting anthropogenic CO_2 in the oceans. *Global Biogeochemical Cycles* **10**, 809–837.

Häkkinen, S., and P. Rhines. 2004. Decline of subpolar North Atlantic circulation during the 1990s. *Science* **304**, 555–559.

Hall, T., T. Haine, and D. Waugh. 2002. Inferring the concentration of anthropogenic carbon in the ocean from tracers. *Global Biogeochemical Cycles*.

Hansen, B., and S. Østerhus. 2000. North Atlantic–Nordic Seas exchanges. *Progress in Oceanography* **45**, 109 – 208.

Hátún, H., A. Sandø, H. Drange, B. Hansen, and H. Valdimarsson. 2005. Influence of the Atlantic subpolar gyre on the thermohaline circulation. *Science* **309**, 1841–1844.

Henson, S. A., I. Robinson, J. T. Allen, and J. J. Waniek. 2006. Effect of meteorological conditions on interannual variability in timing and magnitude of the spring bloom in the Irminger Basin, North Atlantic. *Deep Sea Research Part I: Oceanographic Research Papers* **53**, 1601 – 1615.

Henson, S. A., S. C. Painter, N. Penny Holliday, M. C. Stinchcombe, and S. L. C. Giering. 2013. Unusual subpolar North Atlantic phytoplankton bloom in 2010: Volcanic fertilization or North Atlantic Oscillation?. *Journal of Geophysical Research: Oceans* **118**, 4771–4780.

Hurrell, J. 1996. Influence of variations in extratropical wintertime teleconnections on Northern Hemisphere temperature. *Geophysical Research Letters* **23**, 665–668.

Hurrell, J. W., and C. Deser. 2009. North Atlantic climate variability: The role of the North Atlantic Oscillation. *Journal of Marine Systems* **78**, 28–41.

Jeansson, E., S. Jutterström, B. Rudels, L. G. Anderson, K. A. Olsson, E. P. Jones, W. M. S. Jr., and J. H. Swift. 2008. Sources to the East Greenland Current and its contribution to the Denmark Strait Overflow . *Progress in Oceanography* **78**, 12 – 28.

Knutsen, Ø., H. Svendsen, S. Østerhus, T. Rossby, and B. Hansen. 2005. Direct measurements of the mean flow and eddy kinetic energy structure of the upper ocean circulation in the NE Atlantic. *Geophysical Research Letters*. L14604.

Lauvset, S. K., N. Gruber, P. Landschützer, A. Olsen, and J. Tjiputra. 2015. Trends and drivers in global surface ocean pH over the past 3 decades. *Biogeosciences* **12**, 1285–1298.

Lavender, K., W. Owens, and R. Davis. 2005. The mid-depth circulation of the subpolar North Atlantic Ocean as measured by subsurface floats. *Deep-Sea Research Part I-Oceanographic Research Papers* **52**, 767–785.

Lazier, J., R. Hendry, A. Clarke, I. Yashayaev, and P. Rhines. 2002. Convection and restratification in the Labrador Sea, 1990-2000. *Deep-Sea Research Part I-Oceanographic Research Papers* **49**, 1819–1835.

Le Quéré, C., R. M. Andrew, J. G. Canadell, S. Sitch, J. I. Korsbakken, G. P. Peters, A. C. Manning, T. A. Boden, P. P. Tans, R. A. Houghton, R. F. Keeling, S. Alin, O. D. Andrews, P. Anthoni, L. Barbero, L. Bopp, F. Chevallier, L. P. Chini, P. Ciais,

K. Currie, C. Delire, S. C. Doney, P. Friedlingstein, T. Gkritzalis, I. Harris, J. Hauck, V. Haverd, M. Hoppema, K. Klein Goldewijk, A. K. Jain, E. Kato, A. Körtzinger, P. Landschützer, N. Lefèvre, A. Lenton, S. Lienert, D. Lombardozzi, J. R. Melton, N. Metzl, F. Millero, P. M. S. Monteiro, D. R. Munro, J. E. M. S. Nabel, S.-I. Nakaoka, K. O'Brien, A. Olsen, A. M. Omar, T. Ono, D. Pierrot, B. Poulter, C. Rödenbeck, J. Salisbury, U. Schuster, J. Schwinger, R. Séférian, I. Skjelvan, B. D. Stocker, A. J. Sutton, T. Takahashi, H. Tian, B. Tilbrook, I. T. van der Laan-Luijkx, G. R. van der Werf, N. Viovy, A. P. Walker, A. J. Wiltshire, and S. Zaehle. 2016. Global Carbon Budget 2016. *Earth System Science Data* **8**, 605–649.

Levine, N. M., S. C. Doney, I. Lima, R. Wanninkhof, N. R. Bates, and R. A. Feely. 2011. The impact of the North Atlantic Oscillation on the uptake and accumulation of anthropogenic CO_2 by North Atlantic Ocean mode waters. *Global Biogeochemical Cycles*.

Lherminier, P., H. Mercier, T. Huck, C. Gourcuff, F. F. Pérez, P. Morin, A. Sarafanov, and A. Falina. 2010. The Atlantic Meridional Overturning Circulation and the subpolar gyre observed at the A25-OVIDE section in June 2002 and 2004 . *Deep Sea Research Part I: Oceanographic Research Papers* **57**, 1374 – 1391.

Lueker, T. J., A. G. Dickson, and C. D. Keeling. 2000. Ocean pCO_2 calculated from dissolved inorganic carbon, alkalinity, and equations for K_1 and K_2: validation based on laboratory measurements of CO_2 in gas and seawater at equilibrium. *Marine Chemistry* **70**, 105–119.

Marshall, J., and F. Schott. 1999. Open-ocean convection: Observations, theory, and models. *Reviews of Geophysics* **37**, 1–64.

McKinley, G. A., A. R. Fay, T. Takahashi, and N. Metzl. 2011. Convergence of atmospheric and North Atlantic carbon dioxide trends on multidecadal timescales. *Nature Geoscience* **4**, 606–610.

Mehrbach, C., C. H. Culberson, J. E. Hawley, and R. M. Pytkowicx. 1973. Measurement of the apparent dissociation constants of carbonic acid in seawater at atmospheric pressure. *Limnology and Oceanography* **18**, 897–907.

Metzl, N., A. Corbiere, G. Reverdin, A. Lenton, T. Takahashi, A. Olsen, T. Johannessen, D. Pierrot, R. Wanninkhof, S. R. Olafsdottir, J. Olafsson, and M. Ramonet. 2010. Recent acceleration of the sea surface fCO_2 growth rate in the North Atlantic subpolar gyre (1993-2008) revealed by winter observations. *Global Biogeochemical Cycles*.

Mikaloff Fletcher, S. E., N. Gruber, A. R. Jacobson, S. C. Doney, S. Dutkiewicz, M. Gerber, M. Follows, F. Joos, K. Lindsay, D. Menemenlis, A. Mouchet, S. A. Müller, and J. L. Sarmiento. 2006. Inverse estimates of anthropogenic CO_2 uptake, transport, and storage by the ocean. *Global Biogeochemical Cycles*. GB2002.

Moore, G., and I. Renfrew. 2005. Tip jets and barrier winds: A QuikSCAT climatology of high wind speed events around Greenland. *Journal of Climate* **18**, 3713–3725.

Moore, G. W. K. 2003. Gale force winds over the Irminger Sea to the east of Cape Farewell, Greenland. *Geophysical Research Letters*.

Nansen, F. 1912. Das Bodenwasser und die Abkühlung des Meeres. *Internationale Revue der gesamten Hydrobiologie und Hydrographie* **Band V**, Nr. 1:1–42.

Nightingale, P. D., G. Malin, C. S. Law, A. J. Watson, P. S. Liss, M. I. Liddicoat, J. Boutin, and R. C. Upstill-Goddard. 2000. In situ evaluation of air-sea gas exchange parameterizations using novel conservative and volatile tracers. *Global Biogeochemical Cycles* **14**, 373–387.

NOAA-ESRL 2015. Atmospheric Carbon Dioxide Dry Air Mole Fractions from quasi-continuous measurements at Mauna Loa, Hawaii. *Compiled by K.W. Thoning, D.R. Kitzis, and A. Crotwell. National Oceanic and Atmospheric Administration (NOAA), Earth System Research Laboratory (ESRL), Global Monitoring Division (GMD): Boulder, Colorado, USA.*

Olsen, A., K. R. Brown, M. Chierici, T. Johannessen, and C. Neill. 2008. Sea-surface CO_2 fugacity in the subpolar North Atlantic. *Biogeosciences* **5**, 535–547.

Olsen, A., R. M. Key, S. van Heuven, S. K. Lauvset, A. Velo, X. Lin, C. Schirnick, A. Kozyr, T. Tanhua, M. Hoppema, S. Jutterström, R. Steinfeldt, E. Jeansson, M. Ishii, F. F. Pérez, and T. Suzuki. 2016. The Global Ocean Data Analysis Project version 2 (GLODAPv2) – an internally consistent data product for the world ocean. *Earth System Science Data* **8**, 297–323.

Omar, A. M., and A. Olsen. 2006. Reconstructing the time history of the air-sea CO_2 disequilibrium and its rate of change in the eastern subpolar North Atlantic, 1972–1989. *Geophysical Research Letters.* L04602.

Park, G.-H., R. Wanninkhof, S. C. Doney, T. Takahashi, K. Lee, R. A. Feely, C. L. Sabine, J. Trinanes, and I. D. Lima. 2010. Variability of global net sea–air CO_2 fluxes over the last three decades using empirical relationships. *Tellus B* **62**, 352–368.

Pérez, F. F., H. Mercier, M. Vázquez-Rodríguez, P. Lherminier, A. Velo, P. C. Pardo, G. Roson, and A. F. Ríos. 2013. Atlantic Ocean CO_2 uptake reduced by weakening of the meridional overturning circulation. *Nature Geoscience* **6**, 146–152.

Pérez, F. F., M. Vázquez-Rodríguez, E. Louarn, X. A. Padín, H. Mercier, and A. F. Ríos. 2008. Temporal variability of the anthropogenic CO_2 storage in the Irminger Sea. *Biogeosciences* **5**, 1669–1679.

Pérez, F. F., M. Vázquez-Rodríguez, H. Mercier, A. Velo, P. Lherminier, and A. F. Ríos. 2010. Trends of anthropogenic CO_2 storage in North Atlantic water masses. *Biogeosciences* **7**, 1789–1807.

Pickart, R., F. Straneo, and G. Moore. 2003a. Is Labrador Sea Water formed in the Irminger basin?. *Deep-Sea Research Part I-Oceanographic Research Papers* **50**, 23–52.

Pickart, R., M. Spall, M. Ribergaard, G. Moore, and R. Milliff. 2003b. Deep convection in the Irminger Sea forced by the Greenland tip jet. *Nature* **424**, 152–156.

Rhein, M., J. Fischer, W. Smethie, D. Smythe-Wright, R. Weiss, C. Mertens, D. Min, U. Fleischmann, and A. Putzka. 2002. Labrador Sea Water: Pathways, CFC inventory, and formation rates. *Journal of Physical Oceanography* **32**, 648–665.

Sabine, C., R. Feely, N. Gruber, R. Key, K. Lee, J. Bullister, R. Wanninkhof, C. Wong, D. Wallace, B. Tilbrook, F. Millero, T. Peng, A. Kozyr, T. Ono, and A. Ríos. 2004. The oceanic sink for anthropogenic CO_2. *Science* **305**, 367–371.

Sarmiento, J., and N. Gruber. 2006. *Ocean Biogeochemical Dynamics*. Princton University Press.

Sarmiento, J. L., J. C. Orr, and U. Siegenthaler. 1992. A perturbation simulation of CO_2 uptake in an ocean general circulation model. *Journal of Geophysical Research: Oceans* **97**, 3621–3645.

Schuster, U., and A. J. Watson. 2007. A variable and decreasing sink for atmospheric CO_2 in the North Atlantic. *Journal of Geophysical Research: Oceans*. C11006.

Schwinger, J., J. F. Tjiputra, C. Heinze, L. Bopp, J. R. Christian, M. Gehlen, T. Ilyina, C. D. Jones, D. Salas-Melia, J. Segschneider, R. Seferian, and I. Totterdell. 2014. Nonlinearity of Ocean Carbon Cycle Feedbacks in CMIP5 Earth System Models. *Journal of Climate* **27**, 3869–3888.

Steinfeldt, R., M. Rhein, J. L. Bullister, and T. Tanhua. 2009. Inventory changes in anthropogenic carbon from 1997-2003 in the Atlantic Ocean between 20°S and 65°N. *Global Biogeochemical Cycles*.

Straneo, F., R. Pickart, and K. Lavender. 2003. Spreading of Labrador sea water: an advective-diffusive study based on Lagrangian data. *Deep-Sea Research Part I-Oceanographic Research Papers* **50**, 701–719.

Takahashi, T., S. C. Sutherland, R. Wanninkhof, C. Sweeney, R. A. Feely, D. W. Chipman, B. Hales, G. Friederich, F. Chavez, C. Sabine, A. Watson, D. C. Bakker, U. Schuster, N. Metzl, H. Yoshikawa-Inoue, M. Ishii, T. Midorikawa, Y. Nojiri, A. Körtzinger, T. Steinhoff, M. Hoppema, J. Olafsson, T. S. Arnarson, B. Tilbrook, T. Johannessen, A. Olsen, R. Bellerby, C. Wong, B. Delille, N. Bates, and H. J. de Baar. 2009. Climatological mean and decadal change in surface ocean pCO_2, and net sea-air CO_2 flux over the global oceans . *Deep Sea Research Part II: Topical Studies in Oceanography* **56**, 554–577.

Talley, L. D., and M. S. McCartney. 1982. Distribution and circulation of Labrador Sea-Water. *Journal of Physical Oceanography* **12**, 1189–1205.

Tanhua, T., and R. F. Keeling. 2012. Changes in column inventories of carbon and oxygen in the Atlantic Ocean. *Biogeosciences* **9**, 4819–4833.

Tanhua, T., D. W. Waugh, and D. W. R. Wallace. 2008. Use of SF_6 to estimate anthropogenic CO_2 in the upper ocean. *Journal of Geophysical Research-Oceans*.

Tanhua, T., K. A. Olsson, and E. Jeansson. 2005. Formation of Denmark Strait overflow water and its hydro-chemical composition. *Journal of Marine Systems* **57**, 264–288.

Thomas, H., A. E. F. Prowe, I. D. Lima, S. C. Doney, R. Wanninkhof, R. J. Greatbatch, U. Schuster, and A. Corbiere. 2008. Changes in the North Atlantic Oscillation influence CO_2 uptake in the North Atlantic over the past 2 decades. *Global Biogeochemical Cycles*.

Tjiputra, J. F., A. Olsen, K. Assmann, B. Pfeil, and C. Heinze. 2012. A model study of the seasonal and long-term North Atlantic surface pCO_2 variability. *Biogeosciences* **9**, 907–923.

Ullman, D. J., G. A. McKinley, V. Bennington, and S. Dutkiewicz. 2009. Trends in the North Atlantic carbon sink: 1992-2006. *Global Biogeochemical Cycles*.

UNFCCC 2015. Adoption of the Paris Agreement.

Vázquez-Rodríguez, M., F. Touratier, C. Lo Monaco, D. W. Waugh, X. A. Padín, R. G. J. Bellerby, C. Goyet, N. Metzl, A. F. Ríos, and F. F. Pérez. 2009. Anthropogenic carbon distributions in the Atlantic Ocean: data-based estimates from the Arctic to the Antarctic. *Biogeosciences* **6**, 439–451.

Vázquez-Rodríguez, M., X. A. Padín, P. C. Pardo, A. F. Ríos, and F. F. Pérez. 2012. The subsurface layer reference to calculate preformed alkalinity and air-sea CO_2 disequilibrium in the Atlantic Ocean. *Journal of Marine Systems* **94**, 52–63.

Våge, K., R. S. Pickart, A. Sarafanov, O. Knutsen, H. Mercier, P. Lherminier, H. M. van Aken, J. Meincke, D. Quadfasel, and S. Bacon. 2011. The Irminger Gyre: Circulation, convection, and interannual variability. *Deep-Sea Research Part I-Oceanographic Research Papers* **58**, 590–614.

Våge, K., R. S. Pickart, G. W. K. Moore, and M. H. Ribergaard. 2008. Winter mixed layer development in the central Irminger Sea: The effect of strong, intermittent wind events. *Journal of Physical Oceanography* **38**, 541–565.

Wanninkhof, R. 1992. Relationship between wind speed and gas exchange over the ocean. *Journal of Geophysical Research: Oceans* **97**, 7373–7382.

Wanninkhof, R., S. C. Doney, J. L. Bullister, N. M. Levine, M. Warner, and N. Gruber. 2010. Detecting anthropogenic CO_2 changes in the interior Atlantic Ocean between 1989 and 2005. *Journal of Geophysical Research-Oceans*.

Waugh, D. W., T. M. Hall, B. I. McNeil, R. Key, and R. J. Matear. 2006. Anthropogenic CO_2 in the oceans estimated using transit time distributions. *Tellus Series B-Chemical and Physical Meteorology* **58**, 376–389.

Weiss, R. F. 1974. Carbon dioxide in water and seawater: the solubility of a non-ideal gas. *Marine Chemistry* **2**, 203–215.

Wolf-Gladrow, D. A., R. E. Zeebe, C. Klaas, A. Körtzinger, and A. G. Dickson. 2007. Total alkalinity: The explicit conservative expression and its application to biogeochemical processes. *Marine Chemistry* **106**, 287–300.

Woosley, R. J., F. J. Millero, and R. Wanninkhof. 2016. Rapid anthropogenic changes in CO_2 and pH in the Atlantic Ocean: 2003–2014. *Global Biogeochemical Cycles* **30**, 70–90. 2015GB005248.

Wunsch, C., R. W. Schmitt, and D. J. Baker. 2013. Climate change as an intergenerational problem. *Proceedings of the National Academy of Sciences* **110**, 4435–4436.

Wüst, G. 1943. Der subarktische Bodenstrom in der westatlantischen Mulde. *Annalen der Hydrographie und Maritimen Meteorologie* **IV/VI**, 249–256.

Yashayaev, I., and A. Clarke. 2008. Evolution of North Atlantic Water Masses inferred from Labrador Sea Salinity Series. *Oceanography* **21**, 30–45.

Yashayaev, I., H. M. van Aken, N. P. Holliday, and M. Bersch. 2007a. Transformation of the Labrador Sea Water in the subpolar North Atlantic. *Geophysical Research Letters*.

Yashayaev, I., M. Bersch, and H. M. van Aken. 2007b. Spreading of the Labrador Sea Water to the Irminger and Iceland basins. *Geophysical Research Letters*. L10602.

Zeebe, R., and D. Wolf-Gladrow. 2001. *CO_2 in Seawater: Equilibrium, Kinetics, Isotopes*. Vol. 65. 1st ed.

6 Scientific results

I

Paper I

6.1 Irminger Sea deep convection injects oxygen and anthropogenic carbon to the ocean interior

Fröb, F., A. Olsen, K. Våge, G.W.K. Moore, I. Yashayaev, E. Jeansson, and B. Rajasakaren

Nature Communications, **7**, 13244 (2016)

nature COMMUNICATIONS

ARTICLE

Received 22 Apr 2016 | Accepted 15 Sep 2016 | Published 27 Oct 2016

DOI: 10.1038/ncomms13244 OPEN

Irminger Sea deep convection injects oxygen and anthropogenic carbon to the ocean interior

F. Fröb[1,2], A. Olsen[1,2], K. Våge[1,2], G.W.K. Moore[3], I. Yashayaev[4], E. Jeansson[2,5] & B. Rajasakaren[2,5]

Deep convection in the subpolar North Atlantic ventilates the ocean for atmospheric gases through the formation of deep water masses. Variability in the intensity of deep convection is believed to have caused large variations in North Atlantic anthropogenic carbon storage over the past decades, but observations of the properties during active convection are missing. Here we document the origin, extent and chemical properties of the deepest winter mixed layers directly observed in the Irminger Sea. As a result of the deep convection in winter 2014–2015, driven by large oceanic heat loss, mid-depth oxygen concentrations were replenished and anthropogenic carbon storage rates almost tripled compared with Irminger Sea hydrographic section data in 1997 and 2003. Our observations provide unequivocal evidence that ocean ventilation and anthropogenic carbon uptake take place in the Irminger Sea and that their efficiency can be directly linked to atmospheric forcing.

[1] Geophysical Institute, University of Bergen, Bergen 5007, Norway. [2] Bjerknes Centre for Climate Research, Bergen 5007, Norway. [3] Department of Physics, University of Toronto, Toronto, Ontario, Canada M5S A17. [4] Bedford Institute of Oceanography, Fisheries and Oceans Canada, Dartmouth, Nova Scotia, Canada B2Y 4A2. [5] Uni Climate, Uni Research, Bergen 5007, Norway. Correspondence and requests for materials should be addressed to F.F. (email: friederike.frob@uib.no).

Deep convection is a key process for maintaining the oceanic sink for anthropogenic carbon and ventilating the ocean for atmospheric gases such as CO_2 and oxygen[1]. The renewal of oxygen at depth supports aerobic remineralization of organic matter, and biogeochemical processes respond sensitively to changes in the supply rate from the surface ocean[2]. Regions where ocean ventilation and anthropogenic carbon sequestration occur are limited, for example, 85% of the total volume of the deep ocean is ventilated from only 15% of the surface ocean[3]. The subpolar North Atlantic is such a location. However, the processes that govern deep convection there are highly variable and sensitive to changes in large-scale ocean–atmosphere interactions.

In the northern mid-latitudes, strong declines in oxygen between the 1970s and the 1990s were observed in the upper ocean (100–1,000 m). This decline in oxygen likely resulted from reduced exchange between the surface mixed layer and interior ocean, associated with warming and freshening in the upper ocean[4,5]. Furthermore, a series of papers have shown how reduced deep water formation in the subpolar North Atlantic from the mid-1990s to the mid-2000s affected ocean anthropogenic carbon storage rates[6–8]. A recent acceleration in anthropogenic carbon storage rates has been observed in the North Atlantic from 2003 to 2014 compared with the 1989–2003 period, attributed to changes in water mass ventilation as well as increasing atmospheric CO_2 concentration[9]. The frequency, duration and intensity of deep water formation in the North Atlantic subpolar gyre region is strongly related to atmospheric variability. In particular, variability associated with the North Atlantic oscillation (NAO) is one of the main drivers for hydrographic property changes in the subpolar North Atlantic on interannual to decadal timescales[10,11].

Despite efforts to elucidate the relationship between atmospheric forcing and ventilation processes, a complete mechanistic understanding is still missing. There are insufficient observational data to determine the impact of atmospheric forcing on mixed layer depth and properties in the subpolar gyre, in particular with regard to ocean ventilation and carbon sequestration. Data collected during summer cruises only provide indirect evidence, and signals that are advected from outside the subpolar gyre are challenging to distinguish from signals that reflect local mechanisms of deep water formation. With the installation of mooring stations and the advent of autonomous sampling systems such as Argo the problem of seasonal biases in sampling is now being alleviated[12,13]. However, the type of sensors that are carried are limited and for the collection of high-quality carbon and tracer data, ship-board measurements are required. Since wintertime conditions are extremely harsh in the subpolar gyre, ship data from the convective season are rare. For example, between 1990 and 2014 the Irminger Sea was occupied by more than 30 research cruises, but only once during the potentially convective season[14].

In the Irminger Sea, deep convection takes place under favourable oceanic and atmospheric conditions[15–21]. Here we present new observational data from a unique cruise in winter 2015 that captured such a deep convective event. These observations document the properties of the deepest mixed layers directly recorded in this region and their impact on oxygen and anthropogenic carbon, providing a link between atmospheric forcing and anthropogenic carbon storage and oxygen re-ventilation in the subpolar gyre.

Results

Oxygen and anthropogenic carbon in the water column. Sulfur hexafluoride (SF_6) saturation values, here shown in a potential temperature–salinity diagram based on the 2015 Irminger Sea cruise data (Fig. 1a), indicate that strong local convection took place in the Irminger Sea in winter 2014–2015. The depth of the mixed layer is derived from hydrographic profiles using a threshold criterion[22] (see Methods section). The mean density in the winter mixed layer corresponds to the density of the lighter Labrador Sea Water (LSW) class formed in the subpolar gyre after 2000 (ref. 23). SF_6 is typically undersaturated in the surface ocean during active water mass formation with saturation values of 86% in the North Atlantic[24]. Here, within the winter mixed layer the SF_6 saturation varies strongly between undersaturation and supersaturation, with supersaturated values testifying to the recent formation through convective processes in winter 2014–2015. The highest supersaturated values of SF_6 were observed at the base of the mixed layer with a mean saturation of $116.2 \pm 8.2\%$, possibly driven by bubble formation at the surface induced by high wind speeds[25].

Oxygen and anthropogenic carbon concentrations are presented along the 2015 cruise transect across the Irminger Sea with the coast of Greenland close to Cape Farewell to the west and the Reykjanes Ridge to the east (Fig. 1b,c). Anthropogenic carbon concentrations are computed using the transient time distribution (TTD) method[26]. Within the winter mixed layer, they are based on SF_6 data. In the less recently ventilated water masses below the mixed layer, dichlorodifluoromethane (CFC-12) measurements provide more reliable estimates[24]. Concentrations of oxygen and anthropogenic carbon are high in the entire winter mixed layer, indicative of its recent ventilation. Below lies an older water mass layer with reduced levels of oxygen and anthropogenic carbon. Towards the bottom of the western Irminger Basin, elevated oxygen concentrations are found, a characteristic feature of Denmark Strait Overflow Water. In combination with Iceland Scotland Overflow Water and LSW from the Labrador and Irminger Seas, this water mass forms North Atlantic Deep Water[27], the key component of the lower limb of the Atlantic Meridional Overturning Circulation.

With respect to atmospheric values in 2015, the surface waters are saturated by 94–98% in oxygen and 90–100% in anthropogenic carbon, respectively. Oxygen undersaturation in the northern high latitudes during the convective season has been described as a consequence of gas exchange lagging behind strong heat loss[28,29].

Mixed layer depths in the North Atlantic subpolar gyre. Deep convection in winter 2014–2015 was not confined to the Irminger Sea, but occurred across the entire subpolar gyre. The mixed layer depth estimates we present are based on individual Argo profiles from December 2001 to May 2015, and hydrographic station data from April and May cruises to the Irminger and Labrador Seas in 2015. For consistency with earlier studies[20], we use the 2000–2007 base period of February–April Argo data to contextualize the 2015 data. Compared with climatological conditions, wintertime mixed layer depths were exceptionally deep in the entire subpolar gyre in 2015 (Fig. 2a) and the largest deviation from the long-term mean occurred in the Irminger Sea (Supplementary Fig. 1). Here, mixed layers were deeper than 1,400 m in early 2015 (Fig. 2a). While these are the deepest mixed layers directly observed in the Irminger Sea, exceeding the two previous winters by at least 800 m, there is indirect evidence that even deeper convection took place in the Irminger Sea in the early 1990s (ref. 15).

Convectively formed water masses are partly advected from their main formation region in the Labrador Sea to the Irminger Sea with a travel time of about 2 years, where these weakly stratified water masses can precondition the water column for convection[5,15,17,23]. Alternatively, waters originating from the

NATURE COMMUNICATIONS | DOI: 10.1038/ncomms13244 ARTICLE

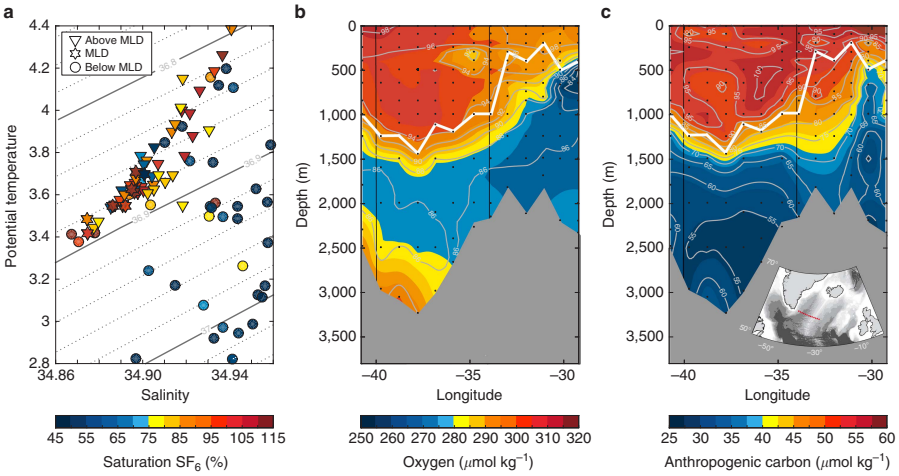

Figure 1 | Sulfur hexafluoride, oxygen and anthropogenic carbon in the water column in winter 2014–2015. (**a**) Irminger Sea potential temperature, salinity and sulfur hexafluoride (SF_6) saturation as observed during the April Irminger Sea cruise (58GS20150410). The contour lines show the potential density anomaly (σ_2 isopycnals). The filled circles show data below the depth of the mixed layer (MLD), the filled triangles show data within the winter mixed layer and the stars highlight properties at the base of the winter mixed layer. (**b**) Interpolated oxygen and (**c**) anthropogenic carbon concentrations in μmol kg^{-1} for a transect across the Irminger Sea based on April Irminger Sea cruise data. The black contour lines indicate saturation degree with respect to 2015 atmospheric concentrations. The white line shows winter mixed layer depth. The vertical lines show longitude bounds for the Irminger Sea region. The black dots show sampling depths. The location of the transect is shown in the map.

region south of Greenland could possibly be advected into the Irminger Sea on shorter timescales, but propagation rates are difficult to determine. In winter 2012–2013, convection was shallow and there was little dense water production in the entire subpolar gyre (Fig. 2b; Supplementary Fig. 1). During the subsequent winter of 2013–2014, dense water masses were produced by deep convection in the Labrador Sea as well as south of Greenland. However, in order for these water masses to potentially precondition the water column in the Irminger Sea for convection in winter 2014–2015, a fast eastward advection would be required. This is implausible given the observed mid-depth large-scale circulation[30]. The February to April mixed layer density evolution also reveals no eastward propagation of dense waters, particularly in 2013–2014. It appears instead that the deep mixed layers in the Irminger Sea arose locally in 2014–2015 by a gradual densification. That winter, deep convection resulted in the production of almost equally dense water masses in the Labrador Sea and the Irminger Sea. Therefore, advection of convectively formed water masses from outside the Irminger Sea cannot explain our observations. Hence, other mechanisms are responsible for the strong local convection.

Atmospheric forcing and water column stratification. The leading mode of atmospheric variability over the mid-latitude North Atlantic is the NAO. The positive phase of the NAO is characterized by a deeper Icelandic Low and stronger westerlies across the North Atlantic[31]. The NAO index (Supplementary Fig. 2) attained the highest value observed since the mid-1990s in winter 2014–2015. Atmospheric conditions during the positive phase of the NAO are conducive for the formation of westerly tip jets[32]. Tip jets are intense, periodic westerly winds that develop over the Irminger Sea as a result of the interaction of passing extra-tropical cyclones with the high topography of southern Greenland[33,34]. These local wind phenomena are typically associated with high wind speeds and elevated sea-air heat fluxes over the Irminger Sea[19]. Due to their small spatial scale, coarse-resolved global climate models fail to simulate the magnitude of tip jet events around Greenland[32,35]. Consistent with the high NAO index, the number of westerly tip jet events as well as the winter mean total oceanic heat loss over the Irminger Sea during the winter of 2014–2015 attained values not seen since the mid-1990s (Fig. 3a; Supplementary Fig. 2).

As a measure of water column stratification we use the buoyancy frequency N, which represents the frequency at which a neutrally buoyant parcel will oscillate in a stably stratified fluid. It is calculated as:

$$N^2 = -\frac{g}{\rho_0}\frac{\mathrm{d}\rho}{\mathrm{d}z}, \qquad (1)$$

with g being the downward acceleration due to gravity and ρ_0 the mean density. A preconditioned water column with reduced stratification, for example through the presence of weakly stratified water at intermediate levels, facilitates deep convection before the onset of the convective season[13]. The temporal evolution of buoyancy frequency with depth based on Argo data from 2002 to 2015 illustrates the interannual variability of preconditioning in the Irminger Sea (Fig. 3b). There is a seasonal cycle of surface stratification connected to local winter convection. The lowest values of buoyancy frequency are observed in the winter mixed layers as a consequence of buoyancy loss from the surface, followed by a period of restratification of the upper 500–1,000 m in spring and summer. The deepest winter mixed layers (white bars) were observed in winters 2007–2008, 2011–2012 and 2014–2015. Compared with the moderate winters before 2007, buoyancy

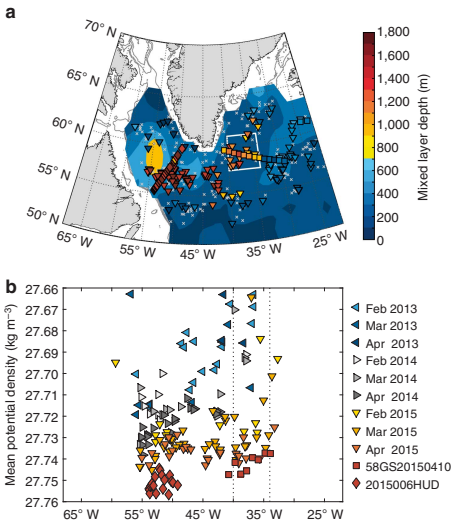

Figure 2 | Wintertime mixed layer depth distribution. February–April mixed layer depths greater than 80% of the deepest recorded mixed layer depth for individual Argo floats (triangles), Irminger Sea cruise data (58GS20150410) collected in April (squares) and Labrador Sea cruise data (2015006HUD) collecteted in May (diamonds). Note that mixed layers for May Labrador Sea cruise data were isolated from the sea surface. Mixed layer depths were calculated using a semi-subjective method following Pickart *et al.*[22]. (**a**) Winter 2014–2015 data with 2000–2007 average winter mixed layer depths as contours[20]. The crosses show locations of all data points. The white box shows the region in the Irminger Sea selected for further analysis. (**b**) Mean potential density anomaly (σ_0) over the winter mixed layer of the February–April Argo data for 2013 (blue scale), 2014 (grey scale) and 2015 (red scale). The vertical lines show longitude bounds for the Irminger Sea region.

frequency at depth has generally been lower after the deep convection in winter 2007–2008 (ref. 20).

The impact of these deep convection events on water column stability becomes more evident by analyzing the mean buoyancy frequency from individual Argo profiles (Fig. 3c). While the features are robust over a wide depth range, the mean buoyancy frequency between 500 and 1,000 m is presented here. During the convective season (February–April, grey bars) in 2008, 2012 and 2015, the mean buoyancy frequency at depth was low as a consequence of convection. Deep convection during these three winters interrupted periods of restratification that led to higher values of mean buoyancy frequency at depth, most likely due to lateral advection or mixing of more stratified water masses into the region. This variability can partly be explained by trends deduced from least-squared fits over the low-passed envelope of mean buoyancy. The envelope was computed by considering every local minimum of the mean buoyancy frequency time series and smoothing the result using a running mean filter for the periods 2002–2007, 2008–2011 and 2012–2015. In general, the Irminger Sea has shifted towards a state of weaker mid-depth stratification after the strong convection in 2007–2008.

Deep convection occurs in the Irminger Sea despite strong initial stratification during severe winters in terms of heat removal from the ocean (for example, winter 2007–2008 (ref. 20)). Although surface buoyancy loss in winter 2013–2014 led to deep mixing in the Labrador Sea and parts of the subpolar gyre, there is, as noted above, no indication that convectively-formed water masses from that winter advected into the Irminger Basin (Fig. 2b). The buoyancy frequency (Fig. 3b) substantiates this. The water column in fall 2014 reveals no particular sign of preconditioning for deep convection in 2014–2015. Combined, all these observations indicate that the strong winter surface buoyancy loss was the primary agent inducing deep convection in the Irminger Sea in winter 2014–2015, while preconditioning of the water column was only of secondary importance.

Discussion

In the early twentieth century, deep convection was thought to occur in the Irminger Sea[36], but in the decades that followed, the Labrador Sea became the main area of interest for subsequent convection studies as it is the primary location for deep water formation in the North Atlantic. The Irminger Sea has, however, been re-identified as a region where deep convection takes place under favourable oceanic and atmospheric conditions[15–21]. The convection in winter 2014–2015 was the third deep water formation event in the Irminger Sea since the winter 2007–2008, with substantial impact on not only ocean circulation and stratification processes but also, as presented here, ocean biogeochemistry and carbon cycle variability.

The effect of convection and its variability in the Irminger Sea on ocean oxygen and anthropogenic carbon is illustrated by comparing saturation profiles at representative stations in April 2015 with cruise data from 1997 (ref. 37) and 2003 (ref. 38) (Fig. 4a,b). The saturation degree of oxygen and anthropogenic carbon in the Irminger Sea has undergone significant changes related to deep water formation variability. The formation of well-ventilated LSW during the mid-1990s is reflected by the elevated oxygen and anthropogenic carbon saturation values between 1,000 and 1,750 m depth in the 1997 profiles (blue curves). In 2003 (black curves) the saturation levels were reduced throughout most of the water column, a consequence of no deep ventilation between 1997 and 2003 and aging of the remnant water masses[6]. In contrast, elevated oxygen and anthropogenic carbon concentrations in 2015 in the Irminger Sea are a result of high convective activity. At the tail end of the convective season in 2015, the mixed layer was nearly saturated in oxygen and anthropogenic carbon ($>90\%$) to a depth of 1,250 m.

The efficiency of the air-to-sea flux ultimately determines the degree of saturation and preformed concentrations of atmospheric gases in seawater. Preformed concentrations are set at the time of water mass formation, that is, the last time a water parcel is in direct contact with the atmosphere before subduction. For oxygen, preformed values are assumed to be close to saturation, however, the exact concentration can only be determined if measured directly. We observed a mean oxygen undersaturation of $3.6 \pm 0.9\%$, possibly driven by solubility effects due to the strong heat loss over winter and by the entrainment of old, less recently ventilated water masses[28]. Since oxygen concentrations at depth reflect the balance between supply and consumption, this needs to be taken into account if apparent oxygen utilization is used as in Feely[2] as a measure of biological activity, to avoid overestimation of respiration processes. The saturation degree of SF_6 in the winter mixed layer varied from undersaturated to supersaturated conditions with supersaturated values occuring at the base of the mixed layer (Fig. 1a). The consistency of this signal across stations indicates that this is not a measurement artefact. Supersaturation of SF_6 is

NATURE COMMUNICATIONS | DOI: 10.1038/ncomms13244 ARTICLE

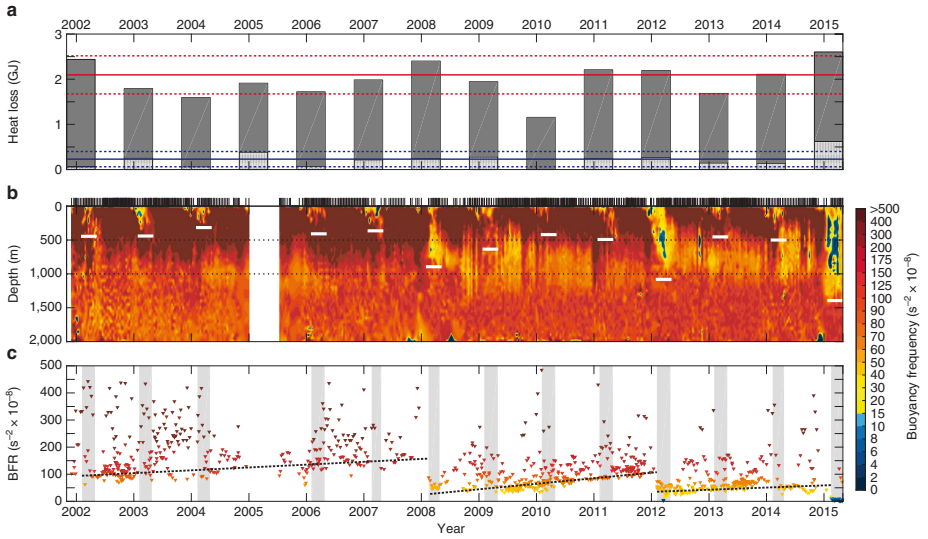

Figure 3 | Temporal evolution of ocean heat loss, buoyancy frequency and mean buoyancy frequency in the Irminger Sea. (**a**) The bars represent the integrated ocean heat loss from November to April based on ERA-Interim reanalysis data. The hatched part indicates the heat loss associated with tip jet events. The red solid line is the mean ocean heat loss from November to April from 1979 to 2015, the red dashed lines represent ±1 s.d. The blue solid line is the mean ocean heat loss associated with tip jet events from November to April from 1979 to 2015, the blue dashed lines represent ±1 s.d. (**b**) Interpolated buoyancy frequency with depth and time, based on Argo data. The white bars represent the 95th percentile of the February–April mixed layer depth (greater than 80% of deepest recorded mixed layer depth of individual floats). The black dotted lines highlight 500 and 1,000 m depth. The vertical bars on top denote the sampling time of each profile in the Irminger Sea. (**c**) Mean buoyancy frequency over 500–1,000 m. The grey bars highlight the convective season (February–April). The black dotted lines are least-square fits over the low-passed envelope of mean buoyancy frequency for 2002–2007 ($R^2 = 0.50$), 2008–2011 ($R^2 = 0.65$) and 2012–2015 ($R^2 = 0.20$).

induced by bubble formation at high wind speeds[25]. The reason why this water is found at the base of the mixed layer is likely because the highest winds speeds also result in the strongest heat loss and most active convection. Our measurements thus show that transient tracers such as SF_6 are not necessarily undersaturated at the time of water mass formation[24], and that physical processes such as bubble-mediated gas transfer may influence saturation values during winter convection.

Changes in the inventory of anthropogenic carbon reflect the interannual variability of the convective activity in the subpolar gyre (Fig. 4c). Exploiting the almost exponential time history of atmospheric CO_2 and evoking the theory of transient steady-state[39], the anthropogenic carbon concentrations in the ocean are expected to increase by 1.90% per year over our considered time period. Therefore, the anthropogenic carbon inventory is expected to increase by 1.20 ± 0.16 mol C m^{-2} per year in the absence of circulation changes and only based on rising atmospheric CO_2 concentrations. In contrast, between 1997 and 2003, anthropogenic carbon inventories increased by 0.63 ± 0.50 mol C m^{-2} per year, which leads to a lower-than-expected inventory in 2003 due to absence of ventilation processes and export of LSW from the western subpolar North Atlantic. Between 2003 and 2015 however, the uptake rate of anthropogenic carbon was 1.94 ± 0.29 mol C m^{-2} per year and clearly larger than expected from the atmospheric CO_2 increase alone. The fact that ocean variability increased the anthropogenic carbon inventory rate by a factor three between 1997 and 2015, indicates that frequent observations of physical and biogeochemical parameters in the subpolar North Atlantic are required to fully quantify anthropogenic carbon uptake variability and to distinguish between trends associated with long-term climate change and signals attributed to natural variability.

Physical properties have been monitored for many decades in the Atlantic, covering several phase shifts and amplitude changes of modes of atmospheric variability such as the NAO. Carbon chemistry data on the other hand have only been systematically collected on a repeat basis since the early 1990s. As the time span of the record is extended, the strong response of ventilation and anthropogenic carbon storage in the Atlantic to variability in atmospheric forcing becomes more evident[5,8,9]. In particular, the observations presented here reveal a strong link between oceanic heat loss enhanced by numerous tip jet events, ventilation and anthropogenic carbon storage in the Irminger Sea, which is one of the deep water formation areas in the North Atlantic. On a broader scale, the variations in ventilation that are being uncovered and attributed with our growing observational data base may also help to understand the decadal variability clearly present in North Atlantic sedimentary records[40,41]. For a robust prediction of future changes in convective processes in the subpolar gyre and their impacts on ocean oxygen and anthropogenic carbon, atmospheric forcing needs to be well-represented in global climate models by resolving small-scale atmospheric patterns such as the Greenland tip jet.

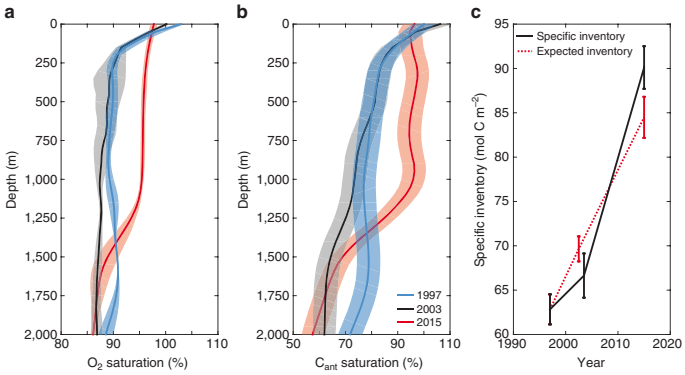

Figure 4 | Water column properties between 0 and 2,000 m for three selected cruises in the Irminger Sea. (**a**) Oxygen and (**b**) anthropogenic carbon mean saturation with depth for selected stations for 1997 (blue curves), 2003 (black curves) and 2014 (red curves) in the Irminger Sea based on cruise data (06MT19970815, 06MT20030723 and 58GS20150410). Note the different scales in (**a**,**b**). (**c**) The specific anthropogenic carbon inventory (black) and the expected evolution of anthropogenic carbon inventory based on actual atmospheric CO_2 increase and 1997 conditions (red) over 100–2,000 m in the Irminger Sea. The shading and the error bars represent ±1 s.d. over the station data, for (**b**,**c**) including the uncertainty of the TTD method.

Methods

Data. The Argo program consists of freely drifting profiling floats, which provide real-time salinity and temperature measurements of the upper 2,000 m of the ocean with accuracies of ±0.01 for salinity and ±0.002 °C for temperature. We use 22,764 Argo profiles obtained in the subpolar gyre from 2002 to 2015 with a quality flag of good (1) or probably good (2). Cruise data was collected during the cruises 58GS20150410, crossing the Irminger Sea from 16–20 April 2015, and 2015006HUD, crossing the Labrador Sea from 2–24 May 2015. The location of the stations, used for Fig. 4, for the Meteor cruises in 1997 (06MT19970815, collected from 15 August to 9 September)[37] and 2003 (06MT20030723, collected from 23 July to 19 August)[38] and 58GS20150410 cruise data are presented in Supplementary Fig. 3.

At 58GS20150410, direct measurements of pressure, conductivity, temperature and dissolved oxygen were obtained with a Seabird 911+ CTD. The CTD measurements were calibrated against *in situ* samples obtained at all Niskin bottle sample depths (usually 12) at every cast, following the Global Ocean Ship-based Hydrographic Investigations Program (GOSHIP) calibration procedure[42]. Bottle salinities were analysed with a salinometer with an accuracy of ±0.003. Winkler titration was performed to analyse oxygen concentration of water samples using a potassium iodate solution as a standard. The precision was ±0.005 ml l^{-1}. CFC-12 and SF_6 was measured with a similar purge and trap system as described in Bullister and Wisegarver[43] and Stoven and Tanhua[44], with gas chromatographic separation and electron capture detection. The precision was ±1.3% for CFC-12 concentrations and, due to some analytical issues, ±6.2% for SF_6 concentrations.

Solubilities of CFCs and SF_6 are estimated from salinity and temperature relations according to Warner and Weiss[45] and Bullister and Wisegarver[46]. The accuracy of the atmospheric record for both CFC-12 and SF_6 is much better than 1%, hence negligible. The accuracy of the solubility functions of CFC-12 and SF_6 are about 1.5% and 2%, respectively. The combined calibration and analytical uncertainties for CFC-12 saturation values is therefore 2.8% and for SF_6 8.2%. According to Weiss[47], the accuracy for the oxygen solubility function in seawater is ±0.015 ml l^{-1}, therefore the combined uncertainty for oxygen saturation values is in the order of 0.3%.

Mixed layer depth estimates. Mixed layer depths were estimated by manual inspection of individual profiles. Following Pickart *et al.*[22], the upper and lower depth limits of the mixed layer were first determined visually; and over that depth range, the mean density and its standard deviation were estimated. If no estimate could be made from the density profile, the temperature or salinity profile was used instead. The intersections between the original profile and the two-standard deviation envelope was defined as the mixed layer depth (Supplementary Fig. 4). This criterion also enabled determination of the depths of mixed layers isolated from the surface (Supplementary Fig. 5), which have been shown to occur in the subpolar gyre, either in the form of stacked multiple mixed layers or during the early phase of surface restratification[19,22]. For consistency with previous studies[20], only mixed layers deeper than 80% of the maximum recorded mixed layer depth for each winter and each float were included in the analysis to avoid a shallow bias associated with the non-uniform spatial and temporal character of convection.

Anthropogenic carbon. The concentration of anthropogenic carbon (C_{ant}) was estimated with the TTD method[26] based on CFC-12 data and SF_6 data. The concentration of any passive, inert tracer is determined at any place x at any time t by the source function of the tracer at sea surface $C^0(t)$ and the transit time distribution $\mathcal{G}(\mathbf{x},\tau)$:

$$C(x,t) = \int_0^\infty C^0(t-\tau)\mathcal{G}(\mathbf{x},\tau)\mathrm{d}\tau' \qquad (2)$$

This method allows to establish a transfer function between measured tracer concentration and C_{ant} with three assumptions made: (1) increasing C_{ant} concentration in the ocean does not affect the biological uptake of carbon, (2) the ocean circulation is in steady-state and (3) $C^0(t)$ has no spatial dependence for a given x (ref. 26).

TTDs can be approximated by inverse Gaussian functions at each location in the interior ocean:

$$\mathcal{G}(\tau,\Gamma,\Delta) = \sqrt{\frac{\Gamma^3}{4\pi\Delta^2\tau^3}}\,exp\left(\frac{-\Gamma(\tau-\Gamma)^2}{4\Delta^2\tau}\right), \qquad (3)$$

where Γ is the mean transit time and Δ defines the width of the TTD. In the subpolar gyre, the ratio Γ/Δ is assumed to be 1 (ref. 6). The source function depends on the atmospheric history (compiled by Bullister[48] for CFCs and SF_6; Mauna Loa updated records for CO_2 (ref. 49)) and the tracer solubility in sea water. Since the atmospheric history of CFCs and SF_6 is well documented, the TTD at any place x can be defined with direct observations of CFC-12 or SF_6, respectively. In case of excess SF_6, that is, supersaturated values within the mixed layers, age estimates are set to zero (ref. 24). Observed temperature (T) and salinity (S) are used to estimate preformed alkalinity (Alk^0)[50]. We use thermodynamic equations of the seawater CO_2 system[51] and the CO_2 dissociation constants of (ref. 52) refitted by (ref. 53) to calculate the time history in the surface mixed layer for anthropogenic CO_2:

$$C_{ant,0}(t) = C_{eq}\left(T, S, Alk^0, pCO_2(t)\right) - C_{eq}\left(T, S, Alk^0, pCO_2{=}280\,\text{p.p.m.}\right) \qquad (4)$$

Here, $C_{ant,0}$ is the difference between the total inorganic carbon C_{eq} at air-sea equilibrium with respect to the atmospheric CO_2 concentration at time t and at preindustrial atmospheric CO_2 levels (280 p.p.m.). The saturation of C_{ant} in the ocean is the ratio between actual C_{ant} concentration and $C_{ant,0}$.

C_{ant} inventories are estimated by integrating C_{ant} concentrations over 100–2,000 m: $INV = \int_0^z C_{ant}\,\varrho\,\mathrm{d}z$. Inventory increase rates are the difference in column inventory divided by the time in years between the measurements. The method-based uncertainty for C_{ant} is ±6 μmol kg^{-1} (ref. 26). For the inventory estimates, uncertainties were calculated by randomly propagating this standard error over depth for the selected stations which led to an uncertainty of ±1 mol C m^{-2}. The expected rise of C_{ant} is 1.9% a^{-1}, calculated for equilibrium

conditions in 1997 using the thermodynamic equations of the seawater CO_2 system and assuming an exponential time history of dissolved CO_2 in the surface mixed layer[6]. Multiplying this expected increase with the C_{ant} concentration in 1997 yields the C_{ant} concentration increase expected from rising atmospheric CO_2 levels only.

Atmospheric forcing. The atmospheric circulation is analysed using the ERA-Interim reanalysis data product, archived by the European Centre for Medium Range Weather Forecasts (ECMWF) and available at http://apps.ecmwf.int/datasets/. The NAO, a large-scale pressure oscillation with centres of action near Iceland and the Azores is the leading mode of variability in the North Atlantic region[54]. An index of the NAO can be defined using the sea-level pressure at Stykkisholmur, Iceland and Lisbon, Portugal[54]. The NAO is said to be in its positive state when the sea-level pressure near Iceland is anomalously low, while that near the Azores is anomalously high. Here, we used the sea-level pressure from the ERA-Interim to define the NAO Index. The heat loss associated with tip jet events is the heat loss during a fixed time period of 24 h, that is, ± 12 h from the peak wind speed during each event.

Data availability. The data that support the findings of this study are available from the corresponding authors (F.F. and A.O., are.olsen@gfi.uib.no) upon request and are available within the article.

References

1. Maier-Reimer, E. & Hasselmann, K. Transport and storage of CO_2 in the ocean - an inorganic ocean-circulation carbon cycle model. *Clim. Dyn.* **2,** 63–90 (1987).
2. Feely, R. A. Oxygen utilization and organic carbon remineralization in the upper water column of the Pacific Ocean. *J. Oceanogr.* **60,** 45–52 (2004).
3. Gebbie, G. & Huybers, P. How is the ocean filled? *Geophys. Res. Lett.* **38,** L06604 (2011).
4. Helm, K. P., Bindoff, N. L. & Church, J. A. Observed decreases in oxygen content of the global ocean. *Geophys. Res. Lett.* **38,** L23602 (2011).
5. Falina, A., Sarafanov, A. & Sokov, A. Variability and renewal of Labrador Sea Water in the Irminger Basin in 1991–2004. *J. Geophys. Res.* **112,** C01006 (2007).
6. Steinfeldt, R., Rhein, M., Bullister, J. L. & Tanhua, T. Inventory changes in anthropogenic carbon from 1997–2003 in the Atlantic Ocean between 20°S and 65°N. *Glob. Biogeochem. Cycles* **23,** GB3010 (2009).
7. Levine, N. M. *et al.* The impact of the North Atlantic Oscillation on the uptake and accumulation of anthropogenic CO_2 by North Atlantic Ocean mode waters. *Glob. Biogeochem. Cycles* **25,** GB3022 (2011).
8. Perez, F. F. *et al.* Atlantic Ocean CO_2 uptake reduced by weakening of the meridional overturning circulation. *Nat. Geosci.* **6,** 146–152 (2013).
9. Woosley, R. J., Millero, F. J. & Wanninkhof, R. Rapid anthropogenic changes in CO_2 and pH in the Atlantic Ocean: 2003–2014. *Glob. Biogeochem. Cycles* **30,** 70–90 (2016).
10. Curry, R. G., McCartney, M. S. & Joyce, T. M. Oceanic transport of subpolar climate signals to mid-depth subtropical waters. *Nature* **391,** 575–577 (1998).
11. Lazier, J., Hendry, R., Clarke, A., Yashayaev, I. & Rhines, P. Convection and restratification in the Labrador Sea, 1990–2000. *Deep-Sea Res. I* **49,** 1819–1835 (2002).
12. Körtzinger, A., Schimanski, J., Send, U. & Wallace, D. The ocean takes a deep breath. *Science* **306,** 1337 (2004).
13. de Jong, M. F., van Aken, H. M., Våge, K. & Pickart, R. S. Convective mixing in the central Irminger Sea: 2002–2010. *Deep-Sea Res. I* **63,** 36–51 (2012).
14. Olsen, A. *et al.* The Global Ocean Data Analysis Project version 2 (GLODAPv2) - an internally consistent data product for the world ocean. *Earth Syst. Sci. Data* **8,** 297–323 (2016).
15. Pickart, R., Straneo, F. & Moore, G. W. K. Is Labrador Sea water formed in the Irminger basin? *Deep-Sea Res. I* **50,** 23–52 (2003a).
16. Pickart, R., Spall, M., Ribergaard, M., Moore, G. W. K. & Milliff, R. Deep convection in the Irminger Sea forced by the Greenland tip jet. *Nature* **424,** 152–156 (2003b).
17. Straneo, F., Pickart, R. & Lavender, K. Spreading of Labrador Sea Water: an advective-diffusive study based on Lagrangian data. *Deep-Sea Res. I* **50,** 701–719 (2003).
18. Bacon, S., Gould, W. & Jia, Y. Open-ocean convection in the Irminger Sea. *Geophys. Res. Lett.* **30,** 1246 (2003).
19. Våge, K., Pickart, R. S., Moore, G. W. K. & Ribergaard, M. H. Winter mixed layer development in the central Irminger Sea: the effect of strong, intermittent wind events. *J. Phys. Oceanogr.* **38,** 541–565 (2008).
20. Våge, K. *et al.* Surprising return of deep convection to the subpolar North Atlantic Ocean in winter 2007–2008. *Nat. Geosci.* **2,** 67–72 (2009).
21. Våge, K. *et al.* The Irminger Gyre: circulation, convection, and interannual variability. *Deep-Sea Res. I* **58,** 590–614 (2011).
22. Pickart, R., Torres, D. & Clarke, R. Hydrography of the Labrador Sea during active convection. *J. Phys. Oceanogr.* **32,** 428–457 (2002).
23. Yashayaev, I., van Aken, H. M., Holliday, N. P. & Bersch, M. Transformation of the Labrador Sea water in the subpolar North Atlantic. *Geophys. Res. Lett.* **34,** L22605 (2007).
24. Tanhua, T., Waugh, D. W. & Wallace, D. W. R. Use of SF_6 to estimate anthropogenic CO_2 in the upper ocean. *J. Geophys. Res.* **113,** C04037 (2008).
25. Stöven, T., Tanhua, T., Hoppema, M. & von Appen, W. J. Transient tracer distributions in the Fram Strait in 2012 and inferred anthropogenic carbon content and transport. *Ocean Sci.* **12,** 319–333 (2016).
26. Waugh, D. W., Hall, T. M., McNeil, B. I., Key, R. & Matear, R. J. Anthropogenic CO_2 in the oceans estimated using transit time distributions. *Tellus Ser. B* **58,** 376–389 (2006).
27. Dickson, R. & Brown, J. The production of North-Atlantic deep-water - sources, rates, and pathways. *J. Geophys. Res.* **99,** 12319–12341 (1994).
28. Ito, T., Follows, M. J. & Boyle, E. A. Is AOU a good measure of respiration in the oceans? *Geophys. Res. Lett.* **31,** L17305 (2004).
29. Olsen, A., Omar, A. M., Jeansson, E., Anderson, L. G. & Bellerby, R. G. J. Nordic seas transit time distributions and anthropogenic CO_2. *J. Geophys. Res.* **115,** C05005 (2010).
30. Palter, J. B. *et al.* Variability of the directly observed, middepth subpolar North Atlantic circulation. *Geophys. Res. Lett.* **43,** 27002708 (2016).
31. Hurrell, J. W. & Deser, C. North Atlantic climate variability: the role of the North Atlantic Oscillation. *J. Mar. Sys* **78,** 28–41 (2009).
32. Moore, G. W. K. Gale force winds over the Irminger Sea to the east of Cape Farewell, Greenland. *Geophys. Res. Lett.* **30,** 1894 (2003).
33. Doyle, J. & Shapiro, M. Flow response to large-scale topography: the Greenland tip jet. *Tellus Ser. A* **51,** 728–748 (1999).
34. Moore, G. W. K. & Renfrew, I. Tip jets and barrier winds: a QuikSCAT climatology of high wind speed events around Greenland. *J. Clim.* **18,** 3713–3725 (2005).
35. DuVivier, A. K. *et al.* Winter atmospheric buoyancy forcing and oceanic response during Strong Wind Events around Southeastern Greenland in the Regional Arctic System Model (RASM) for 1990–2010. *J. Clim* **29,** 975–994 (2016).
36. Nansen, F. Das Bodenwasser und die Abkühlung des Meeres. *Int. Rev. Hydrobiol.* **5,** 1–42 (1912).
37. Rhein, M. *et al.* Labrador Sea water: pathways, CFC inventory, and formation rates. *J. Phys. Oceanogr.* **32,** 648–665 (2002).
38. Rhein, M., Kieke, D. & Steinfeldt, R. Ventilation of the Upper Labrador Sea water, 2003–2005. *Geophys. Res. Lett.* **34,** L06603 (2007).
39. Gammon, R. H., Cline, J. & Wisegarver, D. Chlorofluoromethanes in the Northeast Pacific Ocean - measured vertical distributions and application as transient tracers of upper mixing. *J. Geophys. Res.* **87,** 9441–9454 (1982).
40. Oppo, D. W., McManus, J. F. & Cullen, J. L. Deepwater variability in the Holocene epoch. *Nature* **422,** 277 (2003).
41. Olsen, A. & Ninnemann, U. Large $\delta^{13}C$ Gradients in the preindustrial North Atlantic revealed. *Science* **330,** 658–659 (2010).
42. Hood, E. M., Sabine, C. L. & Sloyan, B. M. (eds). in *The GO-SHIP Repeat Hydrography Manual: A Collection of Expert Reports and Guidelines.* IOCCP Report Number 14, ICPO Publication Series Number 134. Available online at http://www.go-ship.org/HydroMan.html (2010).
43. Bullister, J. L. & Wisegarver, D. The shipboard analysis of trace levels of sulfur hexafluoride, chlorofluorocarbon-11 and chlorofluorocarbon-12 in seawater. *Deep-Sea Res. I* **55,** 10631074 (2008).
44. Stöven, T. & Tanhua, T. Ventilation of the Mediterranean Sea constrained by multiple transient tracer measurements. *Ocean Sci.* **10,** 439–457 (2014).
45. Warner, M. J. & Weiss, R. F. Solubilities of Chlorofluorocarbon-11 and Chlorofluorocarbon-12 in water and seawater. *Deep-Sea Res. A* **32,** 1485–1497 (1985).
46. Bullister, J. L., Wisegarver, D. P. & Menzia, F. A. The solubility of sulfur hexafluoride in water and seawater. *Deep-Sea Res. I* **49,** 175–187 (2002).
47. Weiss, R. F. The solubility of nitrogen, oxygen and argon in water and seawater. *Deep-Sea Res.* **17,** 721–735 (1970).
48. Bullister, J. *Atmospheric Histories (1765–2015) for CFC-11, CFC-12, CFC-113, CCl_4, SF_6 and N_2O* (Carbon Dioxide Information Analysis Center, Oak Ridge National Laboratory, US Department of Energy, Oak Ridge, Tennessee, 2015).
49. NOAA ESRL Global Monitoring Division. *Atmospheric Carbon Dioxide Dry Air Mole Fractions from quasi-continuous measurements at Mauna Loa, Hawaii.* Compiled by K.W. Thoning, D.R. Kitzis, and A. Crotwell (National Oceanic and Atmospheric Administration (NOAA), Earth System Research Laboratory (ESRL), Global Monitoring Division (GMD), 2015.
50. Lee, K. *et al.* Global relationships of total alkalinity with salinity and temperature in surface waters of the world's oceans. *Geophys. Res. Lett.* **33,** L19605 (2006).
51. Dickson, A. G., Sabine, C. L. & Christian, J. R. Guide to best practices for ocean CO_2 measurements. *PICES Spec. Publ* **3,** 191 (2007).

52. Mehrbach, C., Culberson, C. H., Hawley, J. E. & Pytkowicz, R. M. Measurement of the apparent dissociation constants of carbonic acid in seawater at atmospheric pressure. *Limnol. Oceanogr.* **18,** 897–907 (1973).
53. Dickson, A. G. & Millero, F. A comparison of the equilibrium constants for the dissociation of carbonic acid in seawater media. *Deep-Sea Res. I* **34,** 1733–1743 (1987).
54. Hurrell, J. Influence of variations in extratropical wintertime teleconnections on Northern Hemisphere temperature. *Geophys. Res. Lett.* **23,** 665–668 (1996).

Acknowledgements

The authors would like to thank the captain of G.O. SARS, John H. Johnsen, and his crew, and the scientists that took part in the cruise to the Irminger Sea, especially Kristin Jackson, Jörg Schwinger and Ailin Brakstad. Ulysses Ninnemann provided initial input on the paper. The European Centre for Medium-Range Weather Forecasts is acknowledged for access to the the ERA-Interim reanalysis. The Argo Program (part of the Global Ocean Observing System) is acknowledged for collecting data and making these freely available (http://www.argo.ucsd.edu). The 2016 AR7W data used in this work were collected in the 2016-006 cruise of the CCGS Hudson (2015006HUD) performed as a part of the Atlantic Zone Off-Shelf Monitoring Program (AZOMP) by Fisheries and Oceans Canada. The Meteor cruise data were retrieved from GLODAPv2. A.O and F.F appreciate funding from the SNACS project (229752), that is part of the KLIMAFORSK program of the Norwegian Research Council. E.J. and B.R. received funding from the NRC project VENTILATE (229791). Support for this work was provided by the European Union 7th Framework Programme (FP7 2007–2013) under Grant agreement no. 308299 NACLIM Project (K.V.). K.M. received funding from the Natural Sciences and Engineering Research Council of Canada. This is a contribution to the BIGCHANGE project of the Bjerknes Center for Climate Research.

Author contributions

F.F., A.O., E.J. and B.R. collected the 58GS20150410 data and I.Y. provided the 20152006HUD data. F.F. carried out all data analysis, apart from the atmospheric forcing, which was done by K.M. All authors jointly interpreted the results in this paper, which was mainly written by F.F. with contributions from A.O., K.V., I.Y. and K.M.

Additional information

Supplementary Information accompanies this paper at http://www.nature.com/naturecommunications

Competing financial interests: The authors declare no competing financial interests.

Reprints and permission information is available online at http://npg.nature.com/reprintsandpermissions/

How to cite this article: Fröb, F. *et al.* Irminger Sea deep convection injects oxygen and anthropogenic carbon to the ocean interior. *Nat. Commun.* **7,** 13244 doi: 10.1038/ncomms13244 (2016).

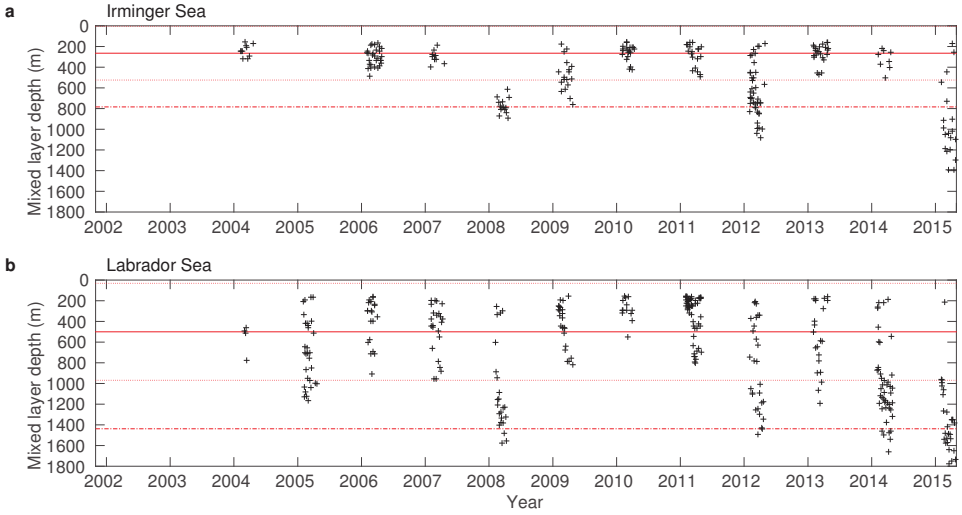

Supplementary Fig. 1: **Mixed layer depth Irminger Sea - Labrador Sea.** February-April mixed layer depth estimates within 80% of deepest recorded mixed layer depth for individual Argo floats for **a** the Irminger Sea and **b** the Labrador Sea (55.6-59 °N, 55-46°W) over 2002 to 2015. Mixed layer depths more shallow than 150 m were excluded. The solid red lines represent the mean mixed layer depth, red dotted lines ± one standard deviation and dashed-dotted lines two standard deviations. The largest deviation from the long-term mean is observed in the Irminger Sea in winter 2014-15.

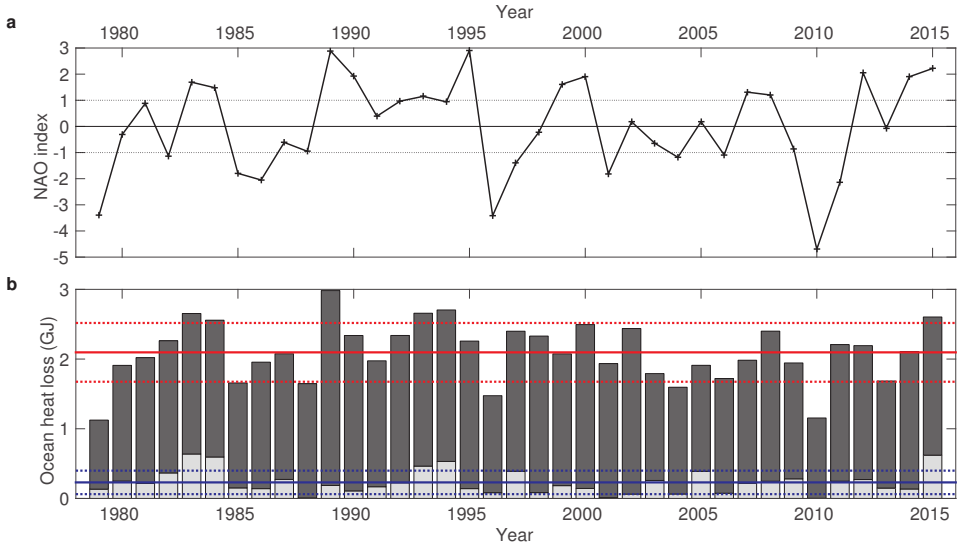

Supplementary Fig. 2: **NAO index and oceanic heat loss over the Irminger Sea. a,** December to February NAO index from 1979 to 2015 based on ERA-Interim reanalysis data. **b,** The winter mean ocean heat loss over the Irminger Sea from November to April from 1979 to 2015 based on ERA-Interim reanalysis data. The light grey shading indicates the heat loss associated with tip jet events. The red solid line is the mean ocean heat loss over 1979 to 2015, the red dotted lines represent ± one standard deviation. The blue solid line is the mean ocean heat loss associated with tip jet events over 1979 to 2015, the blue dotted lines represent ± one standard deviation.

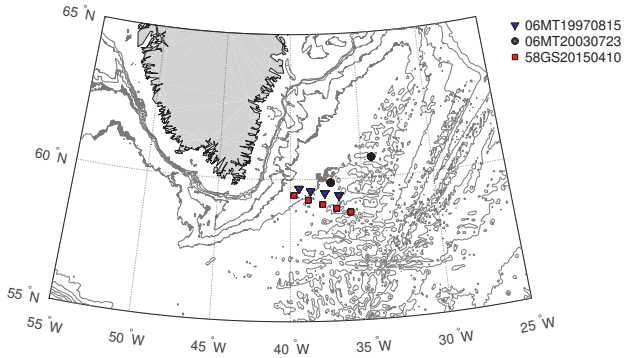

Supplementary Fig. 3: **Location of stations of cruise data.** Selected stations for Fig.4 for 06MT19970815, 06MT20030723 and 58GS20150410 cruise data in the Irminger Sea. Depth contours every 500 m are shown.

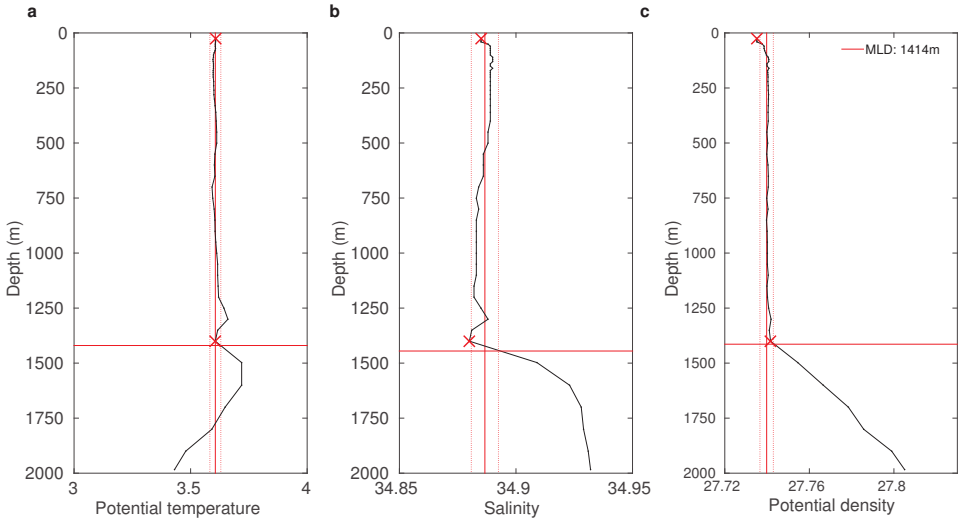

Supplementary Fig. 4: **Mixed layer depth estimates.** Mixed layer depth (MLD) determination for an example Argo profile of **a** potential temperature, **b** salinity and **c** potential density from April 16th, 2015 in the Irminger Sea region. The dotted red lines are the two-standard deviation envelope of the mean over the depth range indicated by the red crosses, close to the mixed layer depth. The intercept of original profile with two-standard deviation envelope marks the mixed layer depth.

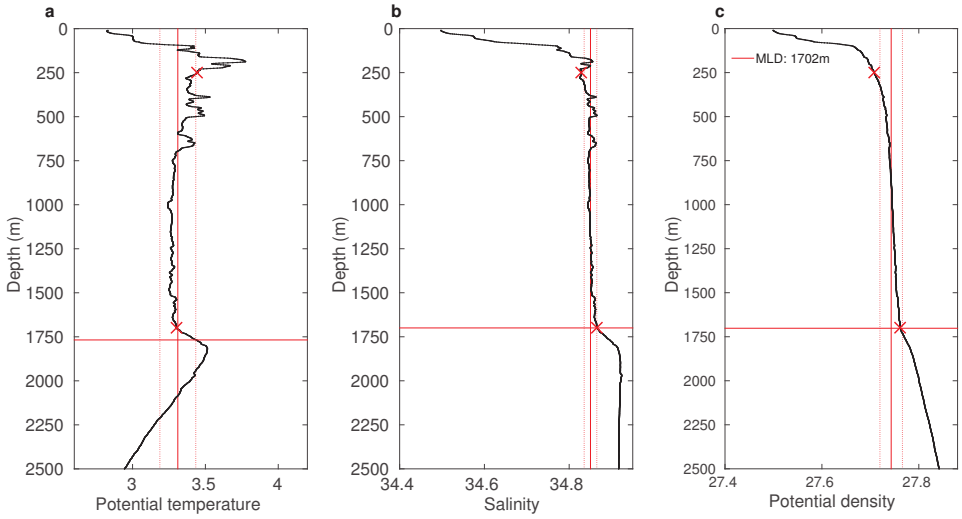

Supplementary Fig. 5: **Estimate of mixed layer depth isolated from the surface.** Mixed layer depth (MLD) determination for a mixed layer that is isolated from the surface for an example CTD profile of **a** potential temperature, **b** salinity and **c** potential density from May 13th, 2015 in the Labrador Sea. The dotted red lines are the two-standard deviation envelope of the mean over the depth range indicated by the red crosses, close to the mixed layer depth. The intercept of original profile with two-standard deviation envelope marks the mixed layer depth.

Paper II

6.2 Inorganic Carbon and Water Masses in the Irminger Sea since 1991

Fröb, F., A. Olsen, F.F. Pérez, M.I. García-Ibáñez, E. Jeansson, A. Omar, and S.K. Lauvset

Biogeosciences Discussions, **27** (2017)

II

Biogeosciences Discuss., doi:10.5194/bg-2017-27, 2017
Manuscript under review for journal Biogeosciences
This is just a preview and not the published paper.

Biogeosciences Discussions Open Access EGU

Inorganic Carbon and Water Masses in the Irminger Sea since 1991

Friederike Fröb[1,2], Are Olsen[1,2], Fiz F. Pérez[3], Maribel I. García-Ibáñez[4], Emil Jeansson[4], Abdirahman Omar[4], and Siv K. Lauvset[4]

[1]Geophysical Institute, University of Bergen, Bergen 5007, Norway.
[2]Bjerknes Centre for Climate Research, Bergen 5007, Norway.
[3]Instituto de Investigaciones Marinas (IIM-CSIC), Vigo 36208, Spain.
[4]Uni Research Climate, Bjerknes Centre for Climate Research, Bergen 5008, Norway.

Correspondence to: Friederike Fröb (friederike.frob@uib.no) and Are Olsen (are.olsen@uib.no)

Abstract.

The subpolar gyre region in the North Atlantic is a major sink for anthropogenic carbon. While the storage rates show large interannual variability related to atmospheric forcing, less is known about variability in the natural Dissolved Inorganic Carbon (DIC) and the combined impact of variations in the two components on the total DIC inventories. Here, data from 15 cruises in the Irminger Sea covering 1991-2015 were used to determine changes in total DIC and its natural and anthropogenic components in relation to the distribution and evolution of the main water masses. The inventory of DIC increased by 1.43±0.17 mol $m^{-2}yr^{-1}$ over the period, mainly driven by the increase in anthropogenic carbon (1.84±0.16 mol $m^{-2}yr^{-1}$), but partially offset by a loss of natural DIC (-0.57±0.22 mol $m^{-2}yr^{-1}$). Changes in the carbon storage rate can be driven by concentration changes in the water column, for example due to ageing of water masses, or by changes in the distribution of water masses with different concentrations, either by local formation or advection. A decomposition of the trends into their main drivers showed that variations of natural DIC inventories are mainly driven by changes in the layer thickness of the main water masses, while anthropogenic carbon is most affected by concentration changes. The storage rates of anthropogenic carbon are sensitive to data selection, while changes in DIC inventory show a robust signal on short timescales, associated with the strength of convection.

1 Introduction

Since the industrial revolution, atmospheric CO_2 levels have been increasing almost exponentially as a result of human activities such as fossil fuel burning, cement production, and land use changes. The global ocean has acted as strong sink for this anthropogenic CO_2 (Sabine et al., 2004) and is currently taking up approximately 25 % of the annual emissions (Le Quéré et al., 2016). While the ocean has capacity to store almost all of the anthropogenic CO_2 released to the atmosphere, the emissions currently outpace the oceanic absorption rates (Sabine and Tanhua, 2010). This is because the transport of anthropogenic CO_2 from the atmosphere into the ocean interior is limited by the rate of vertical exchange between the surface and deep ocean (Sarmiento and Gruber, 2002). Warming of the ocean will decrease this rate as a consequence of the increased stratification, and Earth System Models predict a decline in oceanic anthropogenic CO_2 uptake efficiency over the 21st century (Friedlingstein et al., 2006; Schwinger et al., 2014). Warming of the ocean will also affect CO_2 solubility, primary production

Biogeosciences Discuss., doi:10.5194/bg-2017-27, 2017
Manuscript under review for journal Biogeosciences
This is just a preview and not the published paper.

Biogeosciences Discussions Open Access EGU

and other factors governing the distribution and inventory of natural carbon in the ocean (Arora et al., 2013; Schwinger et al., 2014). It is important to constrain the magnitude of these feedbacks for policy planning, but current estimates vary significantly among models. Observational based quantitative and qualitative insight in carbon cycle climate interactions are important for the further improvement of projections of the future ocean carbon cycle.

Over the past three decades, ocean CO_2 chemistry data have been collected on a regular basis in the world's oceans. As the observational record extends, direct evidence of the climate sensitivity of the marine carbon cycle emerges. For example, the Southern Ocean carbon sink exhibits clear variations in response to atmospheric circulation patterns; the sink was weakening from the early 1980s to the early 2000s (Le Quéré et al., 2007), but has strengthened in the more recent decades (Landschützer et al., 2015). In the subarctic western North Pacific, measurements from 1992 to 2008 at the two time series stations KNOT and K2 reveal decadal trends in total dissolved inorganic carbon (DIC), related to alkalinity driven reductions in CO_2 outgassing (Wakita et al., 2010). In the Mediterranean Sea, changes in the large-scale circulation result in variability of the anthropogenic CO_2 concentration (Touratier and Goyet, 2009). Within the subpolar North Atlantic (SPNA), high-quality carbon data have been collected almost every second year since the early 1990s (Olsen et al., 2016), enabling the determination of subdecadal variability. This shows relationships between the anthropogenic CO_2 storage rate and the extent and intensity of ventilation processes, primarily driven by the North Atlantic Oscillation (NAO) (Pérez et al., 2010; Wanninkhof et al., 2010; Fröb et al., 2016; Woosley et al., 2016).

The SPNA is a key region for the storage and transport of CO_2 in the global ocean (Sabine et al., 2004). While a response of anthropogenic CO_2 storage to atmospheric forcing has been determined as mentioned above, less is known about variations in natural DIC, any relations to atmospheric forcing and relevance for total DIC inventories (Tanhua and Keeling, 2012). Here, we analyse changes in total DIC and its natural and anthropogenic components in the central SPNA, the Irminger Sea, in relation to the distribution and evolution of water masses over a 24-year period from 1991 to 2015, covering three periods of variable convective activity (Fröb et al., 2016).

2 Hydrographic setting

The Irminger Sea, a central sea in the SPNA (Fig. 1), is a climatically sensitive area with strong hydrographic contrasts. The SPNA circulation pattern has been extensively presented in the literature; here the description follows Lavender et al. (2005) and Våge et al. (2011). In the upper ocean, the East Greenland Current (EGC) carries cold and fresh water of Arctic origin southwards, in the west, close to the shelf of Greenland. In the east, the Irminger Current (IC) carries warm and salty water northwards along the Reykjanes Ridge. The salinity and temperature signature of these warm water masses is affected by the strength and shape of the subpolar gyre (SPG) (Häkkinen and Rhines , 2004; Hátún et al., 2005). South of the Denmark Strait, they largely recirculate to the south. In the centre of the cyclonic circulation of the Irminger Gyre, preconditioning conditions for convection are fulfilled (Marshall and Schott, 1999; Bacon et al., 2003; de Jong et al., 2012) and depending on heat loss,

Biogeosciences Discuss., doi:10.5194/bg-2017-27, 2017
Manuscript under review for journal Biogeosciences
This is just a preview and not the published paper.

Biogeosciences Discussions Open Access EGU

deep convection can occur (Pickart et al., 2003a; Våge et al., 2008, 2011; Fröb et al., 2016; de Jong and de Steur, 2016). The extent and strength of convective processes are mainly driven by the state of the NAO, which is the leading mode of atmospheric variability over the mid-North Atlantic (Curry et al., 1998; Hurrell and Deser, 2009).

At depth, the circulation in the Irminger Sea is mainly characterized by the Denmark Strait Overflow Water (DSOW) and the Iceland-Scotland Overflow Water (ISOW). DSOW, to the west, is a relatively recently ventilated water mass enriched in oxygen (O_2) as well as other dissolved atmospheric gases. It is composed of several water masses originating from the Arctic Ocean and the Nordic Seas (Tanhua et al., 2005; Jeansson et al., 2008). ISOW originates from intermediate waters of the Nordic Seas, which are modified as they flow through the Iceland Basin to the Irminger Sea (Hansen and Østerhus, 2000). In combination with ISOW and DSOW, Labrador Sea Water (LSW) forms North Atlantic Deep Water (NADW) (Dickson and Brown, 1994), the key component of the lower limb of the Atlantic Meridional Overturning Circulation. Two main LSW classes are identified in the SPNA: the $LSW_{1987-1994}$ and the LSW_{2000}. $LSW_{1987-1994}$, from now on called classical LSW (cLSW), is a dense, cold and relatively fresh water mass with high concentrations of dissolved atmospheric gases, formed by the recurring winter convection in the mid-1980s and mid-1990s in the Labrador and Irminger Seas (Lazier et al., 2002; Pickart et al., 2003b; Yashayaev et al., 2007). After 2000, the lighter LSW_{2000} or upper Labrador Sea Water (uLSW) has largely replaced cLSW (Yashayaev et al., 2007).

3 Data

Data from 15 cruises in the Irminger Sea covering 1991-2015 are used in this study (see Table 1). Data from the first 13 cruises were extracted from the GLODAPv2 data product, which provides bias-corrected, cruise-based, interior ocean data (Key et al., 2015; Olsen et al., 2016). The more recent data are from the 2012 OVIDE cruise (expocode: 29AH20120623) and the 2015 SNACS cruise (expocode: 58GS20150410). In order to minimize seasonal bias due to primary production, the upper 100 m of the water column are excluded from the inventory analysis. The region between 40.5° W and 31.5° W was covered by all 15 cruises.

All cruises intersect the ocean currents of the Irminger Sea described in the previous section. The cruises occupied either WOCE section A01/AR07E, the FOUREX or the OVIDE section, and locations are presented in Fig. 1. In order for the sections to be fully comparable, a coordinate transformation was performed for the 1997 FOUREX data. The latitude and longitude coordinates were rotated to the AR07E section using Cape Farewell as pivot point. Adjusting the distance between the stations ensured that the adjusted coordinates of the station over the Reykjanes Ridge on the FOUREX line matched the station over the Reykjanes Ridge on the AR07E line. The inventory estimates are sensitive to depth, therefore the pressure coordinates of all cruises were normalized. The location of every station for all cruises was mapped to the one arc-minute global relief model of the Earth's surface (Amante and Eakins, 2009) using a nearest-neighbour interpolation. The ratio between the bottom depth of this bathymetry and the reported cruise station bottom depth was multiplied with the pressure coordinates of each station. This

Biogeosciences Discuss., doi:10.5194/bg-2017-27, 2017
Manuscript under review for journal Biogeosciences
This is just a preview and not the published paper.

Biogeosciences Discussions Open Access EGU

normalization step mainly affected the adjusted FOUREX data, while for the other cruises the normalization changed sampling depths by less than 20 meters.

The accuracy of the GLODAPv2 data product is better than 0.005 in salinity, 1 % in O_2, 2 % in nitrate (NO_3), 2 % in silicate (SiO_2), 2 % in phosphate (PO_4), 4 μmol kg^{-1} in DIC and 6 μmol kg^{-1} in total alkalinity (A_T) (Olsen et al., 2016). For 29AH20120623, the overall accuracy of NO_3, PO_4 and SiO_2 was 1 %; the accuracy of DIC was 2 μmol kg^{-1} and for A_T it was 4 μmol kg^{-1} (Ríos et al., 2015; García-Ibáñez et al., 2016). For the SNACS cruise in 2015, pressure, conductivity, temperature and dissolved O_2 were directly measured with a Seabird 911+ CTD profiler. At every station, water samples were obtained at 12 depths using Niskin bottles, and used to calibrate the CTD measurements following the Global Ocean Ship-based Hydrographic Investigations Program (GOSHIP) calibration procedure (Hood et al., 2010). The accuracy of bottle salinities, analysed with a salinometer, was $\pm$0.003. The accuracy of O_2 concentration measured with Winkler titration using a potassium iodate solution as a standard was 0.2 μmol kg^{-1}. The precision was better than 2 % in PO_4, 1 % in SiO_2 and 1 % in NO_3 as evaluated using samples drawn from sets of Niskin bottles tripped at the same depth. DIC and A_T was measured according to Dickson et al. (2007), with an accuracy of 2 μmol kg^{-1} for both (Fröb et al., 2016).

The seawater CO_2 chemistry can be fully described if at least two of the four variables DIC, A_T, CO_2 partial pressure or pH are known. The measured variables at each of the 15 cruises are listed in Table 1. For six cruises, A_T and pH were measured, therefore DIC was calculated for these, using the dissociation constants of Lueker et al. (2000). For three cruises, only DIC was measured. For these, A_T was approximated using the salinity-alkalinity relationship for the North Atlantic of Lee et al. (2006). This relationship is defined for the surface ocean only, therefore its validity for the deep Irminger Sea was tested (Appendix A). The mean difference between approximated and the measured A_T data available was less than 5 μmol kg^{-1}; this is better than the target accuracy of A_T of the GLODAPv2 data product. No bias with depth or position was evident.

4 Method

The total DIC concentration is partitioned into its natural and anthropogenic components (DIC = DIC_{nat} + C_{ant}). The C_{ant} concentration was estimated with the φC_T^o method (see section 4.1). The DIC_{nat} concentration is the difference between DIC and C_{ant}. For all cruises, the column inventories were estimated for DIC, DIC_{nat} and C_{ant}. The inventories are sensitive to depth, therefore column inventories were only estimated for the part of the transect covered by all 15 cruises, between 40.5° W and 31.5° W. The column inventory is the concentration profile integrated over the entire water column (Tanhua and Keeling, 2012):

$$Inv_s = \int_0^z c_s * \varrho \, dz \quad (1)$$

Biogeosciences Discuss., doi:10.5194/bg-2017-27, 2017
Manuscript under review for journal Biogeosciences
This is just a preview and not the published paper.

Biogeosciences Discussions Open Access EGU

Here, Inv_s is the column inventory of any species s, c_s its concentration, ϱ the density at in situ temperature and pressure and z the depth of the water column. The storage rate is the slope of a linear least-squares regression over the mean column inventories with time. The standard error of the slope is the error of the storage rate. Changes in inventories can be caused by changes in the distribution of water masses with different species concentrations or by changes in species concentration within the water masses. The distribution of water masses was determined using an extended Optimum MultiParameter analysis (eOMP, see section 4.2). The change in concentration within each water mass was determined by applying the concept of water mass mixing averaged concentration, i.e. archetypal concentration (Álvarez-Salgado et al., 2013) (see section 4.2). Assuming linearity, the inventory changes can then be decomposed into contributions from changes in the archetypal concentration of the source water types (SWTs) and from changes in layer thickness of each water mass:

$$\frac{dInv_{tot}}{dt} = \sum_{WM} \left(\frac{\partial Inv}{\partial c}\frac{dc}{dt} + \frac{\partial Inv}{\partial z}\frac{dz}{dt} \right) \quad (2)$$

Here, $\frac{\partial Inv}{\partial c}\frac{dc}{dt}$ is the mean layer thicknesses with variable archetypal SWT concentrations, while $\frac{\partial Inv}{\partial z}\frac{dz}{dt}$ can be calculated as the mean archetypal SWT concentrations multiplied by the layer thickness changes over a specific time period. Hence, the two drivers for the observed inventory variability of total DIC and its natural and anthropogenic components can be identified.

4.1 Anthropogenic CO_2 calculation

The φC_T° method was applied to all cruises in the Irminger Sea to estimate C_{ant} concentrations (Pérez et al., 2008; Vázquez-Rodríguez et al., 2009, 2012). The φC_T° method is a back-calculation method that follows the same principles as the ΔC^* method of Gruber et al. (1996). In the φC_T° method, Cant is quantified as the difference between the preformed DIC at the time t and at preindustrial times (π): $C_{ant} = DIC^{\circ,t} - DIC^{\circ,\pi}$. $DIC^{\circ,t}$ is calculated by correcting the measured DIC for changes due to remineralisation of organic matter and $CaCO_3$ dissolution, while $DIC^{\circ,\pi}$ is quantified as the sum of the saturated DIC concentration with respect to the preindustrial atmosphere and the air-sea CO_2 disequilibrium (ΔC_{dis}). The major advantage of the φC_T° method over other back-calculation methods is that data for age tracers, such as chlorofluorocarbons (CFCs), are not needed. For A_T° and ΔC_{dis} the parametrizations developed by Vázquez-Rodríguez et al. (2012) were adopted. These were determined using data of the subsurface layer (100-200 m), which represents and preserves conditions during water mass formation (Vázquez-Rodríguez et al., 2012). The φC_T° method also takes any spatial and temporal variability of ΔC_{dis} into account. Further, the parametrized A_T° is corrected for effects of $CaCO_3$ dissolution changes and the sea surface temperature increase since preindustrial times. Overall, the uncertainty of φC_T° derived C_{ant} has been reported to be 5 μmol kg^{-1} (Vázquez-Rodríguez et al., 2009).

4.2 Extended Optimum MultiParameter Analysis (eOMP)

The Optimum MultiParameter (OMP) analysis (Tomczak and Large, 1989) is used to estimate the contribution of water masses, which are represented through SWTs, to each water parcel along the Irminger Sea sections. The OMP analysis assumes that all hydrographic parameters describing the water masses are affected by the same mixing processes. For each sampling point

Biogeosciences Discuss., doi:10.5194/bg-2017-27, 2017
Manuscript under review for journal Biogeosciences
This is just a preview and not the published paper.

Biogeosciences Discussions Open Access EGU

the contribution of the various water masses is quantified from an over-determined system of linear mixing equations, which is solved in a non-negative least square sense:

$$Gx - d = R \tag{3}$$

where G is the SWT matrix containing their properties, x the relative contributions of each SWT to the sample, d the observed data and R the residual. The OMP was further developed into the extended OMP (eOMP) analysis, which is used here, by Karstensen and Tomczak (1998) and Poole and Tomczak (1999). This accounts for the non-conservative behaviour of O_2 and nutrients by using Redfield ratios. In the eOMP, the remineralization of NO_3 and PO_4 is numerically related to an oxygen consumption rate, which, if multiplied with a pseudo-age, is similar to apparent oxygen utilization (AOU) (Poole and Tomczak, 1999). OMP and eOMP analyses have previously been used to describe in detail the origin, pathways and transformation of the main water masses in the SPNA (Tanhua et al., 2005; Álvarez et al., 2005; García-Ibáñez et al., 2015). Here, the SWT properties were defined based on the cruise data from 1991, assuming that the properties of the SWTs do not significantly change over time. The data for potential temperature (θ), salinity, O_2, NO_3, PO_4, SiO_2 and potential vorticity (PV) were used to characterize 11 SWTs that combined encompass the property features in the Irminger Sea (Fig. 2). The properties of the SWTs are provided in Table 2, including their standard deviations. These values were determined from the 10 % of data in the relevant density class that were closest to the property maximum or minimum used to delineate the SWT. For example, if a SWT was defined as a salinity minimum, all data points within a specific potential density (σ) range were sorted by salinity and the mean and standard deviation over the first 10 % of the data points, gave the salinity properties for that SWT. The approximate locations of all SWTs are shown in Fig. 3.

DSOW is the densest water mass in the Irminger Sea and defined as an O_2 maximum at σ_2 levels denser than 37.10 kg m^{-3} (Yashayaev et al., 2007). ISOW is defined as a salinity maximum between 36.89 and 37.10 kg m^{-3} (σ_2) and θ between 2.3 and 2.6° C. North East Atlantic Deep Water (NEADW) is formed by the entrainment of ISOW with surrounding waters, mainly deep water of Antarctic origin. In the North Atlantic two classes have been identified, upper and lower NEADW (uNEADW and lNEADW) (Castro et al., 1998), but in the Irminger Sea lNEADW is non-existent (McCartney, 1992), while uNEADW was identified as a maximum in SiO_2 below 2500 m. The mid-depth weakly stratified layer of cLSW in the Irminger Sea was identified by a PV and salinity minimum between 36.90 and 36.94 kg m^{-3} (σ_2). uLSW is less dense than cLSW due to its slightly different θ-salinity signature and was identified as a minimum in PV in the 36.81-36.87 kg m^{-3} σ_2 range.

The Icelandic Slope Water (IcSW), the Intermediate Water (IW), the Irminger Sea Water (ISW) and the uLSW are typically found at intermediate depths. IcSW is a warm and saline water mass, close the Reykjanes Ridge on the Iceland Slope (Tanhua et al., 2005; Yashayaev et al., 2007). Here, IcSW was defined by a minimum in O_2, occupying the 36.80-36.86 kg m^{-3} σ_2 range, effectively separating uLSW and cLSW. IW is a saline water mass, depleted in O_2, and of southern origin (Sarafanov et al., 2008). IW was identified by O_2 values below 250 μmol kg^{-1} at σ_0 between 27.45 and 27.65 kg m^{-3}. ISW

Biogeosciences Discuss., doi:10.5194/bg-2017-27, 2017
Manuscript under review for journal Biogeosciences
This is just a preview and not the published paper.

Biogeosciences Discussions Open Access EGU

is fresh, elevated in O_2, and found between 4 and 5° C.

Finally the Subpolar Mode Water (SPMW), the Subarctic Intermediate Water (SAIW) and the North Atlantic Central Water (NACW) are all typically found in the upper Irminger Sea. SPMW is oxygenated and of subpolar origin. It was defined as a salinity maximum in the 7-8° C θ range. SAIW is a salinity minimum in the 6.5-7.5° C θ range. NACW was defined as the salinity maximum for θ above 9° C.

The seven hydrographic parameters, describing the SWTs, limit the number of SWTs included in one eOMP analysis to a maximum of seven. In addition, the requiered mass conservation over-determines the system of linear equations. Therefore, the Irminger Sea was divided into four regions and for each data point in each region, an eOMP analysis was carried out with a subset of the 11 SWTs. In the deep ocean ($\sigma_0 \geq$ 27.76 kg m^{-3}), SWTs were limited to DSOW, ISOW, uNEADW, cLSW and IcSW. In the intermediate ocean (27.61 $\leq \sigma_0 <$ 27.76 kg m^{-3}), only ISW, IW, IcSW, uLSW and cLSW were included. The upper ocean ($\sigma_0 <$ 27.61 kg m^{-3}) was split into two basins: east of Reykjanes Ridge (NACW, SPMW, IW and SAIW) and west of the Reykjanes Ridge (ISW, SPMW, IW and SAIW). The data presented in Fig. 2 are classified according to these 'mixing figures'. The equations were normalized and weighted, accounting for differences in measurement accuracies and potential environmental variability. Weights were assigned according to the variability and accuracy of the parameters following García-Ibáñez et al. (2015). The highest weight was assigned to mass to ensure its conservation. The second highest weights were assigned to θ and salinity, because they are the most accurate. PV was weighted high as well due to its good accuracy and to enable resolution of both LSW classes. The eOMP results in a ratio r_{ij}, this describes the contribution of each SWT to each data point in space and time.

For reasons of simplicity, the number of SWTs were reduced from 11 to 9, by performing composite analyses for uNEADW and IcSW. The uNEADW was determined to be a composite of 26 % ISOW, 14 % LSW, 58 % lNEADW and 2 % Mediterranean Water (MW), based on salinity, θ and SiO_2 following (van Aken, 2000). Properties for the SWTs representing lNEADW and MW were taken from García-Ibáñez et al. (2015). A decomposition based on salinity and θ showed that IcSW is a composite of 30 % ISOW, 20 % cLSW and 50 % IW.

In order to determine the SWT concentrations of DIC, DIC$_{nat}$ and C$_{ant}$, the mixing-weighted concentration or archetypal concentration, C_i, of these species was calculated for each SWT, i (Álvarez-Salgado et al., 2013):

$$C_i = \frac{\sum_j r_{ij} \times C_j}{\sum_j r_{ij}} \quad (4)$$

Biogeosciences Discuss., doi:10.5194/bg-2017-27, 2017
Manuscript under review for journal Biogeosciences
This is just a preview and not the published paper.

Biogeosciences Discussions Open Access EGU

Here, the concentration in each sampling point j, C_j, is multiplied with the ratio of the SWT in that point r_{ij}. When summed over all points and divided by the total fraction the SWT occupies, this estimates C_i. Further, the layer thickness, Th, of each SWT at each station is estimated according to:

$$Th_{ik} = \frac{\sum_j r_{ij}}{n_k} \times d_{k,max} \quad (5)$$

Here, the sum of the fractions over all sampling point divided by the number of sampling points at each station, n_k, and multiplied by its bottom depth, $d_{k,max}$, gives the layer thickness per station for each SWT. The mean over all stations of the Irminger Sea transect is the mean layer thickness.

4.3 Uncertainty analysis

Uncertainties for the distribution of water masses result from measurement uncertainties and errors of the eOMP analysis. Here, the largest source of errors is the definition of the SWTs. The SWT matrix needs to represent the known features of the circulation (Tanhua et al., 2005), but temporal shifts in SWT characteristics cannot be accounted for with the eOMP analysis. A measure of uncertainty is given by the difference between measured and eOMP calculated values, the residual R in Eq. (3). The total residual, calculated by taking the square of the largest parameter residual at each sampling point (García-Ibáñez et al., 2015), and the individual parameter residuals are shown in Fig. 4. Below 1200 m, the total residual is close to zero, as are the residuals of θ, salinity and O_2. In the intermediate and surface ocean these residuals increase, in particular for O_2, which might be a consequence of gas exchange. The residuals of PO_4, NO_3 and SiO_2 are larger, as expected due to their lower weights in the eOMP, and do not show any trend with depth. The mean error for each parameter is listed in Table 2. These are of similar magnitude as the errors determined for the Irminger Sea eOMP analysis by Tanhua et al. (2005).

In order to test how robust the results of the eOMP analysis are, a Monte-Carlo simulation was performed (Tanhua et al., 2005). The properties of the SWT matrix were randomly perturbed, within the standard deviation of each parameter. 100 of such perturbed SWT matrices were created and the eOMP was solved for each perturbed system. This allows for quantification of the sensitivity of the eOMP to potential temporal variations of the SWT properties. The standard deviation of the mean SWT contribution over all 100 perturbations is shown in the last column of Table 2. The uncertainties are generally low, hence the robustness of the eOMP analysis is high.

The layer thickness uncertainties were estimated by scaling the averaged standard deviation of each SWT, which were quantified with the Monte-Carlo simulation, to the width and depth of the Irminger Sea. The uncertainty of C_{ant} concentrations is 5 μmol kg^{-1}, for DIC and for DIC_{nat} it is 4 μmol kg^{-1}. Errors for the inventories were estimated by propagating the uncertainties of the layer thicknesses and the concentrations through the water column.

Biogeosciences Discuss., doi:10.5194/bg-2017-27, 2017
Manuscript under review for journal Biogeosciences
This is just a preview and not the published paper.

Biogeosciences Discussions Open Access EGU

5 Results

Over the 24-year period considered here, the frequency and the amplitude of the mean-winter NAO changed significantly (Hurrell and Deser, 2009). The convection in the SPG during winter, which is driven by the large-scale atmospheric circulation (Lazier et al., 2002; Pickart et al., 2003b; Yashayaev et al., 2007), has varied in strength and extent accordingly. Three distinctive time periods can be characterized from 1991 to 2015 by different levels of convective activity in the Irminger Sea. In the first period, from 1991 to 1997, several consecutive positive NAO winters led to extensive deep convection in the entire SPG (Pickart et al., 2003a, b). In the second period, from 2000 to 2007, the NAO was in a more neutral state and only shallow convection occurred in the Irminger Sea. In the third period from 2008 to 2015, three deep convective events took place in the Irminger Sea, in 2008, 2012 and 2015 (Våge et al., 2008; de Jong et al., 2012; Fröb et al., 2016; de Jong and de Steur, 2016). The DIC, DIC_{nat} and C_{ant} inventory changes are presented with respect to these three periods and for the entire 24 years of observations in the following sections.

The temporal change in DIC, DIC_{nat} and C_{ant} concentration in the Irminger Sea is clearly visible in Fig. 5, which shows interpolated cruise station data for 1991, 1997, 2007 and 2015, start and end years of the three periods considered here. The increase in DIC is evident throughout the basin. From 1991-1997, cLSW with a low DIC-signature dominates the basin, but a tongue of older IW over the Reykjanes Ridge transports relatively high DIC concentrations into the Irminger Sea. By 2015 the DIC concentration had increased by at least 10 μmol kg^{-1} compared to 1991, as visualized by the disappearance of the 2150 μmol kg^{-1} contour line (Fig. 5a). Temporal changes in DIC_{nat} concentration (Fig. 5b) are small compared to those in DIC and less systematic. The C_{ant} concentration increases over time, not only at the surface, but over the entire water column, which is indicated by the disappearance of the 20 μmol kg^{-1} contour line below 1500 m from 1991 to 2015 (Fig. 5c).

The column inventory time series of DIC, DIC_{nat} and C_{ant}, shown in Fig. 6, quantifies this large temporal change in the Irminger Sea sections. Typically, the DIC inventory increased by 1.43±0.17 mol m^{-2}yr^{-1}, from 1991 to 2015, from approximately 5645 to 5685 mol m^{-2}. The C_{ant} storage rate was 1.84±0.16 mol m^{-2}yr^{-1} in the same time period, this is larger than the rate of DIC inventory change. At the same time, the DIC_{nat} inventory decreased at a rate of -0.57±0.22 mol m^{-2}yr^{-1}. Therefore, the annual change in the DIC inventory is mainly driven by the large C_{ant} storage rate, but partially offset by the loss in DIC_{nat} inventory. The variability of the DIC and C_{ant} inventories over the 24-year period is of similar magnitude, as indicated by the error of the slope in Fig. 6, whereas the DIC_{nat} inventory varies slightly more. It is notable that the C_{ant} inventory increased sharply from 2012 to 2015, while there was a comparably large decline in the DIC_{nat} inventory. This is not an artefact of the method, but can be explained by the fact that the 2015 data were obtained during active convection in the Irminger Sea (Fröb et al., 2016). In contrast to that, the peak in 2005 in the C_{ant} inventory cannot be explained by a similar mechanism, therefore it is unlikely a real signal but rather might reflect the true error or reveal measurement bias.

Biogeosciences Discuss., doi:10.5194/bg-2017-27, 2017
Manuscript under review for journal Biogeosciences
This is just a preview and not the published paper.

Biogeosciences Discussions Open Access EGU

5.1 SWT distribution

The layer thickness of the Irminger Sea SWTs from 1991 to 2015 is presented in Fig. 7. Because their individual contributions are small, the upper ocean SWTs, i.e. NACW, ISW, and SPMW, are combined and titled upper waters (UW). Based on the composite analysis, the contributions of uNEADW and IcSW are divided up and added to cLSW, IW and ISOW. MW and lNEADW only appear in the Iceland Basin and are not included for further analysis. Therefore, not all 11 SWTs used for the eOMP analysis are shown, but only UW, IW, uLSW, cLSW, DSOW and ISOW. Since the FOUREX section, occupied in 1997, was located further south than the AR07E section, covered that year by 06MT19970707, the SWT distribution differs slightly between the two cruises. At the FOUREX section, the ISOW layer is on average 50 m and the SAIW layer about 15 m thicker than further north, while the ISW layer is about 47 m and the SPMW layer 19 m thicker for 06MT19970707 than at the FOUREX section. For the other SWTs, differences are smaller than 8 m. Relatively speaking, 50 m is less than 2 % of the entire water column, so that the discrepancy between the two cruises is small compared to the mean depth of the Irminger Sea.

The distribution of SWTs in the Irminger Sea, as shown in Fig. 7, changes substantially from 1991 to 2015. The overall trend is indicated, but the rates of change are often larger, if sub-periods are considered. For example, the IW layer thickens slightly from 1991 to 2015 at a rate of 6.5±2.0 m yr^{-1}, but there is little change before 2004, while after, the layer thickness increase is much stronger. The uLSW layer thickness increases by an average of 24.1±8.7 m yr^{-1}, but it is very thin before 1997 and the major build up occurs after 2004. In particular, after deep convection in the Irminger Sea in 2008, 2012 and 2015, the layer thickness of uLSW increases substantially. The cLSW layer shows the largest changes in thickness at a loss rate of -54.0±4.3 m yr^{-1} from 1991 to 2015. The convective activity in the SPG in 1991 to 1997 lead to extensive production of cLSW. After that, the cLSW layer was not renewed and strongly diminished until 2015. In contrast to that, the DSOW layer decreases only little in thickness over the 24-year period covered by the data. The ISOW layer thins by -9.9±3.1 m yr^{-1}. Over the entire period from 1991 to 2015 the UW layer thickness increases at a rate of 26.2±4.8 m yr^{-1}, but it has essentially a constant thickness from 1991 to 2000, then thickens until 2007 and decreases in thickness after that. Overall, the change of the distribution of the main SWTs is well captured by the eOMP analysis. Especially the transformation of the two LSW classes seems to match the observations well (Yashayaev et al., 2007).

The mean layer thickness for each SWT in the time periods considered here are summarized in Table 3. The main variability in the distribution of water masses is created by layer thickness changes of cLSW, uLSW and UW. With only small changes over the 24-year period, DSOW, ISOW and IW occupy a little more than a third of the Irminger Sea sections. In the mid-1990s, the cLSW layer occupied close to 50 % of the entire water column, which left thin uLSW and UW layers, corresponding to less than 7 % and around 8 %, respectively, of the entire water column. As cLSW was advected out of the Irminger Sea, while not being re-formed by convection, that layer was replaced mainly by UW in the early 2000s. In 2004, cLSW occupied 37 % of the water column and UW 24 %, while the uLSW layer only accounted for 4 %. With the recurring convection events between 2008 and 2015, uLSW was formed more frequently while displacing UW as well as the remainder of the cLSW layer.

Biogeosciences Discuss., doi:10.5194/bg-2017-27, 2017
Manuscript under review for journal Biogeosciences
This is just a preview and not the published paper.

Biogeosciences Discussions Open Access EGU

The measurements from winter 2015 reveal that by then the fraction of cLSW was as low as 17 %, and that of UW only 5 %, but that uLSW occupied 45 % of the entire water column.

5.2 Archetypal concentration changes

Within the SWTs, the archetypal concentrations of carbon species change over time due to e.g. remineralization of organic matter, which add DIC_{nat}, or air-sea gas exchange, which increases C_{ant} in water masses that are in contact with the atmosphere. The archetypal concentrations of DIC, DIC_{nat} and C_{ant} from 1991 to 2015 are shown in Fig. 8, for the same SWTs as in Fig. 7, and are also summarized in Table 3. In all SWTs, DIC is similar, except for UW, which have a more variable DIC that is generally lower compared to all other SWTs. The older SWTs in the deep ocean have higher DIC_{nat} concentrations and lower C_{ant} concentrations compared to SWTs that have been ventilated more recently. Therefore, the deep SWTs, namely ISOW and DSOW, have the highest archetypal concentrations of DIC_{nat} (both 2136 μmol kg^{-1}) and the lowest archetypal concentrations of C_{ant} (22 μmol kg^{-1} and 20 μmol kg^{-1}), respectively. In contrast, UW have the lowest archetypal concentrations of DIC_{nat} (2112 μmol kg^{-1}) and the highest archetypal concentrations of C_{ant} (40 μmol kg^{-1}), which are almost twice as high as in the deep SWTs.

For all SWTs, the rate of change in the archetypal DIC concentration is similar, except for ISOW, where it is slightly smaller. The archetypal concentration change over time for DIC_{nat} is not statistically different from zero for most SWTs, apart from cLSW, where the DIC_{nat} concentration increases by 0.30$\pm$0.06 μmol kg^{-1}yr^{-1}. In contrast, the archetypal C_{ant} concentration increases significantly in all SWTs over time. Further, the increase rate of the archetypal DIC concentration is not statistically different from the rate of increase of the archetypal C_{ant} concentration. This indicates that the increase in DIC can be explained by the input of C_{ant} to the entire water column. This is true for all SWTs, except cLSW. For this water mass the increase in the archetypal C_{ant} concentration contributes by 0.31$\pm$0.07 μmol kg^{-1}yr^{-1} to the increase in DIC, which is only half of the DIC concentration increase. This is because DIC_{nat} accumulates as cLSW ages, while at the same time, a smaller fraction of C_{ant} is added to this water mass due to less frequent ventilation.

5.3 DIC storage rate decomposition

The decomposition of the inventory rates of change reveals the contribution of changes in the SWT distribution and of changes in the concentration within these SWTs to the trends in DIC and its natural and anthropogenic components. Figure 9 summarizes the storage rates of DIC, DIC_{nat} and C_{ant} over the entire 24-year time period and for the periods 1991-1997, 2000-2007 and 2008-2015. The first bar shows the total storage rate summed over all SWTs. The second bar shows the concentration driven storage rate and the third bar the layer thickness-driven storage rate. In theory, the first bar should be the sum of the last two bars. However, since the storage rates have been calculated using a linear regression over only a small number of data points, the residuals can become quite large, this is especially the case for the shorter time periods. Nevertheless, some conclusions can be drawn. The increase of the DIC inventory from 1991 to 2015 is driven by the increase in the C_{ant} inventory, partially offset by a decrease in DIC_{nat} inventory. The rise in the C_{ant} inventory is primarily due to a rise in C_{ant} concentration, but the

Biogeosciences Discuss., doi:10.5194/bg-2017-27, 2017
Manuscript under review for journal Biogeosciences
This is just a preview and not the published paper.

Biogeosciences Discussions Open Access EGU

contribution from layer thickness-driven changes is also significantly positive (Fig. 9a). While the rise in C_{ant} concentration occurs in all SWTs (Fig. 8), the contribution from the latter factor appears mostly driven by the increase in the thickness of uLSW (Fig. 7), which is rich in C_{ant} (Fig. 8). The decrease in the DIC_{nat} inventory is the result of the layer thickness-driven reduction, which is larger than the concentration driven increase (Fig. 9a). This can be attributed to the replacement of cLSW with uLSW and UW, which both have lower concentrations of DIC_{nat}.

The variations at subdecadal timescales can be understood in terms of the convective activity in the Irminger Sea, although with larger uncertainty. Figure 9b shows the decomposed trends from 1991-1997, a period when convective activity was high in the SPG. The total DIC storage rate is driven by the C_{ant} storage rate, while the changes in the DIC_{nat} inventory are not significantly different from zero. The C_{ant} storage rate is mainly driven by increasing concentrations, which occur in all SWTs (Fig. 8).

From 2000-2007, although the C_{ant} storage rate of 2.14±0.49 mol $m^{-2}yr^{-1}$ was similar to that of the preceding period, the DIC storage rate was much smaller because of the large loss of DIC_{nat}. 2000-2007 has smallest DIC storage rate of all periods considered, 0.65±0.39 mol $m^{-2}yr^{-1}$, compared to 2.53±1.24 and 1.93±0.20 mol $m^{-2}yr^{-1}$ for the earlier and later periods, respectively. Also, unlike the other periods, changes in layer thickness and concentrations were almost equally important for the C_{ant} storage rate. The DIC_{nat} storage rate, on the other hand, was almost entirely driven by changes in layer thickness: -1.20±0.29 mol $m^{-2}yr^{-1}$ of a total of -1.63±0.98 mol $m^{-2}yr^{-1}$. From Fig. 7 and Fig. 8 these features appear to be the result of uLSW and UW replacing cLSW. Their larger concentrations of C_{ant} leads to the relatively large layer thickness-driven storage increase, while the advection of DIC_{nat}-rich cLSW out of the Irminger Sea leads to the negative layer thickness-driven decrease of the DIC_{nat} inventory. The negative concentration-driven storage rate appears primarily driven by the loss of DIC_{nat} from uLSW and UW, outweighing the increase of DIC_{nat} in the cLSW.

For the last period from 2008-2015 (Fig. 9d), the deep convection in 2015 had a large impact on all storage rates, as well as their uncertainty estimates, i.e. the exceptional changes in 2015 incurs a large uncertainty on the regression slopes for this time period. The DIC storage rate is 1.93±0.20 mol $m^{-2}yr^{-1}$ and the result of a large C_{ant} storage rate, the largest in all three periods considered, offset by a negative DIC_{nat} storage rate. Both of these are primarily the result of changes in concentrations, indicative of the ventilation that occurred. As evaluated from Fig. 8, the C_{ant} increase is greatest in IW, uLSW and UW, while the loss of DIC_{nat} occurred primarily in the IW and uLSW. However, also cLSW appears to be affected by the most recent event in 2015.

6 Discussion

The data that have been collected in the Irminger Sea over the past decades provide unequivocal evidence for climate forcing of the carbon cycle in this oceanic region. Over long time scales, the steady trend due to uptake of anthropogenic CO_2 clearly

Biogeosciences Discuss., doi:10.5194/bg-2017-27, 2017
Manuscript under review for journal Biogeosciences
This is just a preview and not the published paper.

Biogeosciences Discussions Open Access EGU

dominates, but at shorter time scales, it varies and can also be significantly masked by variability of DIC_{nat}. In particular, this was the case in the period from 2000 to 2007, when the negative DIC_{nat} storage rate partially offset the increasing C_{ant} storage, resulting in a DIC storage rate that was only about a third of the storage rates in the preceding and later time periods considered here. In that period when convection was shallow, the replacement of relatively DIC_{nat} rich cLSW with relatively DIC_{nat}-poor UW and uLSW led to the loss of DIC_{nat}. Ageing might have increased the DIC_{nat} concentration, but the water masses in which these processes occur were flushed out the study area. Climate feedback mechanisms that involve natural carbon cycling in the ocean are relevant to elucidate. While for example Zunino et al. (2015) found steady-state conditions for the natural carbon cycle in the entire eastern SPNA between 2002 and 2010, this was not the case for the Irminger Sea from 1991-2015. A possible explanation for this discrepancy could be the longer time period considered here, or that if both the Irminger Sea and the Iceland Basin are regarded, inventory changes might cancel each other out. This was shown to be the case for C_{ant} by Steinfeldt et al. (2009), as a consequence of opposite changes in cLSW volume east and west of the Reykjanes Ridge.

The results presented here do not indicate a consistent response in the storage rates for anthropogenic CO_2 to the NAO. The storage rates were similar for the first two periods, with predominantly high and low values of the NAO index, while it was clearly larger for the last period, with predominantly high NAO index. In that time period, the C_{ant} storage rate increased by a factor of 1.6 compared to the period from 2000 to 2007 (Fig. 9). The lack of change in C_{ant} storage rates between the two first periods, contrasts with the results of Pérez et al. (2008), who found that the storage rates were low from 1997-2006. This is a result of the differences in data: when using the same cruises and the same periods of time (i.e 1997-2006 for the middle period) as in Pérez et al. (2008) to estimate C_{ant} storage rates, we estimated a significant decline in C_{ant} storage rates for the middle period compared to the first (C_{ant} storage rates: 2.78$\pm$0.28 mol $m^{-2}yr^{-1}$ for 1991-1997: 1.06 pm0.47 mol $m^{-2}yr^{-1}$ for 1997-2006).

The DIC storage, on the other hand, do show a consistent response to the NAO index, it is larger in the periods with predominantly high NAO index winters (the first and the last) than in the middle period, with a predominance of low NAO index winters. This response was also found when using the same cruises and time periods as Pérez et al. (2008) to calculate the storage rates. Altogether, this shows that while calculation of C_{ant} storage rates over small time periods is sensitive to data selection, calculation of DIC storage rates is not. This is not unreasonable, as estimates of C_{ant} inventories involves more variables (for example AOU and alkalinity), which increases the risk of introducing sampling or measurement biases. Regardless, convective events increase the storage of C_{ant}, this is clearly demonstrated for the 2015 event, also presented in detail by Fröb et al. (2016), who also used an independent approach for estimating C_{ant}. Most likely because the thick layer of C_{ant} rich cLSW was mostly established in 1991 when the first data were collected, no large storage rate is observed for the early NAO positive period included here (Yashayaev et al., 2007).

Biogeosciences Discuss., doi:10.5194/bg-2017-27, 2017
Manuscript under review for journal Biogeosciences
This is just a preview and not the published paper.

Biogeosciences Discussions Open Access EGU

Tanhua and Keeling (2012) calculated North Atlantic column inventory changes of DIC using data extracted from GLODAPv1 (Key et al., 2004) and CARINA (Key et al., 2010). For obtaining further insight on the governing processes, they also included O_2, AOU and DIC_{abio}, which is DIC corrected for the fraction of remineralised carbon and is closely related to anthropogenic carbon. However, their inventories were only estimated over the upper 2000 m of the water column. For DIC, the storage rate in the Labrador and Irminger Seas combined was estimated to be 0.57 mol $m^{-2}yr^{-1}$ (Tanhua and Keeling, 2012). This is only a third of our estimates of 1.43±0.17 mol $m^{-2}yr^{-1}$. This difference is likely the result of the different depth ranges, region and time periods evaluated. It is, however, noteworthy, that the DIC_{abio} storage rate calculated by Tanhua and Keeling (2012) is not significantly different from zero. The entire increase in DIC inventory is explained by an increase of the remineralised fraction, as determined from AOU and their assumed C:O ratio. This implies either that there is no storage of C_{ant} in the region or that any increase in C_{ant} is completely offset by reduced CO_2 solubility.

In order to compare to the Tanhua and Keeling (2012) results here, the DIC_{abio} storage rates as well as O_2 and AOU storage rates are shown in Fig. 10 for the same periods as in Fig. 9. For the Irminger Sea cruise data from 1991-2015, the DIC_{abio} storage rate is 1.40±0.17 mol $m^{-2}yr^{-1}$, and explains the DIC storage rate almost entirely. The negligible trend in AOU explains the lack of difference between the DIC and DIC_{abio} storage rates. The estimated DIC_{abio} storage rate is lower than the C_{ant} storage rate (1.92±0.17 mol $m^{-2}yr^{-1}$, Fig. 6), probably due to a decline in preformed DIC values, i.e. a loss of solubility as a consequence of the positive surface temperature trends in the Irminger Sea from 1991-2015 (Stendardo and Gruber, 2012; Maze et al., 2012). The long-term warming trends in the surface ocean and thus the decreasing O_2 solubility leads to a deoxygenation of -0.8±0.3 mol $m^{-2}yr^{-1}$ over the 24-year period, which is consistent with the suggested loss in preformed DIC.

On shorter timescales (Fig. 10b-c) all variables show large variations in the storage rates consistent with the already discussed changes in hydrography. In contrast to the findings of Tanhua and Keeling (2012), DIC and DIC_{abio} storage rates are positive over all time periods. This might be partly due to the increased data coverage in our study. Over the entire time period, DIC_{abio} underestimates C_{ant} by about 25%. However, if the time period is too short, DIC_{abio} becomes much more variable, because it includes solubility effects. For example, from 2000-2007, the DIC_{abio} underestimates the C_{ant} storage rate by 40 %, (compare Fig. 9c and 10c), while from 2008-2015, the DIC_{abio} overestimates the C_{ant} storage rate by 20 % (compare Fig. 9d and 10d).

Similar to the C_{ant} storage rates, both periods before and after 1997 show a loss in O_2, despite stronger convection in the early 1990s. Again, this is attributed to the fact that cLSW was mostly formed before 1991 (Yashayaev et al., 2007). The mean O_2 saturation degree over the entire water column was 89 % in the period from 1991 to 1997, which resulted in a high O_2 inventory of 750±4 mol m^{-2}, indicative of the recent ventilation. After 1997, no re-ventilation took place and the mean O_2 saturation dropped 2 %, while the inventory decreased to 732±4 mol m^{-2}. From 2008 to 2015, the O_2 saturation values increased to 89 % again due to the strong inventory increase of 4.3±2.6 mol $m^{-2}yr^{-1}$, which was mainly driven by the deep

Biogeosciences Discuss., doi:10.5194/bg-2017-27, 2017
Manuscript under review for journal Biogeosciences
This is just a preview and not the published paper.

Biogeosciences Discussions Open Access EGU

convection in 2015 (Fröb et al., 2016). In fact, the convection in 2015 was strong enough to restore the O_2 inventory levels so that the mean inventory from 2008 to 2015 was 749±4 mol m^{-2}, the level of the well-ventilated early 1990s.

7 Conclusions

The repeat observations within the Irminger Sea show significant changes in total, natural and anthropogenic CO_2 inventories from 1991 to 2015 with large interannual variability in the natural component. The eOMP method results and the decomposition of the inventory changes give valuable insight into the driving mechanisms to interpret the observed variability. Overall, changes in layer thickness of the main water masses appear most important for the DIC_{nat} inventory, while concentration change within these water masses is the key factor for C_{ant}. C_{ant} is typically more important for changes in total DIC inventories than DIC_{nat}. While the DIC inventory changes show a clear signal associated to the NAO, for C_{ant} the signal is less robust, especially before and after 1997, likely because the data used here does not cover the period before 1991, when the thick layer of cLSW was formed. From 1991 to 2015 the mean C_{ant} saturation over the entire water column increased from 52 % to 67 %, increasing the C_{ant} inventory from 53±3 mol m^{-2} to 117±3 mol m^{-2}, mainly driven by the most recent convection in 2015. Despite the negative trend in O_2 inventory from 1991 to 2015, the convection in 2015 was strong enough to replenish O_2 levels at depth, leading to a mean saturation of 89 % and an O_2 inventory of 749±4 mol m^{-2}, which was as high as in 1991. C_{ant} is sensitive to time period considered, while DIC appears more robust to sampling and measurement bias. Therefore, for a comprehensive view on carbon cycle feedback mechanisms, not only C_{ant}, but also natural and total DIC should be taken into account.

Appendix A: Salinity - Alkalinity relationship

The application of the surface relationship between salinity, temperature and A_T by Lee et al. (2006) is tested for Irminger Sea cruise data in the entire water column. Further, the linear relationship between salinity and A_T by Nondal et al. (2009) is applied as well and compared to the Lee et al. (2006) relationship. For all cruise data between 1991 and 2015, the difference between measured and calculated A_T is presented in Fig. A1. Both relationships perform reasonably well. For the Lee et al. (2006) relationship there is no bias with depth, but measured A_T is slightly overestimated. The Nondal et al. (2009) relationship tends to overestimate the measured A_T in the surface ocean and underestimate measured A_T below 2000 m. Therefore the variance of the Nondal et al. (2009) relationship is much larger than for the Lee et al. (2006) relationship. Within this study, the Lee et al. (2006) relationship was chosen in order to calculate A_T.

Further, the impact of the overestimated calculated A_T on C_{ant}, DIC_{nat} and DIC storage rates was tested. For that, 4.5 μmol kg^{-1}, which was the mean difference between measured and calculated A_T based on the Lee et al. (2006) relationship, were added to the calculated A_T for the 3 cruises, where only DIC was measured. The archetypal C_{ant} concentrations for all SWTs were less than 1 μmol kg^{-1} smaller after the correction of A_T. No significant difference between the storage rates was evident.

Biogeosciences Discuss., doi:10.5194/bg-2017-27, 2017
Manuscript under review for journal Biogeosciences
This is just a preview and not the published paper.

Biogeosciences Discussions Open Access EGU

Appendix B: Location SWT

As a result of the eOMP, the fraction of SWTs in each water parcel is estimated. Figure B1 shows this fraction for the 1991 (a) and the 2015 (b) data for IW, uLSW, cLSW, DSOW, ISOW and UW, which is the sum over ISW, NACW and SPMW. Overall, the position of the water masses is well represented through time.

Acknowledgements. F. Fröb and A. Olsen appreciate funding from the SNACS project (229752), that is part of the KLIMAFORSK program of the Norwegian Research Council. E. Jeansson and S.K. Lauvset received funding from the NRC project VENTILATE (229791). F.F. Pérez and M.I. García-Ibáñez were supported by the Spanish Ministry of Economy and Competitiveness through the BOCATS (CTM2013-41048-P) project co-funded by the Fondo Europeo de Desarrollo Regional 2007-2012 (FEDER). This is a contribution to the BIGCHANGE project of the Bjerknes Center for Climate Research.

Biogeosciences Discuss., doi:10.5194/bg-2017-27, 2017
Manuscript under review for journal Biogeosciences
This is just a preview and not the published paper.

Biogeosciences Discussions Open Access EGU

References

Álvarez, M., Pérez, F. F., Shoosmith, D. R., and Bryden, H. L.: Unaccounted role of Mediterranean Water in the drawdown of anthropogenic carbon, Journal of Geophysical Research-Oceans, 110, doi:10.1029/2004JC002633, 2005.

Álvarez-Salgado, X. A., Nieto-Cid, M., Álvarez, M., Pérez, F. F., Morin, P., and Mercier, H.: New insights on the mineralization of dissolved organic matter in central, intermediate, and deep water masses of the northeast North Atlantic, Limnology and Oceanography, 58, 681–696, doi:10.4319/lo.2013.58.2.0681, 2013.

Amante, C. and Eakins, B.: ETOPO1 1 Arc-Minute Global Relief Model: Procedures, Data Sources and Analysis, NOAA Technical Memorandum NESDIS NGDC-24. National Geophysical Data Center, NOAA., [02.10.2015], doi:10.7289/V5C8276M, 2009.

Arora, V. K., Boer, G. J., Friedlingstein, P., Eby, M., Jones, C. D., Christian, J. R., Bonan, G., Bopp, L., Brovkin, V., Cadule, P., Hajima, T., Ilyina, T., Lindsay, K., Tjiputra, J. F., and Wu, T.: Carbon-Concentration and Carbon-Climate Feedbacks in CMIP5 Earth System Models, Journal of Climate, 26, 5289–5314, doi:10.1175/JCLI-D-12-00494.1, 2013.

Bacon, S., Gould, W., and Jia, Y.: Open-ocean convection in the Irminger Sea, Geophysical Research Letters, 30,doi:10.1029/2002GL016271, 2003.

Castro, C., Pérez, F., Holley, S., and Ríos, A.: Chemical characterisation and modelling of water masses in the Northeast Atlantic, Progress in Oceanography, 41, 249 – 279, doi:10.1016/S0079-6611(98)00021-4, 1998.

Curry, R., McCartney, M., and Joyce, T.: Oceanic transport of subpolar climate signals to mid-depth subtropical waters, Nature, 391, 575–577, doi:10.1038/35356, 1998.

de Jong, M. F. and de Steur, L.: Strong winter cooling over the Irminger Sea in winter 2014-2015, exceptional deep convection, and the emergence of anomalously low SST, Geophysical Research Letters, 45, doi:10.1002/2016GL069596, 2016GL069596, 2016.

de Jong, M. F., van Aken, H. M., Våge, K., and Pickart, R. S.: Convective mixing in the central Irminger Sea: 2002-2010, Deep-Sea Research Part I-Oceanographic Research Papers, 63, 36–51, doi:10.1016/j.dsr.2012.01.003, 2012.

Dickson, A., Sabine, C., and Christian, J. E.: Guide to Best Practices for Ocean CO_2 Measurements, PICES Special Publication 3, 3, 191pp, 2007.

Dickson, R. and Brown, J.: The Production of North-Atlantic Deep-Water - Sources, Rates and Pathways, Journal of Geophysical Research - Oceans, 99, 12 319–12 341, doi:10.1029/94JC00530, 1994.

Friedlingstein, P., Cox, P., Betts, R., Bopp, L., Von Bloh, W., Brovkin, V., Cadule, P., Doney, S., Eby, M., Fung, I., Bala, G., John, J., Jones, C., Joos, F., Kato, T., Kawamiya, M., Knorr, W., Lindsay, K., Matthews, H. D., Raddatz, T., Rayner, P., Reick, C., Roeckner, E., Schnitzler, K. G., Schnur, R., Strassmann, K., Weaver, A. J., Yoshikawa, C., and Zeng, N.: Climate-carbon cycle feedback analysis: Results from the C^4MIP model intercomparison, Journal of Climate, 19, 3337–3353, doi:10.1175/JCLI3800.1, 2006.

Fröb, F., Olsen, A., Våge, K., Moore, K., Yashayaev, I., Jeansson, E., and Rajasakaren, B.: Irminger Sea deep convection injects oxygen and anthropogenic carbon to the ocean interior, Nature Communications, 7, 13 244, doi:10.1038/ncomms13244, 2016.

García-Ibáñez et al., M. I., Zunino, P., Fröb, F., Carracedo, L. I., Ríos, A., Mercier, H., Olsen, A., and Pérez, F. F.: Ocean Acidification in the Subpolar North Atlantic: mechanisms controlling pH changes, Biogeosciences, in progress, 2016.

García-Ibáñez, M. I., Pardo, P. C., Carracedo, L. I., Mercier, H., Lherminier, P., Ríos, A. F., and Pérez, F. F.: Structure, transports and transformations of the water masses in the Atlantic Subpolar Gyre, Progress in Oceanography, 135, 18–36, doi:10.1016/j.pocean.2015.03.009, 2015.

Biogeosciences Discuss., doi:10.5194/bg-2017-27, 2017
Manuscript under review for journal Biogeosciences
This is just a preview and not the published paper.

Gruber, N., Sarmiento, J., and Stocker, T.: An improved method for detecting anthropogenic CO_2 in the oceans, Global Biogeochemical Cycles, 10, 809–837, doi:10.1029/96GB01608, 1996.

Häkkinen, S. and Rhines, P.: Decline of subpolar North Atlantic circulation during the 1990s, Science, 304, 555–559, doi:10.1126/science.1094917, 2004.

Hansen, B. and Østerhus, S.: North Atlantic-Nordic Seas exchanges, Progress in Oceanography, 45, 109 – 208, doi:10.1016/S0079-6611(99)00052-X, 2000.

Hátún, H., Sandø, A., Drange, H., Hansen, B., and Valdimarsson, H.: Influence of the Atlantic subpolar gyre on the thermohaline circulation, Science, 309, 1841–1844, doi:10.1126/science.1114777, 2005.

Hood, E.M., Sabine, C.L. & Sloyan, B.M., eds. *The GO-SHIP Repeat Hydrography Manual: A Collection of Expert Reports and Guidelines*. IOCCP Report Number 14, ICPO Publication Series Number 134. Available online at http://www.go-ship.org/HydroMan.html. (2010).

Hurrell, J. W. and Deser, C.: North Atlantic climate variability: The role of the North Atlantic Oscillation, Journal of Marine Systems, 78, 28–41, 2009.

Jeansson, E., Jutterström, S., Rudels, B., Anderson, L. G., Olsson, K. A., Jones, E. P., Smethie Jr., W. M., and Swift, J. H.: Sources to the East Greenland Current and its contribution to the Denmark Strait Overflow , Progress in Oceanography, 78, 12 – 28, doi:10.1016/j.pocean.2007.08.031, 2008.

Johnson, K., Key, R., Millero, F., Sabine, C., Wallace, D., Winn, C., Arlen, L., Erickson, K., Friis, K., Galanter, M., Goen, J., Rotter, R., Thomas, C., Wilke, R., Takahashi, T., and Sutherland, S.: Carbon Dioxide, Hydrographic, and Chemical Data Obtained During the R/V Knorr Cruises in the North Atlantic Ocean on WOCE Sections AR24 (November 2 - December 5, 1996) and A24, A20, and A22 (May 30 - September 3, 1997), Carbon Dioxide Information Analysis Center, Oak Ridge National Laboratory, U.S. Department of Energy, Oak Ridge, Tennessee., 2003.

Karstensen, J. and Tomczak, M.: Age determination of mixed water masses using CFC and oxygen data, Journal of Geophysical Research: Oceans, 103, 18 599–18 609, doi:10.1029/98JC00889, 1998.

Key, R., Kozyr, A., Sabine, C., Lee, K., Wanninkhof, R., Bullister, J., Feely, R., Millero, F., Mordy, C., and Peng, T.: A global ocean carbon climatology: Results from Global Data Analysis Project (GLODAP), Global Biogeochemical Cycles, 18, doi:10.1029/2004GB002247, 2004.

Key, R. M., Tanhua, T., Olsen, A., Hoppema, M., Jutterström, S., Schirnick, C., van Heuven, S., Kozyr, A., Lin, X., Velo, A., Wallace, D. W. R., and Mintrop, L.: The CARINA data synthesis project: introduction and overview, Earth System Science Data, 2, 105–121, doi:10.5194/essd-2-105-2010, 2010.

Key, R. M., Olsen, A., van Heuven, S., Lauvset, S. K., Velo, A., Lin, X., Schirnick, C., Kozyr, A., Tanhua, T., Hoppema, M., Jutterström, S., Steinfeldt, R., Jeansson, E., Ishii, M., Pérez, F. F., and Suzuki, T.: Global Ocean Data Analysis Project, version 2 (GLODAPv2), ORNL/CDIAC-162, NDP-093, Carbon Dioxide Information Analysis Center, Oak Ridge National Laboratory, Oak Ridge, Tennessee, US., 2015.

Körtzinger, A., Rhein, M., and Mintrop, L.: Anthropogenic CO_2 and CFCs in the North Atlantic Ocean - A comparison of man-made tracers, Geophysical Research Letters, 26, 2065–2068, doi:10.1029/1999GL900432, 1999.

Landschützer, P., Gruber, N., Haumann, F. A., Rödenbeck, C., Bakker, D. C. E., van Heuven, S., Hoppema, M., Metzl, N., Sweeney, C., Takahashi, T., Tilbrook, B., and Wanninkhof, R.: The reinvigoration of the Southern Ocean carbon sink, Science, 349, 1221–1224, doi:10.1126/science.aab2620, 2015.

Biogeosciences Discuss., doi:10.5194/bg-2017-27, 2017
Manuscript under review for journal Biogeosciences
This is just a preview and not the published paper.

Lavender, K., Owens, W., and Davis, R.: The mid-depth circulation of the subpolar North Atlantic Ocean as measured by subsurface floats, Deep-Sea Research Part I-Oceanographic Research Papers, 52, 767–785, doi:10.1016/j.dsr.2004.12.007, 2005.

Lazier, J., Hendry, R., Clarke, A., Yashayaev, I., and Rhines, P.: Convection and restratification in the Labrador Sea, 1990-2000, Deep-Sea Research Part I-Oceanographic Research Papers, 49, 1819–1835, doi:10.1016/S0967-0637(02)00064-X, 2002.

Le Quéré, C., Rödenbeck, C., Buitenhuis, E. T., Conway, T. J., Langenfelds, R., Gomez, A., Labuschagne, C., Ramonet, M., Nakazawa, T., Metzl, N., Gillett, N., and Heimann, M.: Saturation of the Southern Ocean CO_2 Sink Due to Recent Climate Change, Science, 316, 1735–1738, doi:10.1126/science.1136188, 2007.

Le Quéré, C., Andrew, R. M., Canadell, J. G., Sitch, S., Korsbakken, J. I., Peters, G. P., Manning, A. C., Boden, T. A., Tans, P. P., Houghton, R. A., Keeling, R. F., Alin, S., Andrews, O. D., Anthoni, P., Barbero, L., Bopp, L., Chevallier, F., Chini, L. P., Ciais, P., Currie, K., Delire, C., Doney, S. C., Friedlingstein, P., Gkritzalis, T., Harris, I., Hauck, J., Haverd, V., Hoppema, M., Klein Goldewijk, K., Jain, A. K., Kato, E., Körtzinger, A., Landschützer, P., Lefèvre, N., Lenton, A., Lienert, S., Lombardozzi, D., Melton, J. R., Metzl, N., Millero, F., Monteiro, P. M. S., Munro, D. R., Nabel, J. E. M. S., Nakaoka, S.-I., O'Brien, K., Olsen, A., Omar, A. M., Ono, T., Pierrot, D., Poulter, B., Rödenbeck, C., Salisbury, J., Schuster, U., Schwinger, J., Séférian, R., Skjelvan, I., Stocker, B. D., Sutton, A. J., Takahashi, T., Tian, H., Tilbrook, B., van der Laan-Luijkx, I. T., van der Werf, G. R., Viovy, N., Walker, A. P., Wiltshire, A. J., and Zaehle, S.: Global Carbon Budget 2016, Earth System Science Data, 8, 605–649, doi:10.5194/essd-8-605-2016, 2016.

Lee, K., Tong, L. T., Millero, F. J., Sabine, C. L., Dickson, A. G., Goyet, C., Park, G.-H., Wanninkhof, R., Feely, R. A., and Key, R. M.: Global relationships of total alkalinity with salinity and temperature in surface waters of the world's oceans, Geophysical Research Letters, 33, doi:10.1029/2006GL027207, 2006.

Lherminier, P., Mercier, H., Huck, T., Gourcuff, C., Pérez, F. F., Morin, P., Sarafanov, A., and Falina, A.: The Atlantic Meridional Overturning Circulation and the subpolar gyre observed at the A25-OVIDE section in June 2002 and 2004 , Deep Sea Research Part I: Oceanographic Research Papers, 57, 1374 – 1391, doi:10.1016/j.dsr.2010.07.009, 2010.

Lueker, T. J., Dickson, A. G., and Keeling, C. D.: Ocean pCO_2 calculated from dissolved inorganic carbon, alkalinity, and equations for K_1 and K_2: validation based on laboratory measurements of CO_2 in gas and seawater at equilibrium, Marine Chemistry, 70, 105 –119, doi:10.1016/S0304-4203(00)00022-0, 2000.

Marshall, J. and Schott, F.: Open-ocean convection: Observations, theory, and models, Reviews of Geophysics, 37, 1–64, doi:10.1029/98RG02739, 1999.

Maze, G., Mercier, H., Thierry, V., Memery, L., Morin, P., and Pérez, F. F.: Mass, nutrient and oxygen budgets for the northeastern Atlantic Ocean, Biogeosciences, 9, 4099–4113, doi:10.5194/bg-9-4099-2012, 2012.

McCartney, M.: Recirculating components to the deep boundary current of the northern North Atlantic, Progress in Oceanography, 29, 283 – 383, doi:10.1016/0079-6611(92)90006-L, 1992.

Mercier, H., Lherminier, P., Sarafanov, A., Gaillard, F., Daniault, N., Desbruyères, D., Falina, A., Ferron, B., Gourcuff, C., Huck, T., and Thierry, V.: Variability of the meridional overturning circulation at the Greenland-Portugal OVIDE section from 1993 to 2010 , Progress in Oceanography, 132, 250 – 261, doi:0.1016/j.pocean.2013.11.001, 2015.

Nondal, G., Bellerby, R. G. J., Olsen, A., Johannessen, T., and Olafsson, J.: Optimal evaluation of the surface ocean CO_2 system in the northern North Atlantic using data from voluntary observing ships, Limnology and Oceanography: Methods, 7, 109–118, doi:10.4319/lom.2009.7.109, 2009.

Biogeosciences Discuss., doi:10.5194/bg-2017-27, 2017
Manuscript under review for journal Biogeosciences
This is just a preview and not the published paper.

Olsen, A., Key, R. M., van Heuven, S., Lauvset, S. K., Velo, A., Lin, X., Schirnick, C., Kozyr, A., Tanhua, T., Hoppema, M., Jutterström, S., Steinfeldt, R., Jeansson, E., Ishii, M., Pérez, F. F., and Suzuki, T.: The Global Ocean Data Analysis Project version 2 (GLODAPv2) – an internally consistent data product for the world ocean, Earth System Science Data, 8, 297–323, doi:10.5194/essd-8-297-2016, 2016.

Pérez, F. F., Vázquez-Rodríguez, M., Louarn, E., Padín, X. A., Mercier, H., and Ríos, A. F.: Temporal variability of the anthropogenic CO_2 storage in the Irminger Sea, Biogeosciences, 5, 1669–1679, doi:10.5194/bg-5-1669-2008, 2008.

Pérez, F. F., Vázquez-Rodríguez, M., Mercier, H., Velo, A., Lherminier, P., and Ríos, A. F.: Trends of anthropogenic CO_2 storage in North Atlantic water masses, Biogeosciences, 7, 1789–1807, doi:10.5194/bg-7-1789-2010, 2010.

Pérez, F. F., Mercier, H., Vázquez-Rodríguez, M., Lherminier, P., Velo, A., Pardo, P. C., Roson, G., and Ríos, A. F.: Atlantic Ocean CO_2 uptake reduced by weakening of the meridional overturning circulation, Nature Geoscience, 6, 146–152, doi:10.1038/NGEO1680, 2013.

Pickart, R., Spall, M., Ribergaard, M., Moore, G., and Milliff, R.: Deep convection in the Irminger Sea forced by the Greenland tip jet, Nature, 424, 152–156, doi:10.1038/nature01729, 2003a.

Pickart, R., Straneo, F., and Moore, G.: Is Labrador Sea Water formed in the Irminger basin?, Deep-Sea Research Part I-Oceanographic Research Papers, 50, 23–52, doi:10.1016/S0967-0637(02)00134-6, 2003b.

Poole, R. and Tomczak, M.: Optimum multiparameter analysis of the water mass structure in the Atlantic Ocean thermocline, Deep-Sea Research Part I-Oceanographic Research Papers, 46, 1895–1921, doi:10.1016/S0967-0637(99)00025-4, 1999.

Ríos, A.F., Pérez, F.F., García-Ibáñez, M.I., Fajar, N.M., Lherminier, P., Branellec, P., Gilcoto, M., Rosón, G., Alonso-Pérez, F., de la Paz, M., Castaño-Carrera, M., Galindo, M., and Velo, A.: Carbon Dioxide, Hydrographic, and Chemical Data Obtained During the R/V Sarmiento de Gamboa Cruise in the North Atlantic Ocean on CLIVAR Repeat Hydrography Section OVIDE-2012 (June 22 - July 20, 2012). Carbon Dioxide Information Analysis Center, Oak Ridge National Laboratory, US Department of Energy, Oak Ridge, Tennessee., 2015.

Sabine, C., Feely, R., Gruber, N., Key, R., Lee, K., Bullister, J., Wanninkhof, R., Wong, C., Wallace, D., Tilbrook, B., Millero, F., Peng, T., Kozyr, A., Ono, T., and Ríos, A.: The oceanic sink for anthropogenic CO_2, Science, 305, 367–371, doi:10.1126/science.1097403, 2004.

Sarafanov, A., Falina, A., Sokov, A., and Demidov, A.: Intense warming and salinification of intermediate waters of southern origin in the eastern subpolar North Atlantic in the 1990s to mid-2000s, Journal of Geophysical Research - Oceans, 113, doi:10.1029/2008JC004975, 2008.

Sarmiento, J. and Gruber, N.: Sinks for anthropogenic carbon, Physics Today, 55, 30–36, doi:10.1063/1.1510279, 2002.

Schwinger, J., Tjiputra, J. F., Heinze, C., Bopp, L., Christian, J. R., Gehlen, M., Ilyina, T., Jones, C. D., Salas-Melia, D., Segschneider, J., Seferian, R., and Totterdell, I.: Nonlinearity of Ocean Carbon Cycle Feedbacks in CMIP5 Earth System Models, JOURNAL OF CLIMATE, 27, 3869–3888, doi:10.1175/JCLI-D-13-00452.1, 2014.

Steinfeldt, R., Rhein, M., Bullister, J. L., and Tanhua, T.: Inventory changes in anthropogenic carbon from 1997-2003 in the Atlantic Ocean between 20○S and 65○N, Global Biogeochemical Cycles, 23, doi:10.1029/2008GB003311, 2009.

Stendardo, I. and Gruber, N.: Oxygen trends over five decades in the North Atlantic, Journal of Geophysical Research - Oceans, 117, doi:10.1029/2012JC007909, 2012.

Stoll, M., van Aken, H., de Baar, H., and de Boer, C.: Meridional carbon dioxide transport in the northern North Atlantic, Marine Chemistry, 55, 205 – 216, doi:10.1016/S0304-4203(96)00057-6, 1996.

Tanhua, T. and Keeling, R. F.: Changes in column inventories of carbon and oxygen in the Atlantic Ocean, Biogeosciences, 9, 4819–4833, doi:10.5194/bg-9-4819-2012, 2012.

Tanhua, T., Olsson, K. A., and Jeansson, E.: Formation of Denmark Strait overflow water and its hydro-chemical composition, Journal of Marine Systems, 57, 264–288, doi:10.1016/j.jmarsys.2005.05.003, 2005.

Biogeosciences Discuss., doi:10.5194/bg-2017-27, 2017
Manuscript under review for journal Biogeosciences
This is just a preview and not the published paper.

Thomas, H. and Ittekkot, V.: Determination of anthropogenic CO_2 in the North Atlantic Ocean using water mass ages and CO_2 equilibrium chemistry, Journal of Marine Systems, 27, 325 – 336, doi:10.1016/S0924-7963(00)00077-4, 2001.

Tomczak, M. and Large, D. G. B.: Optimum Multimparameter Analysis of Mixing in the Thermocline of the Eastern Indian-Ocean, Journal of Geophysical Research-Oceans, 94, 16 141–16 149, doi:10.1029/JC094iC11p16141, 1989.

Touratier, F. and Goyet, C.: Decadal evolution of anthropogenic CO_2 in the northwestern Mediterranean Sea from the mid-1990s to the mid-2000s, Deep Sea Research Part I: Oceanographic Research Papers, 56, 1708 – 1716, doi:10.1016/j.dsr.2009.05.015, 2009.

van Aken, H.: The hydrography of the mid-latitude Northeast Atlantic Ocean II: The intermediate water masses, Deep-Sea Research Part I-Oceanographic Research Papers, 47, 789–824, doi:10.1016/S0967-0637(99)00112-0, 2000.

van Heuven, S., Zemmelink, H., Bakker, K., van Aken, H., and Veth, C.: Carbon Dioxide, Hydrographic, and Chemical Data Obtained During the R/V Pelagia Repeat Hydrography Cruise in the Atlantic Ocean: CLIVAR CO_2 Section AR07E2005 (September 7 - October 5, 2005), Carbon Dioxide Information Analysis Center, Oak Ridge National Laboratory, US Department of Energy, Oak Ridge, Tennessee., 2012.

van Heuven, S., Brummer, G.-J., van Ooijen, J., and van Aken, H.: Carbon Dioxide, Hydrographic, and Chemical Data Obtained During the R/V Pelagia Repeat Hydrography Cruise in the Atlantic Ocean: CLIVAR CO_2 Section AR07E2007 (August 30 - September 27, 2007), Carbon Dioxide Information Analysis Center, Oak Ridge National Laboratory, US Department of Energy, Oak Ridge, Tennessee., 2013.

Vázquez-Rodríguez, M., Touratier, F., Lo Monaco, C., Waugh, D. W., Padín, X. A., Bellerby, R. G. J., Goyet, C., Metzl, N., Ríos, A. F., and Pérez, F. F.: Anthropogenic carbon distributions in the Atlantic Ocean: data-based estimates from the Arctic to the Antarctic, Biogeosciences, 6, 439–451, 2009.

Vázquez-Rodríguez, M., Padín, X. A., Pardo, P. C., Ríos, A. F., and Pérez, F. F.: The subsurface layer reference to calculate preformed alkalinity and air-sea CO_2 disequilibrium in the Atlantic Ocean, Journal of Marine Systems, 94, 52–63, doi:10.1016/j.jmarsys.2011.10.008, 2012.

Våge, K., Pickart, R. S., Moore, G. W. K., and Ribergaard, M. H.: Winter mixed layer development in the central Irminger Sea: The effect of strong, intermittent wind events, Journal of Physical Oceanography, 38, 541–565, doi:10.1175/2007JPO3678.1, 2008.

Våge, K., Pickart, R. S., Sarafanov, A., Knutsen, O., Mercier, H., Lherminier, P., van Aken, H. M., Meincke, J., Quadfasel, D., and Bacon, S.: The Irminger Gyre: Circulation, convection, and interannual variability, Deep-Sea Research Part I-Oceanographic Research Papers, 58, 590–614, doi:10.1016/j.dsr.2011.03.001, 2011.

Wakita, M., Watanabe, S., Murata, A., Tsurushima, N., and Honda, M.: Decadal change of dissolved inorganic carbon in the subarctic western North Pacific Ocean, Tellus B, 62, 1600–0889, doi:10.1111/j.1600-0889.2010.00476.x, 2010.

Wanninkhof, R., Doney, S. C., Bullister, J. L., Levine, N. M., Warner, M., and Gruber, N.: Detecting anthropogenic CO_2 changes in the interior Atlantic Ocean between 1989 and 2005, Journal of Geophysical Research-Oceans, 115, doi:10.1029/2010JC006251, 2010.

Woosley, R. J., Millero, F. J., and Wanninkhof, R.: Rapid anthropogenic changes in CO_2 and pH in the Atlantic Ocean: 2003-2014, Global Biogeochemical Cycles, 30, 70–90, doi:10.1002/2015GB005248, 2015GB005248, 2016.

Yashayaev, I., Bersch, M., and van Aken, H. M.: Spreading of the Labrador Sea Water to the Irminger and Iceland basins, Geophysical Research Letters, 34, n/a–n/a, doi:10.1029/2006GL028999, l10602, 2007.

Yashayaev, I., van Aken, H. M., Holliday, N. P., and Bersch, M.: Transformation of the Labrador Sea Water in the subpolar North Atlantic, Geophysical Research Letters, 34, doi:10.1029/2007GL031812, 2007.

Zunino, P., Lherminier, P., Mercier, H., Padín, X. A., Ríos, A. F., and Pérez, F. F.: Dissolved inorganic carbon budgets in the eastern subpolar North Atlantic in the 2000s from in situ data, Geophysical Research Letters, 42, 9853–9861, doi:10.1002/2015GL066243, 2015GL066243, 2015.

Biogeosciences Discuss., doi:10.5194/bg-2017-27, 2017
Manuscript under review for journal Biogeosciences
This is just a preview and not the published paper.

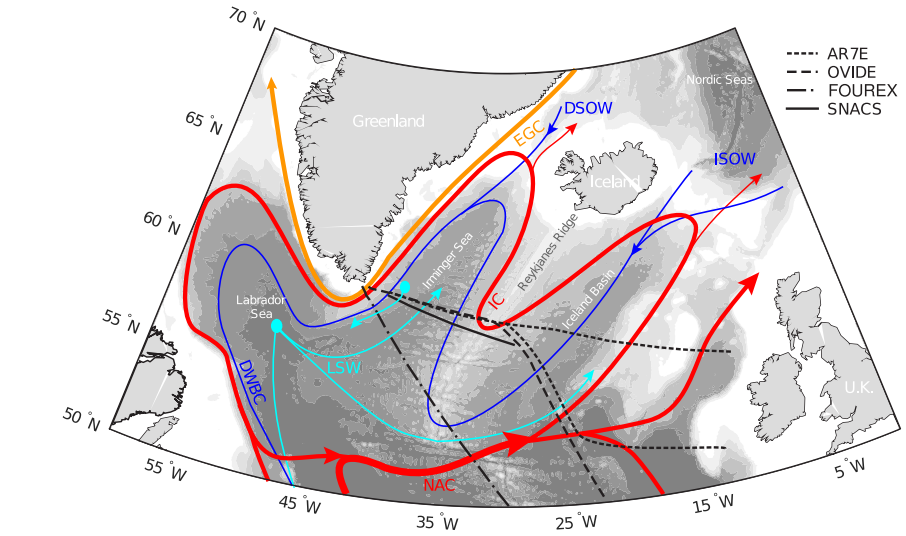

Figure 1. Schematic subpolar North Atlantic circulation. The location of the AR7E, OVIDE, FOUREX and SNACS lines are plotted in black on the bathymetry (500 m intervals). The branches of the North Atlantic Current (NAC) turning into the Irminger Current (IC) are shown in red and the East Greenland Current (EGC) is plotted in orange. The dark blue currents illustrate the spreading of the Iceland-Scotland Overflow Water (ISOW) and the Denmark Strait Overflow Water (DSOW) at depth, which jointly with the Labrador Sea Water (LSW), in cyan, contribute to the Deep Western Boundary Current (DWBC). Adapted from Lherminier et al. (2010) and Pérez et al. (2013).

Biogeosciences Discuss., doi:10.5194/bg-2017-27, 2017
Manuscript under review for journal Biogeosciences
This is just a preview and not the published paper.

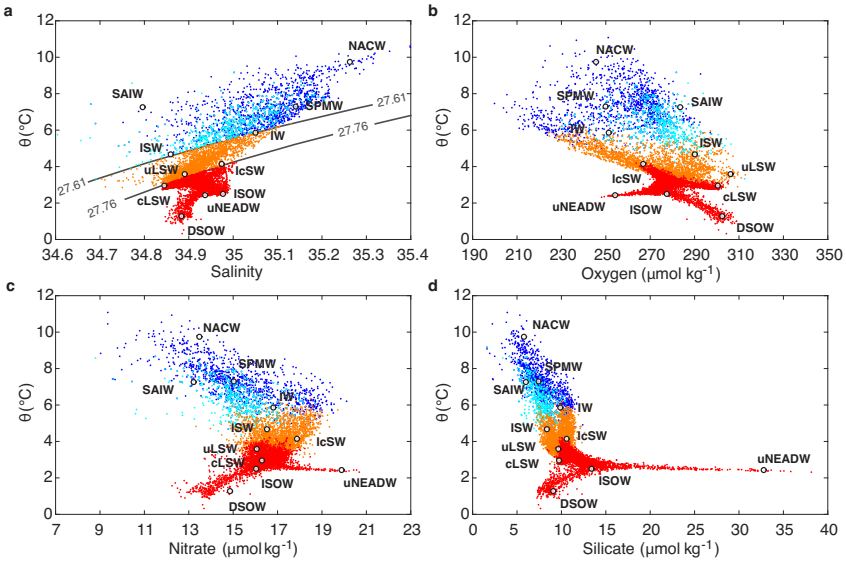

Figure 2. Source water type (SWT) parameters presented in a potential temperature - a) salinity, including potential density (σ_0) levels, b) oxygen, c) nitrate and d) silicate space for Irminger Sea cruise-data from 1991-2015. The colours represent different mixing figures for the eOMP analysis: red for the deep ocean ($\sigma_0 \geq 27.76$ kg m^{-3}), orange for the intermediate ocean ($27.61 \leq \sigma_0 < 27.76$ kg m^{-3}) and surface ocean ($\sigma_0 < 27.61$ kg m^{-3}), east of Reykjanes Ridge (dark blue) and west of Reykjanes Ridge region (cyan).

Biogeosciences Discuss., doi:10.5194/bg-2017-27, 2017
Manuscript under review for journal Biogeosciences
This is just a preview and not the published paper.

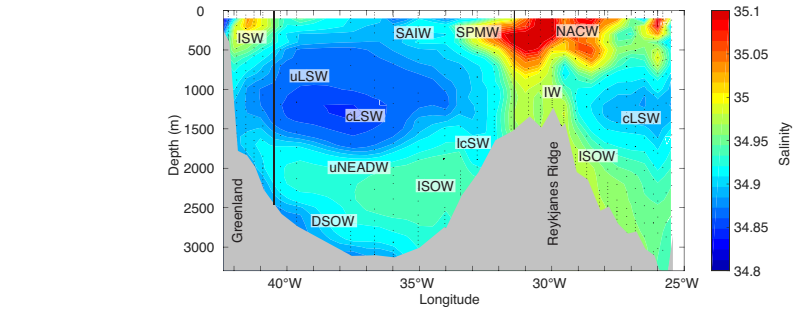

Figure 3. Vertical cross section through the Irminger Sea showing interpolated salinity based on the 1991 cruise data (06MT19910902). The approximate location of the main water masses of the eOMP analysis, shown in Appendix B, is illustrated: Subarctic Intermediate Water (SAIW), Intermediate Water (IW), classical and upper Labrador Sea Water (cLSW and uLSW), Denmark Strait Overflow Water (DSOW), upper Northeast Atlantic Deep Water (uNEADW), Iceland-Scotland Overflow Water (ISOW), Icelandic Slope Water (IcSW), Irminger Sea Water (ISW), Subpolar Mode Water (SPMW), North Atlantic Central Water (NACW). The longitudinal boundaries for the inventory estimates at 40.5° W and 31.5° W are shown (black lines).

Biogeosciences Discuss., doi:10.5194/bg-2017-27, 2017
Manuscript under review for journal Biogeosciences
This is just a preview and not the published paper.

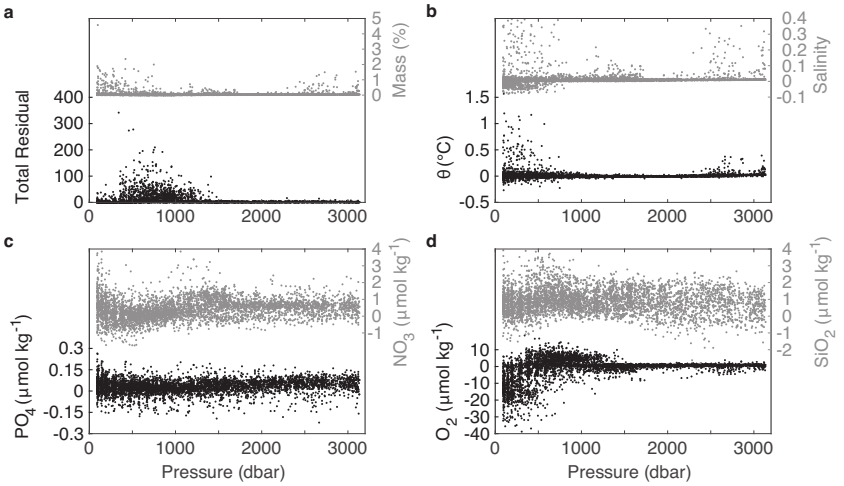

Figure 4. Residuals of the eOMP analysis for all Irminger Sea cruise-data from 1991-2015 for the a) total residual as the squared largest singular value for the set of residuals (García-Ibáñez et al., 2015), and the residual of mass conservation in %, b) residuals of potential temperature and salinity, c) residuals of phosphate and nitrate and d) residuals of oxygen and silicate with respect to pressure.

Biogeosciences Discuss., doi:10.5194/bg-2017-27, 2017
Manuscript under review for journal Biogeosciences
This is just a preview and not the published paper.

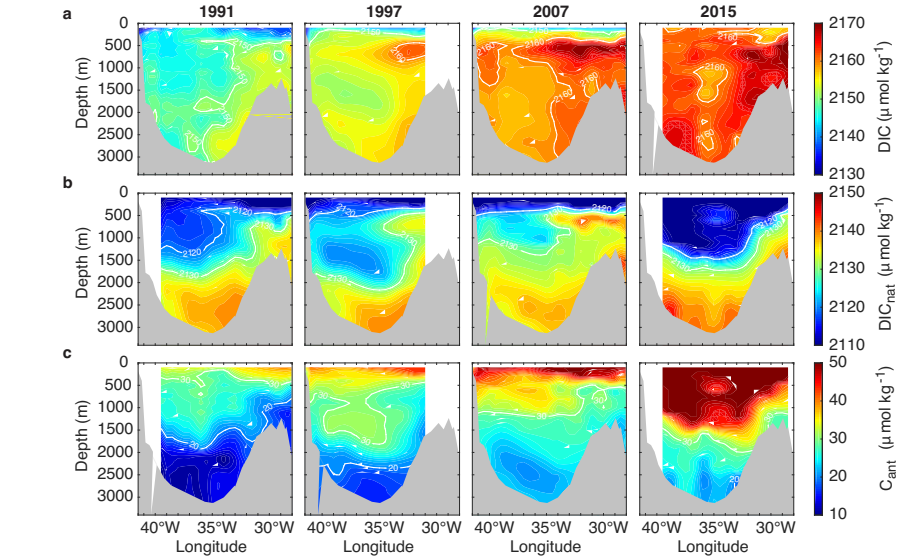

Figure 5. Vertical cross sections through the Irminger Sea showing interpolated cruise station data of a) DIC b) DIC_{nat} and c) C_{ant} concentration in 1991 (first row), 1997 (second row), 2007 (third row) and 2015 (last row). The white contour lines illustrate selected concentration levels. All panels have a the same span of values of 40 μmol kg^{-1}.

Biogeosciences Discuss., doi:10.5194/bg-2017-27, 2017
Manuscript under review for journal Biogeosciences
This is just a preview and not the published paper.

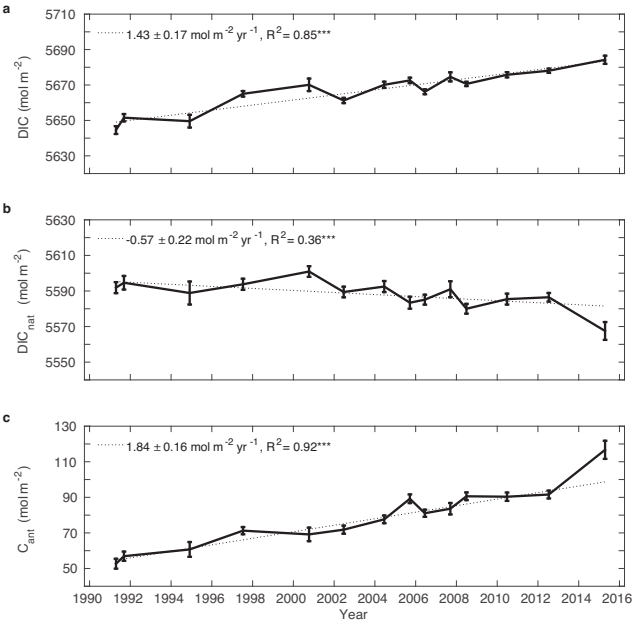

Figure 6. Total inventory for a) DIC, b) DIC_{nat} and c) C_{ant} for Irminger Sea cruise-data from 1991-2015. The rates of change between 1991 and 2015 are given, including the R-squared value of the linear regression model. The significance on the 99 % level (***) is indicated. Values of the two cruises in 1997 were averaged and are shown as one data point.

Biogeosciences Discuss., doi:10.5194/bg-2017-27, 2017
Manuscript under review for journal Biogeosciences
This is just a preview and not the published paper.

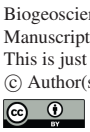

Biogeosciences Discussions Open Access EGU

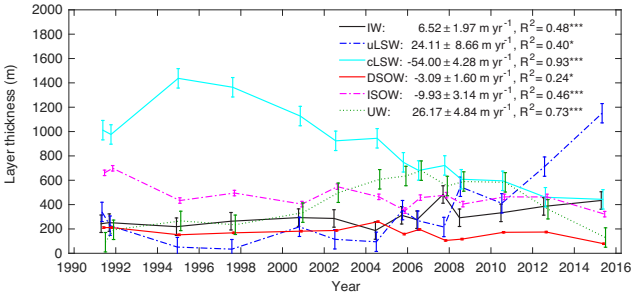

Figure 7. Layer thickness for IW, uLSW, cLSW, DSOW, ISOW and the sum over the upper ocean waters (UW) based on Irminger Sea cruise-data from 1991-2015. The mean depth between 40.5° W and 31.5° W is 2650 m. The error bars show the uncertainty based on a Monte Carlo simulation scaled to width and depth of the Irminger Sea. The rates of thickness change between 1991 and 2015 are given for all SWTs, including the R-squared value of the linear regression model. The significance on the 90 % level (*) or the 99 % level (***) is indicated. Values of the two cruises in 1997 were averaged and are shown as one data point. All markers are slightly offset in time for clarity.

Biogeosciences Discuss., doi:10.5194/bg-2017-27, 2017
Manuscript under review for journal Biogeosciences
This is just a preview and not the published paper.

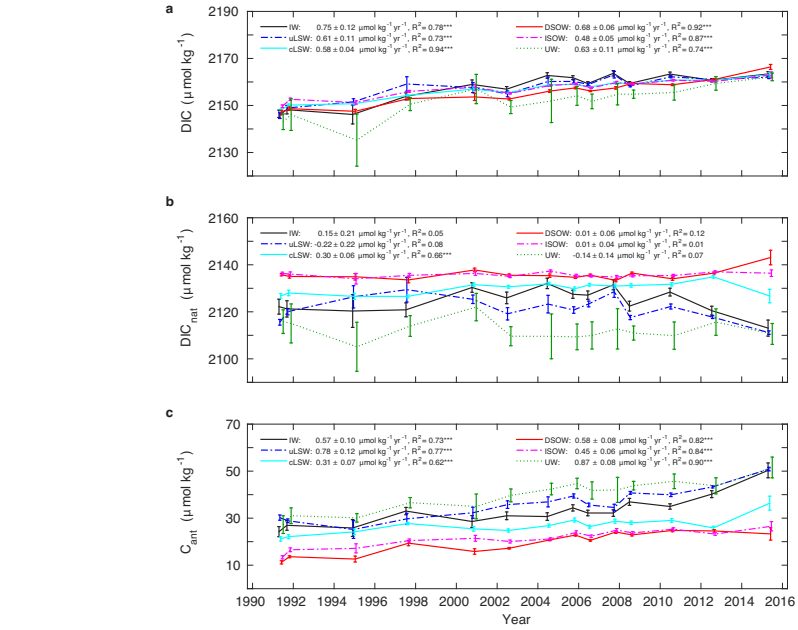

Figure 8. Archetypal concentration for IW, uLSW, cLSW, DSOW, ISOW and the sum over the upper ocean waters (UW) in the Irminger Sea from 1991 to 2015 for a) DIC, b) DIC_{nat} and c) C_{ant}. The error bars represent σ. The storage rates between 1991 and 2015 are given for all SWTs, including the R-squared value of the linear regression model. The significance on the 90 % level (*) or the 99 % level (***) is indicated. Values of the two cruises in 1997 were averaged and are shown as one data point. All markers are slightly offset in time for clarity.

Biogeosciences Discuss., doi:10.5194/bg-2017-27, 2017
Manuscript under review for journal Biogeosciences
This is just a preview and not the published paper.

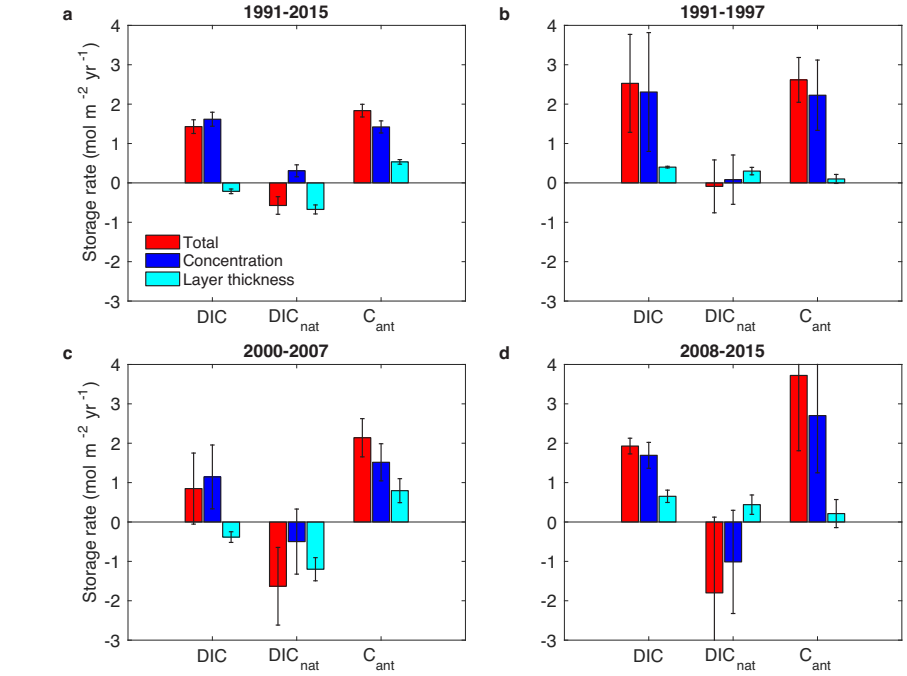

Figure 9. Decomposition of the total storage rates (red bars) into the concentration-driven storage rate (blue bars) and the layer thickness-driven storage rate rate (cyan bars) for DIC, C_{ant} and DIC_{nat} from a) 1991-2015, b) 1991-1997, c) 2000-2007 and d) 2008-2015. The error bars represent the error of the linear regression model.

Biogeosciences Discuss., doi:10.5194/bg-2017-27, 2017
Manuscript under review for journal Biogeosciences
This is just a preview and not the published paper.

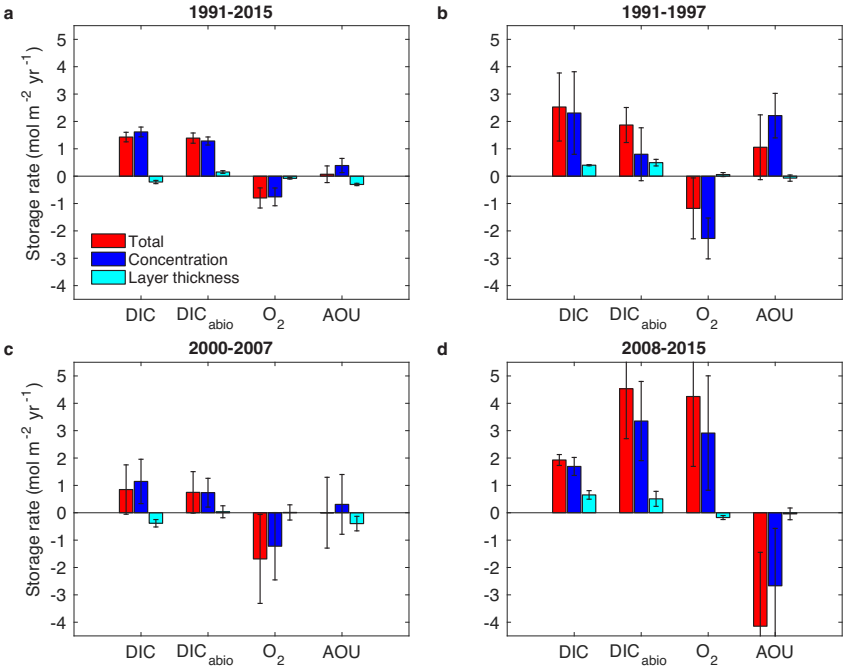

Figure 10. Decomposition of the total storage rates (red bars) into the concentration-driven storage rate (blue bars) and the layer thickness-driven storage rate (cyan bars) for DIC, DIC_{abio}, O_2 and AOU from a) 1991-2015, b) 1991-1997, c) 2000-2007 and d) 2008-2015. The error bars represent the error of the linear regression model.

Biogeosciences Discuss., doi:10.5194/bg-2017-27, 2017
Manuscript under review for journal Biogeosciences
This is just a preview and not the published paper.

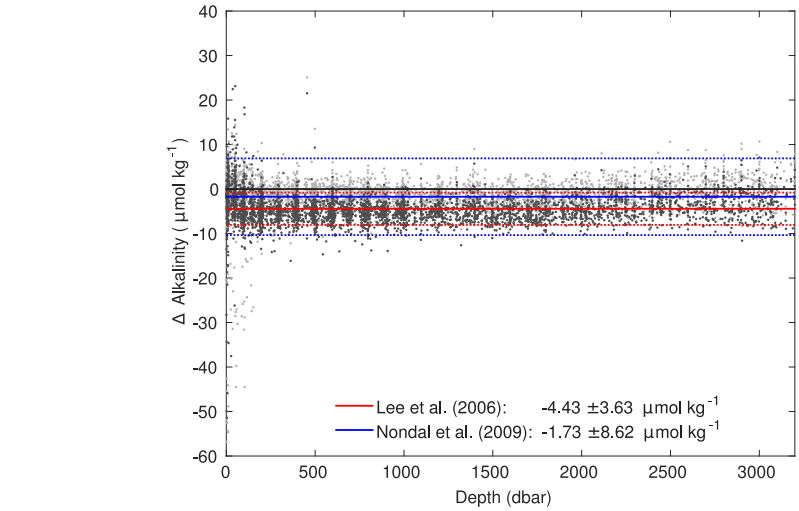

Figure A 1. Difference between measured and calculated alkalinity for Irminger Sea cruise data. The dark grey dots use the salinity-alkalinity relationship following Lee et al. (2006) and the light grey dots use the relationship following Nondal et al. (2009). The solid lines represent the mean difference and dotted lines ± one standard deviation.

Biogeosciences Discuss., doi:10.5194/bg-2017-27, 2017
Manuscript under review for journal Biogeosciences
This is just a preview and not the published paper.

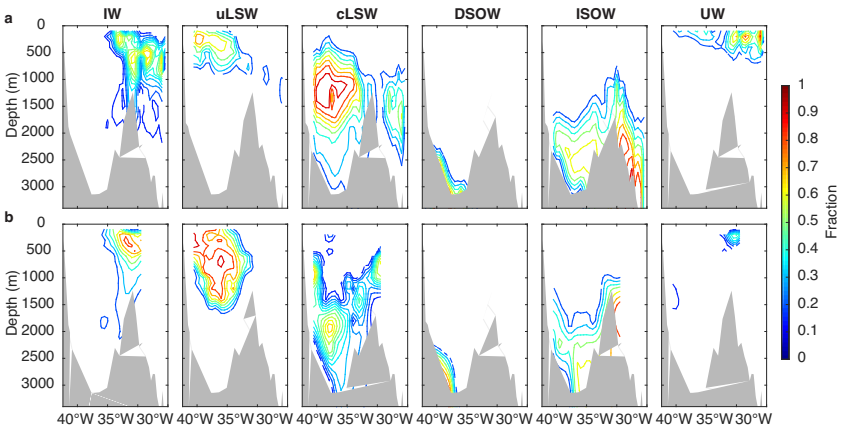

Figure B 1. Vertical cross section of fraction of water masses (IW, cLSW, uLSW, DSOW, ISOW and UW) in a) 1991 and b) 2015. Ratios below 0.1 are set to zero for clarity.

Biogeosciences Discuss., doi:10.5194/bg-2017-27, 2017
Manuscript under review for journal Biogeosciences
This is just a preview and not the published paper.

Biogeosciences Discussions Open Access EGU

Table 1. Irminger Sea cruise information. The measured variables of the seawater CO_2 chemistry are indicated.

Alias	Expocode	Month/Year	Ship	Data	Reference
AR07E	64TR19910408	04-05/1991	Tyro	DIC	Stoll et al. (1996)
A01E	06MT19910902	09/1991	Meteor	DIC, A_T	Meincke and Becker (1993)
A01	06MT19941115	11-12/1994	Meteor	DIC	Thomas and Ittekkot (2001)
FOUREX	316N19970530	05-07/1997	Knorr	DIC, A_T, pH	Johnson et al. (2003)
AR07W	06MT19970707	07-08/1997	Meteor	DIC, A_T	Körtzinger et al. (1999)
AR7E	64PE20000926	09-10/2000	Pelagia	DIC	Yashayaev et al. (2007)
OVIDE 2002	35TH20020611	06-07/2002	Thalassa	A_T, pH	Lherminier et al. (2010)
OVIDE 2004	35TH20040604	06-07/2004	Thalassa	A_T, pH	Lherminier et al. (2010)
AR07E	64PE20050907	09-10/2005	Pelagia	DIC, A_T	van Heuven et al. (2012)
OVIDE 2006	06MM20060523	05-06/2006	Maria S. Merian	A_T, pH	Pérez et al. (2008)
AR07E	64PE20070830	09/2007	Pelagia	DIC, A_T	van Heuven et al. (2013)
OVIDE 2008	35TH20080610	06-07/2008	Thalassa	A_T, pH	Mercier et al. (2015)
OVIDE 2010	35TH20100610	06/2010	Thalassa	A_T, pH	Mercier et al. (2015)
OVIDE 2012	29AH20120623	06-07/2012	Sarmiento de Gamboa	A_T, pH	García-Ibáñez et al. (2016)
SNACS	58GS20150410	04/2015	G.O. Sars	DIC, A_T	Fröb et al. (2016)

Biogeosciences Discuss., doi:10.5194/bg-2017-27, 2017
Manuscript under review for journal Biogeosciences
This is just a preview and not the published paper.

Biogeosciences Discussions Open Access EGU

Table 2. Source water type (SWT) parameters and their standard deviation used for the eOMP analysis for Subarctic Intermediate Water (SAIW), Intermediate Water (IW), classical and upper Labrador Sea Water (cLSW ans uLSW), Denmark Strait Overflow Water (DSOW), upper Northeast Atlantic Deep Water (uNEADW), Iceland-Scotland Overflow Water (ISOW), Icelandic Slope Water (IcSW), Irminger Sea Water (ISW), Subpolar Mode Water (SPMW) and North Atlantic Central Water (NACW). Definitions for Mediterraneum Water (MW) and lower Northeast Atlantic Deep Water (lNEADW) (*) from García-Ibáñez et al. (2015) are used only for the composite analysis but not in the eOMP. The weights for the equations are given. The mass weight is 150. The mean parameter residual is given (error). The last column gives an uncertainty estimate (per one) for the SWT contribution based on a Monte Carlo simulation.

SWT	θ	S	O_2	PO_4	NO_3	SiO_2	PV	Uncertainty
	°C		μmol kg^{-1}	μmol kg^{-1}	μmol kg^{-1}	μmol kg^{-1}	10^{-8} m^{-1}s^{-1}	
IW	5.85± 0.25	35.05 ± 0.01	251.3± 1.7	1.17 ± 0.03	16.82 ± 0.56	9.87 ± 0.27	0.0547 ± 0.0184	0.030
SAIW	7.25± 0.07	34.80 ± 0.04	283.5± 6.1	0.86 ± 0.07	13.21 ± 1.53	6.01 ± 1.20	0.1100 ± 0.0158	0.005
uLSW	3.57± 0.12	34.89 ± 0.07	296.0± 9.3	1.06 ± 0.02	16.07 ± 0.35	9.68 ± 0.47	0.0009 ± 0.0169	0.034
cLSW	2.96± 0.01	34.85 ± 0.01	300.3± 1.0	1.07 ± 0.02	16.21 ± 0.23	9.74 ± 0.13	0.0003 ± 0.0186	0.034
DSOW	1.11± 0.16	34.88 ± 0.01	303.6± 1.0	0.95 ± 0.02	14.16 ± 0.35	9.23 ± 0.30	0.0479 ± 0.0184	0.003
uNEADW	2.42± 0.05	34.94 ± 0.01	254.3± 1.6	1.35 ± 0.04	19.88 ± 0.34	32.82 ± 2.46	0.0364 ± 0.0158	$3.6*10^{-6}$
ISOW	2.50± 0.05	34.98 ± 0.01	277.5± 0.7	1.11 ± 0.03	16.04 ± 0.14	13.38 ± 0.51	0.0264 ± 0.0173	0.010
IcSW	4.13± 0.12	34.97 ± 0.01	267.0± 3.4	1.12 ± 0.01	17.87 ± 0.20	10.59 ± 0.30	0.0309 ± 0.0184	0.038
ISW	4.68± 0.30	34.86 ± 0.02	290.2± 1.0	1.07 ± 0.02	16.51 ± 0.90	8.35 ± 0.85	0.0364 ± 0.0158	0.017
SPMW	7.28± 0.25	35.14 ± 0.02	250.0± 0.2	0.98 ± 0.06	15.03 ± 1.00	7.44 ± 0.11	0.0479 ± 0.0096	0.016
NACW	9.74± 0.13	35.26 ± 0.02	245.7± 5.6	0.89 ± 0.01	13.47 ± 0.17	5.76 ± 0.42	0.0547 ± 0.0158	0.006
MW*	11.70	36.50	210	0.7	10.9	4.88	-	-
lNEADW*	1.98	34.90	252	1.5	22.6	48	-	-
Weight	25	15	8	2	2	1	3	
Error	0.006	0.015	0.881	0.031	0.421	0.927	0.001	

Biogeosciences Discuss., doi:10.5194/bg-2017-27, 2017
Manuscript under review for journal Biogeosciences
This is just a preview and not the published paper.

Biogeosciences Discussions Open Access EGU

Table 3. Mean layer thickness and concentration of DIC, DIC_{nat} and C_{ant} in IW, uLSW, cLSW, DSOW, ISOW and UW in the time periods from 1991-2015,1991-1997, 2000-2007 and 2008-2015.

Period	Variable	IW	uLSW	cLSW	DSOW	ISOW	UW
1991-2015	Thickness (m)	301	338	860	170	474	411
	DIC (μmol kg^{-1})	2158	2157	2157	2157	2155	2152
	DIC_{nat} (μmol kg^{-1})	2125	2121	2130	2136	2136	2112
	C_{ant} (μmol kg^{-1})	33	36	27	20	22	40
1991-1997	Thickness (m)	244	163	1197	186	572	196
	DIC (μmol kg^{-1})	2149	2151	2151	2149	2152	2144
	DIC_{nat} (μmol kg^{-1})	2121	2123	2127	2135	2136	2113
	C_{ant} (μmol kg^{-1})	28	29	24	14	17	31
2000-2007	Thickness (m)	306	211	858	182	450	551
	DIC (μmol kg^{-1})	2161	2159	2158	2156	2158	2153
	DIC_{nat} (μmol kg^{-1})	2129	2123	2131	2135	2136	2112
	C_{ant} (μmol kg^{-1})	32	36	27	20	22	41
2008-2015	Thickness (m)	361	705	527	136	413	416
	DIC (μmol kg^{-1})	2162	2161	2161	2161	2161	2158
	DIC_{nat} (μmol kg^{-1})	2121	2117	2131	2138	2136	2112
	C_{ant} (μmol kg^{-1})	41	44	30	24	25	46

Paper III

6.3 Impact of recent North Atlantic freshening and cooling on the carbon cycle

Fröb, F., A. Olsen, M. Becker, L. Chafik, T. Johanessen, G. Reverdin, and A. Omar.
prepared for submission to GRL

III

Paper IV

6.4 Ocean Acidification in the Subpolar North Atlantic: mechanisms controlling pH changes

García-Ibáñez, M. I., P. Zunino, F. Fröb, L.I. Carracedo, A. Ríos, H. Mercier, A. Olsen, and F.F. Pérez.

Biogeosciences, **13**, 3701-3715 (2016)

IV

Biogeosciences, 13, 3701–3715, 2016
www.biogeosciences.net/13/3701/2016/
doi:10.5194/bg-13-3701-2016

Biogeosciences Open Access EGU

Ocean acidification in the subpolar North Atlantic: rates and mechanisms controlling pH changes

Maribel I. García-Ibáñez[1], Patricia Zunino[2], Friederike Fröb[3], Lidia I. Carracedo[4], Aida F. Ríos[†], Herlé Mercier[5], Are Olsen[3], and Fiz F. Pérez[1]

[1]Instituto de Investigaciones Marinas, IIM-CSIC, Vigo, E36208, Spain
[2]Ifremer, Laboratoire d'Océanographie Physique et Spatiale, UMR 6523 CNRS/Ifremer/IRD/UBO, Ifremer Centre de Brest, Plouzané, CS 10070, France
[3]Geophysical Institute, University of Bergen and Bjerknes Centre for Climate Research, Bergen, N5007, Norway
[4]Faculty of Marine Sciences, University of Vigo, Vigo, E36200, Spain
[5]CNRS, Laboratoire d'Océanographie Physique et Spatiale, UMR 6523 CNRS/Ifremer/IRD/UBO, Ifremer Centre de Brest, Plouzané, CS 10070, France
[†]deceased

Correspondence to: Maribel I. García-Ibáñez (maribelgarcia@iim.csic.es)

Received: 24 February 2016 – Published in Biogeosciences Discuss.: 29 February 2016
Revised: 24 May 2016 – Accepted: 27 May 2016 – Published: 23 June 2016

Abstract. Repeated hydrographic sections provide critically needed data on and understanding of changes in basin-wide ocean CO_2 chemistry over multi-decadal timescales. Here, high-quality measurements collected at twelve cruises carried out along the same track between 1991 and 2015 have been used to determine long-term changes in ocean CO_2 chemistry and ocean acidification in the Irminger and Iceland basins of the North Atlantic Ocean. Trends were determined for each of the main water masses present and are discussed in the context of the basin-wide circulation. The pH has decreased in all water masses of the Irminger and Iceland basins over the past 25 years with the greatest changes in surface and intermediate waters (between -0.0010 ± 0.0001 and -0.0018 ± 0.0001 pH units yr^{-1}). In order to disentangle the drivers of the pH changes, we decomposed the trends into their principal drivers: changes in temperature, salinity, total alkalinity (A_T) and total dissolved inorganic carbon (both its natural and anthropogenic components). The increase in anthropogenic CO_2 (C_{ant}) was identified as the main agent of the pH decline, partially offset by A_T increases. The acidification of intermediate waters caused by C_{ant} uptake has been reinforced by the aging of the water masses over the period of our analysis. The pH decrease of the deep overflow waters in the Irminger basin was similar to that observed in the upper ocean and was mainly linked to the C_{ant} increase, thus reflecting the recent contact of these deep waters with the atmosphere.

1 Introduction

The oceanic uptake of a fraction of the anthropogenic CO_2 (i.e. C_{ant}; CO_2 released from humankind's industrial and agricultural activities) has resulted in long-term changes in ocean CO_2 chemistry, commonly referred to as ocean acidification (OA; e.g. Caldeira and Wickett, 2003, 2005; Raven et al., 2005; Doney et al., 2009; Feely et al., 2009). The changes in the ocean CO_2 chemistry result in declining pH and reduced saturation states for $CaCO_3$ minerals (e.g. Bates et al., 2014). The average pH ($-\log_{10}[H^+]$) of ocean surface waters has decreased by about 0.1 pH units since the beginning of the industrial revolution (1750), and based on model projections we expect an additional drop of 0.1–0.4 by the end of this century, even under conservative CO_2 emission scenarios (Caldeira and Wickett, 2005; Orr, 2011; Ciais et al., 2013). The rate of change in pH is at least a hundred times faster than at any time since the last ice age (Feely et al., 2004; Raven et al., 2005), clearly outpacing natural processes in ocean chemistry that have occurred in the past due to geological processes (Raven et al., 2005). These changes

in ocean CO_2 chemistry will most likely have adverse effects on organisms, particularly calcifying ones; ecosystems (e.g. Langdon et al., 2000; Riebesell et al., 2000; Pörtner et al., 2004) and major marine biogeochemical cycles (e.g. Gehlen et al., 2011; Matear and Lenton, 2014).

The global ocean has absorbed $\sim 30\,\%$ of the C_{ant} emitted to the atmosphere between 1750 and the present (Sabine et al., 2004; Khatiwala et al., 2013; DeVries, 2014; Le Quéré et al., 2015). This C_{ant} is not evenly distributed throughout the oceans (Sabine et al., 2004), but enters the interior ocean preferentially in regions of deep convective overturning and subduction (Maier-Reimer and Hasselmann, 1987; Sarmiento et al., 1992; Lazier et al., 2002). This explains why the meridional overturning circulation (MOC) makes the North Atlantic Ocean one of the most important C_{ant} sinks of the global ocean, storing 25 % of the global oceanic C_{ant} (Sabine et al., 2004; Khatiwala et al., 2013) despite being only 11 % of the global ocean volume (Eakins and Sharman, 2010). The MOC transports C_{ant}-laden surface waters from the Equator to the northern North Atlantic Ocean (e.g. Wallace, 2001; Anderson and Olsen, 2002; Olsen et al., 2006; Zunino et al., 2015), where deep water formation provides a pathway for C_{ant} into the interior ocean (Lazier et al., 2002; Pérez et al., 2008, 2013; Steinfeldt et al., 2009). Being regions close to deep water formation areas and where water mass transformation occurs (Sarafanov et al., 2012; García-Ibáñez et al., 2015), the Irminger and Iceland basins are geographically well placed to monitor temporal changes in the Atlantic MOC (Mercier et al., 2015) and to determine the rates of C_{ant} penetration to the deep ocean and its consequence for OA.

In this paper, we examine high-quality direct measurements of ocean CO_2 chemistry from twelve cruises conducted across the Irminger and Iceland basins between 1991 and 2015. Previous studies focused on C_{ant} uptake and its storage and effect on pH in the Irminger and Iceland basins (e.g. Pérez et al., 2008; Olafsson et al., 2009; Bates et al., 2012; Vázquez-Rodríguez et al., 2012b). Here we quantify the pH change for a 25-year period and identify its chemical and physical drivers by decomposing the observed pH change into five numerically estimated factors (temperature, salinity, alkalinity, anthropogenic CO_2 and non-anthropogenic CO_2), all based on direct measurements.

2 Materials and methods

2.1 Datasets

2.1.1 Cruise Information

We used data from twelve cruises along the same track across the Irminger and Iceland basins, with the cruise dates spanning 25 years (1991–2015; Table 1, Fig. 1a). The bottle data were accessed from the merged data product of the

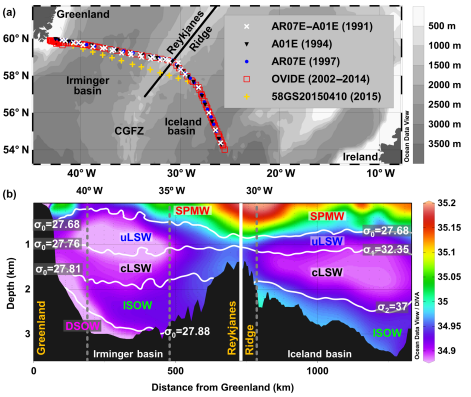

Figure 1. (a) Sampling locations of the twelve cruises used in this study (1991–2015) plotted on bathymetry (500 m intervals). The black line shows the boundary between the Irminger and the Iceland basins constituted by the Reykjanes Ridge. CGFZ stands for Charlie–Gibbs Fracture Zone. **(b)** Limits of the layers and basins considered in this study plotted on top of the salinity distribution for the 2004 cruise. The isopycnals delineating the layers are defined by potential density (referenced to 0 dbar, σ_0; 1000 dbar, σ_1; and 2000 dbar, σ_2; all in kg m^{-3}) and the vertical white line is the limit (Reykjanes Ridge) between the Irminger (left) and Iceland basins (right). The dashed vertical lines represent the longitude axis marks. The layer acronyms are Subpolar Mode Water (SPMW), upper and classical Labrador Sea Water (uLSW and cLSW, respectively), Iceland–Scotland Overflow Water (ISOW) and Denmark Strait Overflow Water (DSOW).

Global Data Analysis Project version 2 (GLODAPv2; Olsen et al., 2016) at http://cdiac.ornl.gov/oceans/GLODAPv2, except for more recent data collected during the OVIDE 2012 and 2014 cruises and the 2015 cruise (58GS20150410). The data of the 1991 cruises (64TR91_1 and 06MT18_1) were merged and treated as a single cruise.

2.1.2 Ocean CO_2 chemistry measurements

The twelve cruises selected for our study have high-quality measurements of the seawater CO_2 system variables (Table 1). Total alkalinity (A_T) was analysed by potentiometric titration and determined by developing either a full titration curve (Millero et al., 1993; Dickson and Goyet, 1994; Ono et al., 1998) or from single point titration (Pérez and Fraga, 1987; Mintrop et al., 2000) and was calibrated with certified reference materials (CRMs) with an overall accuracy of 4 µmol kg^{-1}. For samples without direct A_T measurements, A_T was estimated using a 3-D moving window multilinear regression algorithm (3DwMLR), using potential temperature (θ), salinity, nitrate, phosphate, silicate and

Table 1. List of hydrographic cruises used in this study (Fig. 1a). P.I. denotes principal investigator, #St the number of stations used here and "Measurements" refers to the seawater CO_2 system measurements performed during these cruises.

Cruise name	Expocode	Month yr^{-1}	Vessel	P.I.	#St	Measurements	Reference
AR07E	64TR91_1	04–05/1991	*Tyro*	H. M. van Aken	12	DIC	Stoll et al. (1996)
A01E	06MT18_1	09/1991	*Meteor*	J. Meincke	15	A_T and DIC	Meincke and Becker (1993)
A01E	06MT30_3	11–12/1994	*Meteor*	J. Meincke	27	DIC	Koltermann et al. (1996)
AR07E	06MT39_5	08–09/1997	*Meteor*	A. Sy	32	DIC	Rhein et al. (2002)
OVIDE 2002	35TH20020610	06–07/2002	*Thalassa*	H. Mercier	38	pH and A_T	Lherminier et al. (2007)
OVIDE 2004	35TH20040604	06–07/2004	*Thalassa*	T. Huck	56	pH and A_T	Lherminier et al. (2010)
OVIDE 2006	06MM20060523	05–06/2006	*Maria S. Merian*	P. Lherminier	44	pH and A_T	Gourcuff et al. (2011)
OVIDE 2008	35TH20080610	06–07/2008	*Thalassa*	H. Mercier	45	pH and A_T	Mercier et al. (2015)
OVIDE 2010	35TH20100610	06/2010	*Thalassa*	T. Huck; H. Mercier	46	pH and A_T	Mercier et al. (2015)
CATARINA*	29AH20120623	06–07/2012	*Sarmiento de Gamboa*	A. F. Ríos	44	pH and A_T	This work
GEOVIDE*	35PQ20140517	05–06/2014	*Pourquoi Pas?*	G. Sarthou	31	pH and A_T	This work
58GS20150410	58GS20150410	04–05/2015	*G.O. Sars*	A. Olsen	10	A_T and DIC	Fröb et al. (2016)

* Both CATARINA (http://catarina.iim.csic.es/en) and GEOVIDE (http://www.geovide.obs-vlfr.fr) cruises contain the OVIDE section (http://www.umr-lops.fr/Projets/Projets-actifs/OVIDE) and in the study are referred to as OVIDE 2012 and 2014, respectively.

oxygen as predictor parameters (Velo et al., 2013). The total dissolved inorganic carbon (DIC) samples were analysed with coulometric titration techniques (Johnson et al., 1993) and calibrated with CRMs, achieving an overall accuracy of 2 µmol kg^{-1}. For the cruises for which direct DIC measurements had not been performed, it was computed from A_T and pH using the thermodynamic equations of the seawater CO_2 system (Dickson et al., 2007) and the CO_2 dissociation constants of Mehrbach et al. (1973) refitted by Dickson and Millero (1987). These calculated DIC values have an associated uncertainty of 4 µmol kg^{-1}, calculated by random propagation of the reported A_T and pH accuracies. pH was determined at 25 °C and 1 atm with a spectrophotometric method (Clayton and Byrne, 1993) using diode array spectrophotometers and m-cresol purple as an indicator. The spectrophotometric pH determination has a typical precision of 0.0002–0.0004 pH units (Clayton and Byrne, 1993; Liu et al., 2011). However, Carter et al. (2013) reported an inherent uncertainty of spectrophotometric pH determinations of 0.0055 pH units, associated to the tris-buffer used for calibration. When direct pH measurements were not performed, pH was computed from A_T and DIC using the thermodynamic equations of the seawater CO_2 system (Dickson et al., 2007) and the CO_2 dissociation constants of Mehrbach et al. (1973) refitted by Dickson and Millero (1987). For these calculated pH values, we estimated an uncertainty of 0.006 pH units by random propagation of the reported A_T and DIC accuracies. A_T values differing by more than two times the standard deviation (7 µmol kg^{-1}) of the difference between measured A_T and 3DwMLR-predicted A_T were replaced with the predicted A_T value. Note that the effect of A_T corrections on pH trends is negligible, since A_T corrections of 4 µmol kg^{-1} lead to pH changes lower than a thousandth. The pH values reported here are at in situ conditions (of temperature and pressure) and on the total scale ($pH_{T_{is}}$).

2.1.3 Anthropogenic CO_2 (i.e. C_{ant}) estimation

C_{ant} concentrations were estimated using the back-calculation method φC_T^0 (Pérez et al., 2008; Vázquez-Rodríguez, 2009a) that has previously been applied for the entire Atlantic Ocean (Vázquez-Rodríguez et al., 2009b). Back-calculation methods determine C_{ant} for any sample in the water column as the difference between DIC concentration at the time of the measurement and the DIC concentration it would have had in preindustrial times. Following Gruber et al. (1996), this is represented as the difference in preformed DIC between the time of observation and the preindustrial:

$$C_{ant} = DIC_{meas} - \Delta C_{bio} - DIC_{preind} - \Delta C_{diseq}, \quad (1)$$

where the preformed DIC for the time of observation is represented as the measured DIC (DIC_{meas}) minus any DIC added to the water due to organic matter remineralisation and calcium carbonate dissolution (ΔC_{bio}). The preindustrial preformed concentration is represented by the DIC concentration the water would have if in equilibrium with the preindustrial atmosphere (DIC_{preind}) minus any offset from such an equilibrium value, known as the disequilibrium term (ΔC_{diseq}). The procedure requires DIC and A_T as input parameters, and the empirical parameterisation of the preformed A_T (A_T^0) for the computation of the calcium carbonate dissolution and of the ΔC_{diseq} term (Vázquez-Rodríguez et al., 2012a). The A_T^0 is based on the concept of potential alkalinity ($PA_T = A_T + NO_3 + PO_4$) and is defined as $A_T^0 = PA_T - (NO_3^0 + PO_4^0)$ (Vázquez-Rodríguez et al., 2012a), where NO_3^0 and PO_4^0 are the preformed nitrate and phosphate concentrations, respectively. NO_3^0 and PO_4^0 are determined as $NO_3^0 = NO_3 - AOU / R_{ON}$ and $PO_4^0 = PO_4 - AOU / R_{OP}$. In the former equations AOU (apparent oxygen utilisation) is the difference between the saturated concentrations of oxygen calculated using the equations of Benson and Krause (1984) and the measured con-

centrations of oxygen, while R_{ON} and R_{OP} are the Redfield ratios proposed by Broecker (1974).

The φC_T^0 method presents two main advantages relative to the previous method proposed by Gruber et al. (1996). First, the spatiotemporal variability of A_T^0 is taken into account. And second, the parameterisations of A_T^0 and ΔC_{diseq} are determined using the subsurface layer as a reference (Vázquez-Rodríguez et al., 2012a), where the age of the water parcel, and therefore its C_{ant} concentration, is estimated using CFC measurements (Waugh et al., 2006). The overall uncertainty of the φC_T^0 method has been estimated at 5.2 µmol kg^{-1} (Pérez et al., 2008; Vázquez-Rodríguez, 2009a).

2.1.4 Trend uncertainty

The uncertainties and reproducibilities of the analysis and calculation methods were determined from the deep waters sampled at the Iberian Abyssal Plain during the seven repetitions of the OVIDE line, since these waters are expected to be in near steady state. The standard deviations of those samples for each cruise (Table 2) were taken as an estimate of the uncertainty at each cruise. The uncertainties of the AOU, A_T and $pH_{T_{is}}$ for the seven cruises were similar. The standard deviations of C_{ant} (1.2–1.6 µmol kg^{-1}) and $pH_{T_{is}}$ (0.002–0.003 pH units) for each of the seven cruises are lower than the inherent uncertainty of the φC_T^0 estimates (5.2 µmol kg^{-1}) and the accuracy of the spectrophotometric pH measurements (0.0055 pH units), which provides confidence that these data are suitable for trend determination. The standard deviations of the C_{ant} estimates are rather similar to those from other regions where C_{ant} has been compared across many cruises (i.e. 2.4 µmol kg^{-1} in the South Atlantic Ocean, Ríos et al. (2003); 2.7 µmol kg^{-1} in the equatorial Atlantic Ocean, 24° N, Guallart et al. (2015); and 2.7 µmol kg^{-1} reported from a transect along the western boundary of the Atlantic Ocean from 50° S to 36° N, Ríos et al., 2015). The standard deviations of the mean values of the Iberian Abyssal Plain samples across all (last row of Table 2) were taken as an estimate of the reproducibility of the methodologies. The high reproducibility of the pH measurements, at an order of magnitude higher than the uncertainty (0.0055 pH units, Carter et al., 2013), is suggestive of high quality data. Using these standard deviations for the seven cruises, and taking into account the 25 years considered in this study, the threshold of detectability of pH trends at 95 % of confidence is 0.00012 pH units yr^{-1}, which renders confidence to the estimated trends.

2.2 Water mass characterisation

Changes in ocean CO_2 chemistry were determined for the main water masses in the Irminger and Iceland basins. These are (1) Subpolar Mode Water (SPMW), (2) upper and classical Labrador Sea Water (uLSW and cLSW, respectively), (3) Iceland–Scotland Overflow Water (ISOW) and (4) Denmark Strait Overflow Water (DSOW; Fig. 1b). The layers defining the water masses were delimited using potential density following Azetsu-Scott et al. (2003), Kieke et al. (2007), Pérez et al. (2008) and Yashayaev et al. (2008). The advantage of working in layers is the relatively low variability of the physical and chemical properties within the layers, allowing us to assume linearity in the ocean CO_2 system.

To better determine the limits between layers and the average value of each variable in each layer, cruise bottle data were linearly interpolated onto each dbar before determining average variable values, an improvement with respect to the previous approaches of Pérez et al. (2008, 2010) and Vázquez-Rodríguez et al. (2012b). Then, the interpolated profiles were averaged over each density layer, defined in Figure 1b. Finally, the average values in each density layer were determined for each cruise taking into account the thickness of the layer and the separation between stations. The exception comes with $pH_{T_{is}}$, which is pressure sensitive and for which we needed to define a unique reference pressure to remove pressure effects due to varying sampling strategies. $pH_{T_{is}}$ was calculated using the layer average values of DIC and A_T for the considered year but using the time-averaged pressure of the layer over the studied time period as reference pressure. To reduce the influence of seasonal differences in sampling on the interannual trends, only samples with pressure $\geq$ 75 dbar were considered. The 75 dbar level was determined by the depth of the seasonal nutrients drawdown along the section. The average values of the variables for each layer and their standard deviations can be found in the Supplement (Table S1).

2.3 pH deconvolution

Changes in ocean pH may be brought about by changes in in situ temperature (T_{is}), salinity (S), A_T and/or DIC. Changes in the latter may be brought about by C_{ant} uptake or by natural processes (C_{nat}) such as remineralisation. C_{nat} is determined as the difference between measured DIC and estimated C_{ant}. Changes in temperature and salinity influence the equilibrium constants of the oceanic CO_2 system. Additionally, changes in salinity influence the borate concentration, which is taken into account by the relationship proposed by Uppström (1974).

To estimate how much each of these five factors have contributed to the observed change in pH, we assumed linearity and decomposed the observed pH changes into these potential drivers:

$$\left(\frac{\mathrm{d}pH_{T_{is}}}{\mathrm{d}t}\right)_{total} = \frac{\partial pH_{T_{is}}}{\partial T_{is}}\frac{\mathrm{d}T_{is}}{\mathrm{d}t} + \frac{\partial pH_{T_{is}}}{\partial S}\frac{\mathrm{d}S}{\mathrm{d}t} + \frac{\partial pH_{T_{is}}}{\partial A_T}\frac{\mathrm{d}A_T}{\mathrm{d}t} + \frac{\partial pH_{T_{is}}}{\partial DIC}\left(\frac{\mathrm{d}C_{ant}}{\mathrm{d}t} + \frac{\mathrm{d}C_{nat}}{\mathrm{d}t}\right). \quad (2)$$

To estimate $\frac{\partial pH_{T_{is}}}{\partial var}$ (where "var" refers to each of the drivers: T_{is}, S, A_T and DIC) we calculated a $pH_{T_{is}}$ for each layer and

Table 2. Mean values of pressure (in dbar), potential temperature (θ, in °C), salinity, apparent oxygen utilisation (AOU, in µmol kg^{-1}), total alkalinity (A_T, in µmol kg^{-1}), anthropogenic CO_2 (C_{ant}, in µmol kg^{-1}) and pH at total scale and in situ conditions of temperature and pressure ($pH_{T_{is}}$) for the bottom waters of the Iberian Abyssal Plain sampled during the seven OVIDE cruises. "N" represents the number of data considered in each cruise and "±" the standard deviation. The last row represents the intercruise standard deviation of the mean values.

Year (N)	Pressure	θ	Salinity	AOU	A_T	C_{ant}	$pH_{T_{is}}$
2002 (144)	4205	2.182 ± 0.080	34.913 ± 0.008	86.1 ± 2.0	2351 ± 3	6.4 ± 1.3	8. 013 ± 0.003
2004 (158)	4263	2.162 ± 0.075	34.908 ± 0.007	87.1 ± 1.4	2352 ± 3	6.2 ± 1.2	8.013 ± 0.003
2006 (132)	4252	2.170 ± 0.082	34.913 ± 0.008	85.4 ± 1.6	2350 ± 3	6.2 ± 1.3	8.014 ± 0.003
2008 (125)	4206	2.179 ± 0.075	34.911 ± 0.007	84.9 ± 1.8	2353 ± 4	7.0 ± 1.6	8.016 ± 0.003
2010 (131)	4312	2.163 ± 0.077	34.908 ± 0.008	85.9 ± 1.6	2351 ± 3	7.0 ± 1.2	8.013 ± 0.002
2012 (102)	4397	2.149 ± 0.077	34.909 ± 0.008	87.9 ± 1.6	2352 ± 3	5.1 ± 1.2	8.015 ± 0.002
2014 (54)	4441	2.141 ± 0.069	34.904 ± 0.007	87.4 ± 1.36	2353 ± 3	5.5 ± 1.5	8.016 ± 0.003
		0.015	0.003	1.1	1.1	0.7	0.0015

year using the layer average value of "var" for each year but keeping the values of the other drivers constant and equal to the time-average value for the layer over the studied time period. Given that the variability of the physicochemical properties within each layer is relatively low (see standard deviations of the averaged values in Table S1), we can assume that these derivatives are constant over the studied time period and use a constant derivative value for each layer. Note that the sensitivity of $pH_{T_{is}}$ to changes in C_{ant} is the same as the sensitivity to changes in C_{nat} since both are DIC; therefore only $\frac{\partial pH_{T_{is}}}{\partial DIC}$ is necessary. To estimate each $\frac{dvar}{dt}$ term we performed a linear regression between var and time for each layer.

Due to the small range of pH change with which we are working and the relatively low pH variability within each layer, we can consider that pH follows a linear scale instead of a logarithmic scale. As a consequence the contributions of each of the terms considered in Eq. (2) to pH change are equivalent to the contributions in terms of $[H^+]$.

Trends of all variables involved in Eq. (2) were calculated based on the annual interpolation of the observed values to avoid the bias due to the reduced availability of cruises during the 1990s compared to the 2000s.

3 Results and discussion

3.1 Distribution of water mass properties

The Irminger and Iceland basins in the North Atlantic are characterised by warm and saline surface waters as well as cold and less saline intermediate and deep waters (Fig. 2a, b). The central waters (here represented by the SPMW layer), which dominates the upper ∼ 700 m, are warmer and saltier in the Iceland basin than in the Irminger basin, reflecting the water mass transformation that takes place along the path of the North Atlantic Current (NAC) (Brambilla and Talley, 2008). In particular, the mixing of the SPMW layer with the surrounding waters while flowing around the Reykjanes Ridge (evident in the salinity distribution; see also García-Ibáñez et al., 2015), in conjunction with the air–sea heat loss, results in a colder and fresher SPMW layer in the Irminger basin. The uLSW and cLSW layers below the SPMW layer are saltier in the Iceland basin due to their mixing with the surrounding waters during their journey from their formation regions (Bersch et al., 1999; Pickart et al., 2003; García-Ibáñez et al., 2015). The ISOW layer dominates at depths beneath the cLSW layer. This layer is saltier in the Iceland basin, reflecting its circulation. ISOW comes from the Iceland–Scotland sill and flows southwards into the Iceland basin, where it mixes with the older North Atlantic Deep Water (NADW). Then it crosses the Reykjanes Ridge through the Charlie–Gibbs Fracture Zone (Fig. 1a), where it mixes with the cLSW and DSOW, becoming fresher. At the bottom of the Irminger basin a fifth layer, DSOW, being the coldest and freshest layer of the section, is distinguished.

The general pattern of $pH_{T_{is}}$ (Fig. 2c) by and large follows the distribution expected from the surface production of organic material and remineralisation at depth. Consequently, high pH values (> 8.05) are found in upper layers, while the values generally decrease with depth down to < 7.95 in the deepest layers. This overall pattern is disrupted at ∼ 500 m in the Iceland basin by a layer with relatively low $pH_{T_{is}}$ values (< 7.98), coinciding with relatively high AOU and DIC values (Fig. 2e, f). This layer could be associated with an area of slower circulation where the products of the remineralisation of the organic matter accumulate. This thermocline layer could also be influenced by waters of southern origin (Sarafanov et al., 2008) which are advected into the region by the NAC, which has an extension that is closely related to the North Atlantic Oscillation (Desbruyères et al., 2013). The presence of this low pH layer lowers the average pH of our SPMW layer in the Iceland basin compared to the Irminger basin (Fig. 3). The opposite pattern is found in the uLSW layer. The water mass formation occurring in the Irminger basin (Pickart et al., 2003; García-Ibáñez et al., 2015; Fröb et al., 2016; Piron et al., 2016) transfers recently ventilated low DIC and high pH waters to depth, which causes the mean

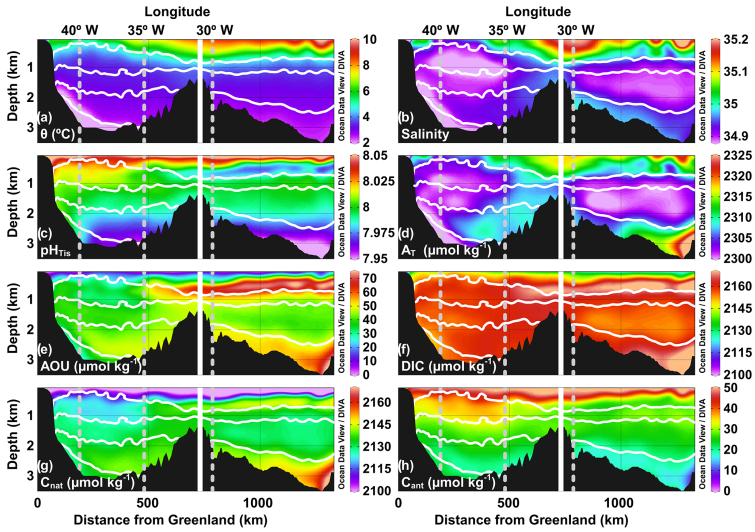

Figure 2. Distributions along the cruise track from Greenland (left) to the Iceland basin (right) over the study period (1991–2015) for **(a)** potential temperature (θ, in °C), **(b)** salinity, **(c)** pH at total scale and in situ conditions ($pH_{T_{is}}$), **(d)** total alkalinity (A_T, in µmol kg^{-1}), **(e)** apparent oxygen utilisation (AOU, in µmol kg^{-1}), **(f)** total dissolved inorganic carbon (DIC; in µmol kg^{-1}), **(g)** natural DIC (C_{nat}, in µmol kg^{-1}) and **(h)** anthropogenic CO_2 (C_{ant}, in µmol kg^{-1}) for the 2004 cruise. The dashed vertical lines represent the longitude axis marks, and isopycnals delineating the layers are shown as white lines.

pH of uLSW in the Irminger basin to be higher than in the Iceland basin. Finally, the layers that contain the overflow waters have the lowest pH values. The presence of the older NADW in the ISOW layer in the Iceland basin decreases the mean pH of this layer here, making it lower than in the Irminger basin.

The upper layer waters of the section have low DIC values, which rapidly increase when increasing depth (Fig. 2f). The low DIC values in the uppermost ∼ 200 m are a consequence of the photosynthetic activity that withdraws DIC from seawater. Below ∼ 200 m the DIC distribution is almost homogeneous, only disrupted by relatively high values in the Iceland basin at ∼ 500 m, associated with the thermocline layer, and at the bottom, associated with the old NADW. The gradients in anthropogenic and natural components of DIC are much stronger. The C_{ant} values are high, close to saturation (approximately 80 % of the C_{ant} concentration expected from a surface ocean in equilibrium with the atmospheric CO_2), near the surface and decrease with depth (Fig. 2h), because C_{ant} enters the ocean from the atmosphere. The C_{nat} distribution has an opposite pattern, with low surface values and high bottom values (Fig. 2g), similar to that of the AOU distribution (Fig. 2e), since C_{nat} is linked to the ventilation of water masses, i.e. respiration and renewal of the water mass.

The A_T distribution along the section resembles the salinity distribution, with high values associated with the relatively saline central waters and relatively low and almost homogeneous values in the rest of the section (Fig. 2d). The exception comes with the ISOW layer. The high A_T values found in the ISOW layer of the Iceland basin are not mirrored in the salinity distribution. This reflects the influence of NADW that is traced by the relatively large amounts of silicate related to the influence of the Antarctic Bottom Water, which provides high A_T from dissolution of $CaCO_3$. The influence of these high A_T values is then transported by the ISOW circulation to the Irminger basin.

3.2 Water mass acidification and drivers

Trends of $pH_{T_{is}}$ in each layer and basin are presented in Table 3, in Fig. 3 and in Supplement Fig. S1. The $pH_{T_{is}}$ has decreased in all layers of the Irminger and Iceland basins during a time period of more than 20 years (1991–2015) that is covered by the data. The trends are stronger in the Irminger basin due to the presence of younger waters. The rate of pH decline decreases with depth, except for the DSOW layer that has acidification rates close to those found in the cLSW layer. This indicates that DSOW is a newly formed water mass that

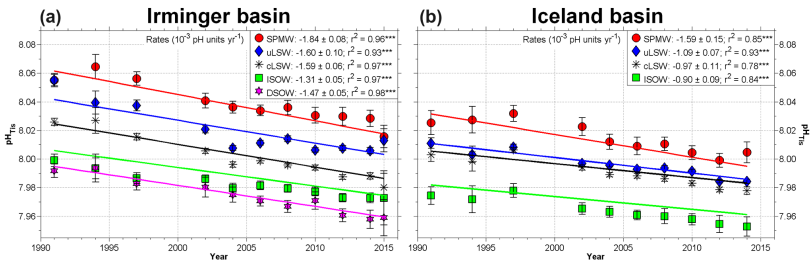

Figure 3. Temporal evolution of average pH at total scale and in situ conditions of temperature and pressure ($pH_{T_{is}}$) in the main water masses of the Irminger **(a)** and Iceland **(b)** basins between 1991 and 2015. Each point represents the average $pH_{T_{is}}$ of a particular layer (SPMW (red dots), uLSW (blue diamonds), cLSW (black asterisks), ISOW (green squares) and DSOW (magenta stars)) at the time of each cruise (Table S1). The error bars are two times the error of the mean ($2\sigma = 2\times$(Standard Deviation)$/\sqrt{N}$, where "N" is the number of samples of each layer). The legends also give the trends (in 10^{-3} pH units yr^{-1}) ± standard error of the estimate and the correlation coefficients (r^2), resulting from the annually interpolated values. *** denotes that the trend is statistically significant at the 99 % level (p value < 0.01). Consult Fig. 1 for layer acronyms.

has recently been in contact with the atmosphere. Moreover, the acidification rate in the ISOW layer in the Irminger basin is relatively low, which could be related to the increasing importance of the relatively old NADW in this layer, with the reduction in cLSW formation since the mid-90s (Lazier et al., 2002; Yashayaev, 2007).

The observed rate of $pH_{T_{is}}$ decrease in the SPMW layer of the Iceland basin (-0.0016 ± 0.0001 pH units yr^{-1}; Table 3, Fig. 3b) is in agreement with that observed at the Iceland Sea time series (68° N, 12.66° W; Olafsson et al., 2009, 2010) for the period 1983–2014 (-0.0014 ± 0.0005 pH units yr^{-1}; Bates et al., 2014). However, our rate of $pH_{T_{is}}$ decrease in the SPMW layer in the Irminger basin (-0.0018 ± 0.0001 pH units yr^{-1}) is lower than that observed in the sea surface waters of the Irminger Sea time series (64.3° N, 28° W; Olafsson et al., 2010) for the period 1983–2014 (-0.0026 ± 0.0006 pH units yr^{-1}; Bates et al., 2014), which is exceptionally high compared to the other time series summarised here. Bates et al. (2014) linked the high acidification rate found at the Irminger Sea time series to the high rate of increase in DIC (1.62 ± 0.35 µmol kg^{-1} yr^{-1}) observed at this site, which is almost three times our rate of increase in DIC (0.64 ± 0.07 µmol kg^{-1} yr^{-1}, Fig. 5c). This is based on data from only one site, further north than our section, and indicates that spatial variations are substantial in this region. Besides, the acidification rates in the SPMW layer of both basins reported here are in agreement with the rates of -0.0020 ± 0.0004 pH units yr^{-1} determined for the North Atlantic subpolar seasonally stratified biome for the period 1991–2011 (Lauvset et al., 2015). Compared to the subtropical Atlantic time series stations, our rates in the SPMW layer of both basins are in agreement with those observed at ESTOC (European Station for Time series in the ocean) (29.04° N, 15.50° W; Santana-Casiano et al., 2007; González-Dávila et al., 2010) for the period 1995–2014 (-0.0018 ± 0.0002 pH units yr^{-1}; Bates et al., 2014) and BATS (Bermuda Atlantic Time-series Study) (32° N, 64° W; Bates et al., 2014) for the period 1983–2014 (-0.0017 ± 0.0001 pH units yr^{-1}; Bates et al., 2014). Compared to the Pacific Ocean, the OA rates in the Iceland and Irminger basins are in agreement with those reported for the central North Pacific based on data from the time series station HOT (Hawaii Ocean Time-series) (22.45° N, 158° W; Dore et al., 2009) for the period 1988–2014 (-0.0016 ± 0.0001 pH units yr^{-1}; Bates et al., 2014), but are slightly higher than those determined by Wakita et al. (2013) in the winter mixed layer at the subarctic western North Pacific (time series stations K2 and KNOT) for the period 1997–2011 (-0.0010 ± 0.0004 pH units yr^{-1}). Wakita et al. (2013) attributed the lower-than-expected pH trends to an increasing A_T trend.

To infer the causes of the acidification trends reported here, we decomposed the pH trends into their individual components as described in Sect. 2.2. The values of each term, $\frac{\partial pH_{T_{is}}}{\partial var}$ and $\frac{dvar}{dt}$ (where "var" refers to each of the drivers), described in Sect. 2.2 can be found in the Supplement in Table S2 and Figs. 4–6, respectively. The results of solving Eq. (2) are presented in Table 3. The sum of the pH changes caused by the individual drivers, i.e. $\left(\frac{dpH_{T_{is}}}{dt}\right)_{total}$ matches the observed pH trends $\left(\left(\frac{dpH_{T_{is}}}{dt}\right)_{obs}\right)$, which renders confidence to the method.

The temperature changes (Fig. 4a, b) have generally resulted in small-to-negligible pH declines (Table 3). Specifically, warming corresponds to a pH decrease of at least 0.0002 pH units yr^{-1} in the SPMW layer of the Iceland basin

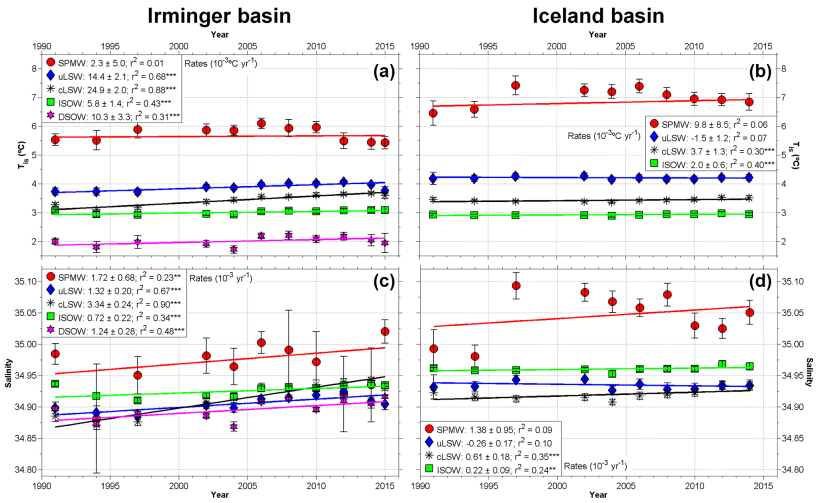

Figure 4. Temporal evolution between 1991 and 2015 of average **(a, b)** in situ temperature (T_{is}, in °C) and **(c, d)** salinity in the main water masses of the Irminger **(a, c)** and Iceland **(b, d)** basins. Each point represents the average property of a particular layer (SPMW (red dots), uLSW (blue diamonds), cLSW (black asterisks), ISOW (green squares) and DSOW (magenta stars)) at the time of each cruise (Table S1). The error bars are 2σ. The legends also give the trends (in 10^{-3} units yr^{-1}) ± standard error of the estimate and the correlation coefficients (r^2), resulting from the annually interpolated values. ** denotes that the trend is statistically significant at the 95 % level (p value < 0.05) and *** at the 99 % level (p value < 0.01). Consult Fig. 1 for layer acronyms.

and in the LSW and DSOW layers of the Irminger basin, while the effect of temperature changes on pH in the other layers is negligible. Temperature-driven pH change is larger in the LSW layers in the Irminger than in the Iceland basin. In the case of the uLSW layer, this is possibly explained by the deep convection occurring in the Irminger basin (Pickart et al., 2003; García-Ibáñez et al., 2015; Fröb et al., 2016; Piron et al., 2016). In the case of the cLSW layer, the higher pH changes driven by temperature changes in the Irminger basin could be explained by the rapid advection of the water mass from the Labrador Sea to this basin (Yashayaev et al., 2007). Temperature driven pH change in the DSOW layer could be related to the entrainment of LSW into DSOW that takes place downstream of the Greenland–Iceland sills (Read, 2000; Yashayaev and Dickson, 2008). The temperature effect on pH evaluated here is thermodynamic. The same applies to the salinity effect, which however is small to negligible, reflecting how salinity changes in the region (Fig. 4c, d) are insufficiently large to significantly change pH.

Overall, the A_T has increased in the Irminger and Iceland basins (Fig. 5a, b), corresponding to increasing pH (Table 3), which counteracts the acidification from the CO_2 absorption. The contribution from A_T to reduce ocean acidification is significant in all layers except for uLSW of the Iceland basin (where the trend in A_T is decreasing, but not significant; Fig. 5b). The similar behaviour of the salinity and A_T trends over time may indicate that the changes in A_T are mainly driven by changes in salinity. The A_T increasing trends observed in the SPMW layer could be related to the increasing presence of waters of subtropical origin (with higher A_T) as the subpolar gyre was shrinking from the mid-90s into the 2000s (e.g. Flatau et al., 2003; Häkkinen and Rhines, 2004; Böning et al., 2006). In the case of the LSW layers, the increase in A_T can be explained by the mid-90s cessation of the cLSW formation (Lazier et al., 2002; Yashayaev, 2007), with the consequent salinisation (and increase in A_T) of this water mass. The signal of the cLSW salinisation was then transmitted to the overflow layers due to the entrainment events (Sarafanov et al., 2010).

The DIC increase (Fig. 5c, d) is the main cause of the observed pH decreases (Table 3) and corresponds to pH drops between -0.00099 ± 0.00014 and -0.00205 ± 0.00011 pH units yr^{-1}. The waters in both the Irminger and Iceland basins gained DIC in response to the increase in atmospheric CO_2; the convection processes occurring in the former basin (Pickart et al., 2003; Thierry et al., 2008; de Boisséson et al., 2010; García-Ibáñez et al., 2015; Fröb et al., 2016; Piron et al., 2016) and in the sur-

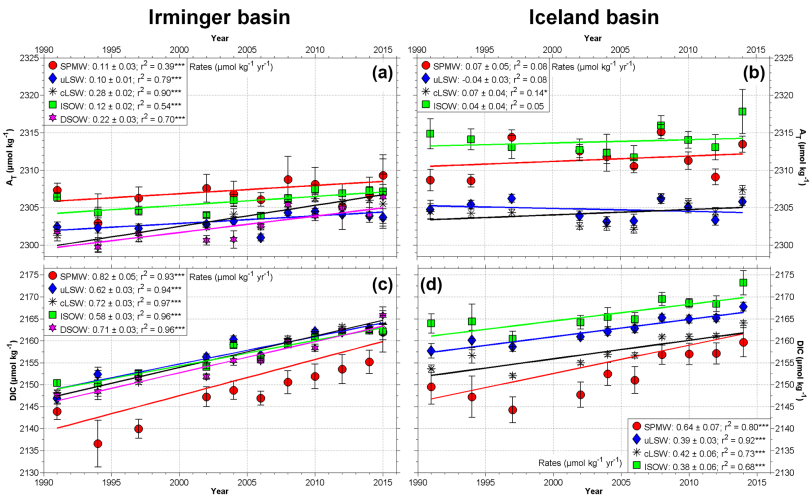

Figure 5. Temporal evolution between 1991 and 2015 of average **(a, b)** total alkalinity (A_T, in µmol kg^{-1}) and **(c, d)** total dissolved inorganic carbon (DIC, in µmol kg^{-1}) in the main water masses of the Irminger **(a, c)** and Iceland **(b, d)** basins. Each point represents the average property of a particular layer (SPMW (red dots), uLSW (blue diamonds), cLSW (black asterisks), ISOW (green squares) and DSOW (magenta stars)) at the time of each cruise (Table S1). The error bars are 2σ. The legends also give the trends (in µmol kg^{-1} yr^{-1}) ± standard error of the estimate and the correlation coefficients (r^2), resulting from the annually interpolated values. * denotes that the trend is statistically significant at the 90 % level (p value < 0.1) and *** at the 99 % level (p value < 0.01). Consult Fig. 1 for layer acronyms.

rounding ones (i.e. Labrador and Nordic seas) provide an important pathway for DIC to pass from the surface mixed layer to the intermediate and deep layers. The effect of the DIC increase on pH is generally dominated by the anthropogenic component (Table 3). The exception comes with the cLSW layer of the Irminger basin, where the natural component resulting from the aging of the layer dominates. In general, the Irminger basin layers have higher C_{ant} increase rates than the Iceland basin layers (Fig. 6a, b) and therefore larger pH declines, presumably a result of convection in the Irminger basin itself and advection of newly ventilated waters from the Labrador Sea. The highest C_{ant} increase rates are found in the SPMW layers, owing to their direct contact with the atmosphere, and result in the strongest rates of pH decrease. In the Irminger basin, the rise in C_{ant} levels of the SPMW layer correspond to about 87 % of the rate expected from a surface ocean maintaining its degree of saturation with the atmospheric CO_2 rise (computed using the globally averaged marine surface annual mean pCO_2 data from the NOAA as a reference, ftp://aftp.cmdl.noaa.gov/products/trends/co2/co2_annmean_gl.txt), while in the Iceland basin, this rate is about 73 % of the expected rate. The lower fraction in the Iceland basin compared to the Irminger basin is a consequence of the inclusion of the aforementioned poorly ventilated thermocline waters in our SPMW layer (Fig. 2e, h). Note than none of the C_{ant} trends of the SPMW layers correspond to 100 % of the rate expected from assuming saturation with the atmospheric CO_2 rise. This can be explained by the fact that surface water CO_2 concentration rise lags behind that of the atmosphere by between two and five years in this region (Biastoch et al., 2007; Jones et al., 2014). We also note that the temperature and A_T changes impact the pH of the SPMW layer, decreasing and increasing it, respectively. This could indicate that the increasing presence of warmer and more saline (with higher A_T) waters of subtropical origin partially counteracts the effects of increasing DIC values, because A_T effects dominate (as stated before, the effect of salinity change on pH is negligible). Overall this change can be explained as the result of the contraction of the subpolar gyre that took place since the mid-90s (e.g. Flatau et al., 2003; Häkkinen and Rhines, 2004; Böning et al., 2006). Wakita et al. (2013) also found lower-than-expected acidification rates in the surface waters of the Pacific Ocean, which they explained as being the consequence of increasing A_T. Finally, the strong influence of the anthropogenic component on the pH decrease of the DSOW layer stands out and is the main agent of the pH decline in this layer.

The pH changes related to C_{nat} changes (Fig. 6c, d) can be interpreted as changes related to ventilation of water masses and water mass changes (with different A_T and DIC).

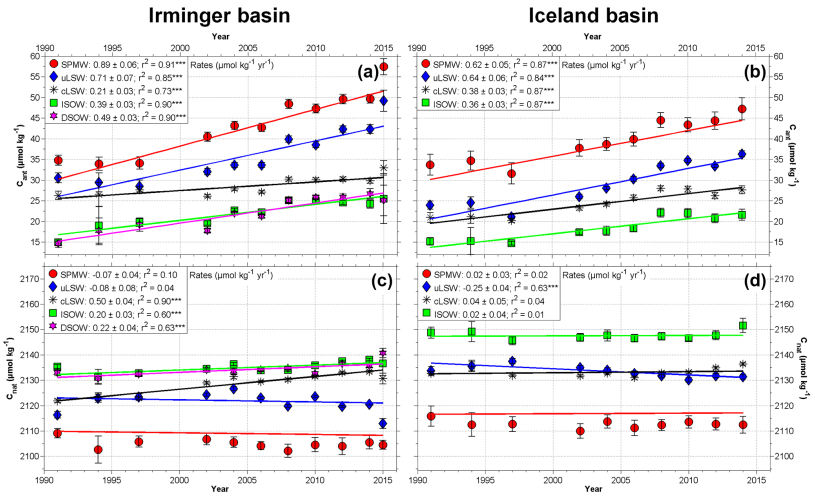

Figure 6. Temporal evolution between 1991 and 2015 of average **(a, b)** anthropogenic CO_2 (C_{ant}, in µmol kg^{-1}) and **(c, d)** natural DIC ($C_{nat} = DIC - C_{ant}$, in µmol kg^{-1}) values in the main water masses of the Irminger **(a, c)** and Iceland **(b, d)** basins. Each point represents the average property of a particular layer (SPMW (red dots), uLSW (blue diamonds), cLSW (black asterisks), ISOW (green squares) and DSOW (magenta stars)) at the time of each cruise (Table S1). The error bars are 2σ. The legends also give the trends (in µmol kg^{-1} yr^{-1}) ± standard error of the estimate and the correlation coefficients (r^2), resulting from the annually interpolated values. *** denotes that the trend is statistically significant at the 99 % level (p value < 0.01). Consult Fig. 1 for layer acronyms.

Stronger pH decreases related to C_{nat} changes indicate a lack of ventilation and accumulation of DIC from remineralised organic material. This is clearly the case for the cLSW layer, where the observed pH decrease is caused by a combination of the effects of C_{ant} and C_{nat} (Table 3). The greater influence of C_{nat} in the cLSW layer is the result of the ageing of this water mass after its last formation event in the mid-90s (e.g. Lazier et al., 2002; Azetsu-Scott et al., 2003; Kieke et al., 2007; Yashayaev, 2007). A similar effect of C_{nat} changes on pH is observed in the overflow layers of the Irminger basin, which are influenced by the mixing with cLSW (García-Ibáñez et al., 2015). Finally, there is a contrast between the C_{nat} influence on the pH of the uLSW layer in both basins. The interannual variability of the uLSW properties attenuates due to mixing over the length and timescales of the transit from the Labrador Sea (Cunningham and Haine, 1995; Paillet et al., 1998), which causes the interannual variability in the C_{nat} values of the uLSW layer in the Iceland basin to be smoother than in the Irminger basin (Fig. 6c, d). Therefore, the lower interannual variability in the C_{nat} values of the uLSW layer in the Iceland basin promotes better detectability of the ventilation of the uLSW layer, resulting in an offset up to 60 % of the effects of acidification on the uLSW layer of the Iceland basin.

Vázquez-Rodríguez et al. (2012b) previously studied the pH changes in the different water masses of the Irminger and Iceland basins. These authors carried out a pH normalisation to avoid potential biases due to different ventilation stages and rates of each layer from the different spatial coverage of the evaluated cruises. The normalised pH values (pH_N) for each layer were obtained using multiple linear regressions between the observed mean pH_{SWS25} (pH at seawater scale and 25 °C) and the observed mean values of θ, salinity, silicate and AOU, referring to the mean climatological values of θ, salinity, silicate and AOU compiled in WOA05 (http://www.nodc.noaa.gov/OC5/WOA05/pr_woa05.html). This normalisation, combined with the different temporal coverage (1981–2008), causes the rates reported by Vázquez-Rodríguez et al. (2012b) to differ from those obtained in the present work. The pH_N trends reported for the SPMW and uLSW layers of the Irminger basin and for the ISOW layer of the Iceland basin are very similar to our $pH_{T_{is}}$ trends for these layers. However, the pH_N trends reported by Vázquez-Rodríguez et al. (2012b) for the cLSW layer in both basins and for the ISOW layer in the Irminger basin are significantly different from our $pH_{T_{is}}$ trends for these layers, but are very similar to pH changes derived from C_{ant} changes: $\frac{\partial pH_{T_{is}}}{\partial DIC}\frac{dC_{ant}}{dt}$ (Table 3). In the case of the DSOW

Table 3. Observed temporal changes of pH at total scale and in situ temperature and pressure conditions: $\left(\frac{\mathrm{dpH_{T_{IS}}}}{\mathrm{d}t}\right)_{\mathrm{obs}}$ for the main water masses in the Irminger and Iceland basins for the period 1991–2015. pH changes caused by the main drivers (in situ temperature, T_{IS}; salinity, S; total alkalinity, A_T; total dissolved inorganic carbon, DIC; the latter decomposed into its anthropogenic and natural components, C_{ant} and C_{nat}, respectively) are also shown, as well as the pH changes determined as the sum of the pH changes caused by the individual drivers $\left(\left(\frac{\mathrm{dpH_{T_{IS}}}}{\mathrm{d}t}\right)_{\mathrm{total}}\right)$. All the trends are calculated based on the annually interpolated values and are in 10^{-3} pH units yr^{-1}. Values in parenthesis are the percentages of the observed pH change explained by each one of its drivers. Consult Fig. 1 for water mass acronyms.

		$\left(\frac{\mathrm{dpH_{T_{IS}}}}{\mathrm{d}t}\right)_{\mathrm{obs}}$	$\frac{\partial \mathrm{pH_{T_{IS}}}}{\partial T_{IS}}\frac{\mathrm{dT_{IS}}}{\mathrm{d}t}$	$\frac{\partial \mathrm{pH_{T_{IS}}}}{\partial S}\frac{\mathrm{dS}}{\mathrm{d}t}$	$\frac{\partial \mathrm{pH_{T_{IS}}}}{\partial A_T}\frac{\mathrm{dA_T}}{\mathrm{d}t}$	$\frac{\partial \mathrm{pH_{T_{IS}}}}{\partial \mathrm{DIC}}\frac{\mathrm{dDIC}}{\mathrm{d}t}$	$\frac{\partial \mathrm{pH_{T_{IS}}}}{\partial \mathrm{DIC}}\frac{\mathrm{dC_{ant}}}{\mathrm{d}t}$	$\frac{\partial \mathrm{pH_{T_{IS}}}}{\partial \mathrm{DIC}}\frac{\mathrm{dC_{ant}}}{\mathrm{d}t}$	$\left(\frac{\mathrm{dpH_{T_{IS}}}}{\mathrm{d}t}\right)_{\mathrm{total}}$
Irminger	SPMW	−1.84 ± 0.08	−0.04 ± 0.08 (2)	−0.021 ± 0.008 (1)	0.26 ± 0.07 (−14)	−2.05 ± 0.11 (111)	−2.21 ± 0.14 (120)	0.16 ± 0.10 (−9)	−1.85 ± 0.15 (100.5)
	uLSW	−1.60 ± 0.10	−0.23 ± 0.03 (14)	−0.016 ± 0.002 (1)	0.25 ± 0.03 (−16)	−1.61 ± 0.08 (101)	−1.83 ± 0.16 (114)	0.22 ± 0.21 (−14)	−1.61 ± 0.09 (100.6)
	cLSW	−1.59 ± 0.06	−0.40 ± 0.03 (25)	−0.040 ± 0.003 (3)	0.70 ± 0.05 (−44)	−1.85 ± 0.07 (116)	−0.55 ± 0.07 (34)	−1.31 ± 0.09 (82)	−1.60 ± 0.09 (100.3)
	ISOW	−1.31 ± 0.05	−0.09 ± 0.02 (7)	−0.009 ± 0.003 (1)	0.29 ± 0.06 (−22)	−1.50 ± 0.07 (115)	−0.99 ± 0.07 (76)	−0.50 ± 0.09 (39)	−1.31 ± 0.09 (100.1)
	DSOW	−1.47 ± 0.05	−0.16 ± 0.05 (11)	−0.015 ± 0.003 (1)	0.55 ± 0.07 (−37)	−1.85 ± 0.08 (126)	−1.27 ± 0.09 (87)	−0.58 ± 0.09 (39)	−1.48 ± 0.12 (100.6)
Iceland	SPMW	−1.59 ± 0.15	−0.16 ± 0.13 (10)	−0.016 ± 0.011 (1)	0.17 ± 0.12 (−11)	−1.60 ± 0.17 (101)	−1.54 ± 0.13 (97)	−0.06 ± 0.08 (4)	−1.60 ± 0.24 (100.9)
	uLSW	−1.09 ± 0.07	0.02 ± 0.02 (−2)	0.003 ± 0.002 (0)	−0.10 ± 0.07 (9)	−1.03 ± 0.06 (95)	−1.68 ± 0.15 (154)	0.65 ± 0.11 (−60)	−1.10 ± 0.10 (101.0)
	cLSW	−0.97 ± 0.11	−0.06 ± 0.02 (6)	−0.007 ± 0.002 (1)	0.18 ± 0.09 (−18)	−1.09 ± 0.14 (112)	−0.98 ± 0.08 (100)	−0.12 ± 0.11 (12)	−0.98 ± 0.17 (101.0)
	ISOW	−0.90 ± 0.09	−0.03 ± 0.01 (4)	−0.003 ± 0.001 (0)	0.11 ± 0.10 (−12)	−0.99 ± 0.14 (110)	−0.95 ± 0.08 (105)	−0.04 ± 0.11 (5)	−0.91 ± 0.18 (101.6)

layer, the $\mathrm{pH_N}$ trend is also in agreement with $\frac{\partial \mathrm{pH_{T_{IS}}}}{\partial \mathrm{DIC}}\frac{\mathrm{d}C_{\mathrm{ant}}}{\mathrm{d}t}$ trends. This suggests that the normalisation carried out by Vázquez-Rodríguez et al. (2012b) could remove some of the impact of the natural component (represented here by C_{nat}) over pH changes, essentially due to the use of AOU in the normalisation.

4 Conclusions

The progressive acidification of the North Atlantic waters has been assessed from direct observations obtained over the last 25 years (1991–2015), with the greatest pH decreases observed in surface and intermediate waters. From the study of the main drivers of the observed pH changes we conclude that the observed pH decreases are mainly a consequence of the oceanic C_{ant} uptake. In addition we find that they have been partially offset by A_T increases. Thus, while the C_{ant} concentration of the upper layer roughly keeps up with the concentration expected from rising atmospheric CO_2, the pH decreases at a lower rate than expected from C_{ant} increase. The increasing arrival of saline and alkaline subtropical waters transported by the NAC to the study region, related to the contraction of the subpolar gyre since the mid-90s, buffers the acidification caused by the C_{ant} increase in the upper layer. The acidification rates in intermediate waters are similar to those in the surface waters and are caused by a combination of anthropogenic and non-anthropogenic components. The acidification of cLSW due to the C_{ant} uptake is reinforced by the aging of this water mass from the end of the 1990s onwards. The pH of the deep waters of the Irminger basin, DSOW, has clearly decreased in response to anthropogenic forcing. We also infer that water mass warming contributes between 2 and 25 % to the pH decrease of the upper and intermediate waters of the Irminger basin, and 10 % to the pH decrease of the upper waters of the Iceland basin.

5 Data availability

OVIDE 2012 data was accessed from the Clivar & Carbon Hydrographic Data Office (CCHDO; http://cchdo.ucsd.edu/cruise/29AH20120622), and OVIDE 2014 data is publicly available at http://www.obs-vlfr.fr/proof/ftpfree/geovide/ALKALINITY_PH/. The data from the 58GS20150410 cruise is unpublished and can be obtained per request to Are Olsen (are.olsen@gfi.uib.no). They have not yet been made public in order to protect the interest of a PhD student who relies heavily on them for her work. It is our intention to release them when that has been completed, in 2017.

The Supplement related to this article is available online at doi:10.5194/bg-13-3701-2016-supplement.

Author contributions. All authors contributed extensively to the work presented in this paper. Maribel I. García-Ibáñez, Aida F. Ríos, Herlé Mercier, Are Olsen and Fiz F. Pérez designed the research. Maribel I. García-Ibáñez, Patricia Zunino, Friederike Fröb, Lidia I. Carracedo, Aida F. Ríos, Herlé Mercier, Are Olsen and Fiz F. Pérez analysed the physical and chemical data. Maribel I. García-Ibáñez and Patricia Zunino developed the code for processing the data. Maribel I. García-Ibáñez and Fiz F. Pérez determined the anthropogenic CO_2 concentrations, average layer properties and rates, and estimated the uncertainties. Maribel I. García-Ibáñez wrote the manuscript and prepared all figures, with contributions from all co-authors.

Acknowledgements. We are grateful to the captains, staff and researchers who contributed to the acquisition and processing of hydrographic data. The research leading to these results was supported through the EU FP7 project CARBOCHANGE "Changes in carbon uptake and emissions by oceans in a changing climate", which received funding from the European Commission's Seventh Framework Programme under grant agreement no. 264879. For this work M. I. Garcia-Ibáñez, A. F. Rios and F. F. Pérez were supported by the Spanish Ministry of Economy and Competitiveness through the BOCATS (CTM2013-41048-P) project co-funded by the Fondo Europeo de Desarrollo Regional 2007–2012 (FEDER). P. Zunino was supported by the GEOVIDE project as well as by IFREMER. L. I. Carracedo was funded by the University of Vigo, through the Galician I2C Plan for postdoctoral research. H. Mercier was supported by the French National Centre for Scientific Research (CNRS). F. Fröb and A. Olsen were supported by a grant from the Norwegian Research Council (SNACS, project 229756/E10).

Edited by: J. Middelburg

References

Anderson, L. G. and Olsen, A.: Air–sea flux of anthropogenic carbon dioxide in the North Atlantic, Geophys. Res. Lett., 29, 1835, doi:10.1029/2002GL014820, 2002.

Azetsu-Scott, K., Jones, E. P., Yashayaev, I., and Gershey, R. M.: Time series study of CFC concentrations in the Labrador Sea during deep and shallow convection regimes (1991–2000), J. Geophys. Res., 108, 3354, doi:10.1029/2002JC001317, 2003.

Bates, N., Astor, Y., Church, M., Currie, K., Dore, J., González-Dávila, M., Lorenzoni, L., Muller-Karger, F., Olafsson, J., and Santa-Casiano, M.: A Time-Series View of Changing Ocean Chemistry Due to Ocean Uptake of Anthropogenic CO_2 and Ocean Acidification, Oceanography, 27, 126–141, doi:10.5670/oceanog.2014.16, 2014.

Bates, N. R., Best, M. H. P., Neely, K., Garley, R., Dickson, A. G., and Johnson, R. J.: Detecting anthropogenic carbon dioxide uptake and ocean acidification in the North Atlantic Ocean, Biogeosciences, 9, 2509–2522, doi:10.5194/bg-9-2509-2012, 2012.

Benson, B. B. and Krause, D.: The concentration and isotopic fractionation of oxygen dissolved in freshwater and seawater in equilibrium with the atmosphere, Limnol. Oceanogr., 29, 620–632, doi:10.4319/lo.1984.29.3.0620, 1984.

Bersch, M., Meincke, J., and Sy, A.: Interannual thermohaline changes in the northern North Atlantic 1991–1996, Deep-Sea Res. Pt. II, 46, 55–75, doi:10.1016/S0967-0645(98)00114-3, 1999.

Biastoch, A., Völker, C., and Böning, C. W.: Uptake and spreading of anthropogenic trace gases in an eddy-permitting model of the Atlantic Ocean, J. Geophys. Res., 112, C09017, doi:10.1029/2006JC003966, 2007.

Böning, C. W., Scheinert, M., Dengg, J., Biastoch, A., and Funk, A.: Decadal variability of subpolar gyre transport and its reverberation in the North Atlantic overturning, Geophys. Res. Lett., 33, L21S01, doi:10.1029/2006GL026906, 2006.

Brambilla, E. and Talley, L. D.: Subpolar Mode Water in the northeastern Atlantic: 1. Averaged properties and mean circulation, J. Geophys. Res., 113, C04025, doi:10.1029/2006JC004062, 2008.

Broecker, W. S.: "NO" a conservative water mass tracer, Earth Planet. Sc. Lett., 23, 8761–8776, doi:10.1016/0012-821X(74)90036-3, 1974.

Caldeira, K. and Wickett, M.E.: Oceanography: Anthropogenic carbon and ocean pH, Nature, 425, 365–365, doi:10.1038/425365a, 2003.

Caldeira, K. and Wickett, M. E.: Ocean model predictions of chemistry changes from carbon dioxide emissions to the atmosphere and ocean, J. Geophys. Res., 110, C09S04, doi:10.1029/2004JC002671, 2005.

Carter, B. R., Radich, J. A., Doyle, H. L., and Dickson, A. G.: An automated system for spectrophotometric seawater pH measurements, Limnol. Oceanogr.-Meth., 11, 16–27, doi:10.4319/lom.2013.11.16, 2013.

Ciais, P., Sabine, C., Bala, G., Bopp, L., Brovkin, V., Canadell, J., Chhabra, A., DeFries, R., Galloway, J., Heimann, M., Jones, C., Le Quéré, C., Myneni, R. B., Piao, S., and Thornton, P.: Carbon and other biogeochemical cycles, in: Climate Change 2013: The Physical Science Basis. Contribution of Working Group I to the Fifth Assessment Report of the Intergovernmental Panel on Climate Change, edited by: Stocker, T. F., Qin, D., Plattner, G.-K., Tignor, M., Allen, S. K., Boschung, J., Nauels, A., Xia, Y., Bex, V., and Midgley, P. M., Cambridge University Press, Cambridge, United Kingdom and New York, NY, USA, 465–570, 2013.

Clayton, T. D. and Byrne, R. H.: Spectrophotometric seawater pH measurements: total hydrogen ion concentration scale calibration of m-cresol purple and at-sea results, Deep-Sea Res. Pt. I, 40, 2115–2129, doi:10.1016/0967-0637(93)90048-8, 1993.

Cunningham, S. A. and Haine, T. W. N.: Labrador Sea Water in the eastern North Atlantic. Part II: mixing dynamics and the advective-diffusive balance, J. Phys. Oceanogr., 14, 103–127, doi:10.1175/1520-0485(1995)025<0666:LSWITE>2.0.CO;2, 1995.

de Boisséson, E., Thierry, V., Mercier, H., and Caniaux, G.: Mixed layer heat budget in the Iceland Basin from Argo, J. Geophys. Res.-Oceans, 115, C10055, doi:10.1029/2010JC006283, 2010.

Desbruyères, D., Thierry, V., and Mercier, H.: Simulated decadal variability of the meridional overturning circulation across the A25-Ovide section, J. Geophys. Res.-Oceans, 118, 462–475, doi:10.1029/2012JC008342, 2013.

DeVries, T.: The oceanic anthropogenic CO_2 sink: Storage, air-sea fluxes, and transports over the industrial era, Global Biogeochem. Cy., 28, 631–647, doi:10.1002/2013GB004739, 2014.

Dickson, A. and Goyet, C.: Handbook of methods for the analysis of the various parameters of the carbon dioxide system in sea water, Version 2, Oak Ridge National Laboratory, Oak Ridge, TN, doi:10.2172/10107773, 198 pp., 1994.

Dickson, A. and Millero, F.: A comparison of the equilibrium constants for the dissociation of carbonic acid in seawater media, Deep-Sea Res., 34, 1733–1743, doi:10.1016/0198-0149(87)90021-5, 1987.

Dickson, A. G., Sabine, C. L., and Christian, J. R.: Guide to best practices for ocean CO_2 measurements, PICES Spec. Publ., 3, North Pacific Marine Science Organization Sidney, British Columbia, 191 pp., 2007.

Doney, S. C., Fabry, V. J., Feely, R. A., and Kleypas, J. A.: Ocean acidification: the other CO_2 problem, Annu. Rev. Mar. Sci., 1, 169–192, doi:10.1146/annurev.marine.010908.163834, 2009.

Dore, J. E., Lukas, R., Sadler, D. W., Church, M. J., and Karl, D. M.: Physical and biogeochemical modulation of ocean acidification in the central North Pacific, P. Natl. Acad. Sci. USA, 106, 12235–12240, doi:10.1073/pnas.0906044106, 2009.

Eakins, B. W. and Sharman, G. F.: Volumes of the World's Oceans from ETOPO1, NOAA National Geophysical Data Center, Boulder, CO, 2010.

Feely, R. A., Sabine, C. L., Lee, K., Berelson, W., Kleypas, J., Fabry, V. J., and Millero, F. J.: Impact of Anthropogenic CO_2 on the $CaCO_3$ System in the Oceans, Science, 305, 362–366, doi:10.1126/science.1097329, 2004.

Feely, R. A., Doney, S. C., and Cooley, S. R.: Ocean acidification: Present and future changes in a high-CO_2 world, Oceanography, 22, 36–47, doi:10.5670/oceanog.2009.95, 2009.

Flatau, M. K., Talley, L., and Niiler, P. P.: The North Atlantic Oscillation, Surface Current Velocities, and SST Changes in the Subpolar North Atlantic, J. Clim., 16, 2355–2369, doi:10.1175/2787.1, 2003.

Fröb, F., Olsen, A., Våge, K., Moore, K., Yashayaev, I., Jeannson, E., and Rajasakaren, B.: Record deep convection in the Irminger Sea in winter 2014-15, OSM, New Orleans, Louisiana, USA, 21–16 February 2016, HE11A-02, 2016.

García-Ibáñez, M. I., Pardo, P. C., Carracedo, L. I., Mercier, H., Lherminier, P., Ríos, A. F., and Pérez, F. F.: Structure, transports and transformations of the water masses in the Atlantic Subpolar Gyre, Prog. Oceanogr., 135, 18–36, doi:10.1016/j.pocean.2015.03.009, 2015.

Gehlen, M., Gruber, N., Gangstø, R., Bopp, L., and Oschlies, A.: Biogeochemical consequences of ocean acidification and feedbacks to the earth system, in: Ocean Acidification, Vol. 1, edited by: Gattuso, J.-P. and Hansson, L., Oxford University Press, 230–248, 2011.

González-Dávila, M., Santana-Casiano, J. M., Rueda, M. J., and Llinás, O.: The water column distribution of carbonate system variables at the ESTOC site from 1995 to 2004, Biogeosciences, 7, 3067—3081, doi:10.5194/bg-7-3067-2010, 2010.

Gourcuff, C., Lherminier, P., Mercier, H., and Le Traon, P. Y.: Altimetry Combined with Hydrography for Ocean Transport Estimation, J. Atmos. Ocean. Tech., 28, 1324–1337, doi:10.1175/2011JTECHO818.1, 2011.

Gruber, N., Sarmiento, J. L., and Stocker, T. F.: An improved method for detecting anthropogenic CO_2 in the oceans, Global Biogeochem. Cy., 10, 809–837, doi:10.1029/96GB01608, 1996.

Guallart, E. F., Fajar, N. M., Padín, X. A., Vázquez-Rodríguez, M., Calvo, E., Ríos, A. F., Hernández-Guerra, A., Pelejero, C., and Pérez, F. F.: Ocean acidification along the 24.5° N section in the subtropical North Atlantic, Geophys. Res. Lett., 42, 450–458, doi:10.1002/2014GL062971, 2015.

Häkkinen, S. and Rhines, P. B.: Decline of subpolar North Atlantic circulation during the 1990s, Science, 304, 555–559, doi:10.1126/science.1094917, 2004.

Johnson, K. M., Wills, K. D., Butler, D. B., Johnson, W. K., and Wong, C. S.: Coulometric total carbon dioxide analysis for marine studies: maximizing the performance of an automated gas extraction system and coulometric detector, Mar. Chem., 44, 167–187, doi:10.1016/0304-4203(93)90201-X, 1993.

Jones, D. C., Ito, T., Takano, Y., and Hsu, W.-C.: Spatial and seasonal variability of the air-sea equilibration timescale of carbon dioxide, Glob. Biogeochem. Cy., 28, 1163–1178, doi:10.1002/2014GB004813, 2014.

Khatiwala, S., Tanhua, T., Mikaloff Fletcher, S., Gerber, M., Doney, S. C., Graven, H. D., Gruber, N., McKinley, G. A., Murata, A., Ríos, A. F., and Sabine, C. L.: Global ocean storage of anthropogenic carbon, Biogeosciences, 10, 2169–2191, doi:10.5194/bg-10-2169-2013, 2013.

Kieke, D., Rhein, M., Stramma, L., Smethie, W. M., Bullister, J. L., and LeBel, D. A.: Changes in the pool of Labrador Sea Water in the subpolar North Atlantic, Geophys. Res. Lett., 34, L06605, doi:10.1029/2006GL028959, 2007.

Koltermann, K. P., Pfannkuche, O., and Meincke, J.: JGOFS, OMEX and WOCE in the North Atlantic 1994, cruise no. 30: 7 September to 22 December 1994, Meteor-Berichte, 96-3, Universität Hamburg, Hamburg, 148 pp., 1996.

Langdon, C., Takahashi, T., Sweeney, C., Chipman, D., Goddard, J., Marubini, F., Aceves, H., Barnett, H., and Atkinson, M. J.: Effect of calcium carbonate saturation state on the calcification rate of an experimental coral reef, Global Biogeochem. Cy., 14, 639–654, doi:10.1029/1999GB001195, 2000.

Lauvset, S. K., Gruber, N., Landschützer, P., Olsen, A., and Tjiputra, J.: Trends and drivers in global surface ocean pH over the past 3 decades, Biogeosciences, 12, 1285–1298, doi:10.5194/bg-12-1285-2015, 2015.

Lazier, J., Hendry, R., Clarke, A., Yashayaev, I., and Rhines, P.: Convection and restratification in the Labrador Sea, 1990–2000, Deep-Sea Res. Pt. I, 49, 1819–1835, doi:10.1016/S0967-0637(02)00064-X, 2002.

Le Quéré, C., Moriarty, R., Andrew, R. M., Canadell, J. G., Sitch, S., Korsbakken, J. I., Friedlingstein, P., Peters, G. P., Andres, R. J., Boden, T. A., Houghton, R. A., House, J. I., Keeling, R. F., Tans, P., Arneth, A., Bakker, D. C. E., Barbero, L., Bopp, L., Chang, J., Chevallier, F., Chini, L. P., Ciais, P., Fader, M., Feely, R. A., Gkritzalis, T., Harris, I., Hauck, J., Ilyina, T., Jain, A. K., Kato, E., Kitidis, V., Klein Goldewijk, K., Koven, C., Landschützer, P., Lauvset, S. K., Lefèvre, N., Lenton, A., Lima, I. D., Metzl, N., Millero, F., Munro, D. R., Murata, A., Nabel, J. E. M. S., Nakaoka, S., Nojiri, Y., O'Brien, K., Olsen, A., Ono, T., Pérez, F. F., Pfeil, B., Pierrot, D., Poulter, B., Rehder, G., Rödenbeck, C., Saito, S., Schuster, U., Schwinger, J., Séférian, R., Steinhoff, T., Stocker, B. D., Sutton, A. J., Takahashi, T., Tilbrook, B., van der Laan-Luijkx, I. T., van der Werf, G. R., van Heuven, S., Vandemark, D., Viovy, N., Wiltshire, A., Zaehle, S., and Zeng, N.:

Global Carbon Budget 2015, Earth Syst. Sci. Data, 7, 349–396, doi:10.5194/essd-7-349-2015, 2015.

Lherminier, P., Mercier, H., Gourcuff, C., Alvarez, M., Bacon, S., and Kermabon, C.: Transports across the 2002 Greenland-Portugal Ovide section and comparison with 1997, J. Geophys. Res., 112, C07003, doi:10.1029/2006JC003716, 2007.

Lherminier, P., Mercier, H., Huck, T., Gourcuff, C., Perez, F. F., Morin, P., Sarafanov, A., and Falina, A.: The Atlantic Meridional Overturning Circulation and the subpolar gyre observed at the A25-OVIDE section in June 2002 and 2004, Deep-Sea Res. Pt. I, 57, 1374–1391, doi:10.1016/j.dsr.2010.07.009, 2010.

Liu, X., Patsavas, M. C., and Byrne, R. H.: Purification and Characterization of meta-Cresol Purple for Spectrophotometric Seawater pH Measurements, Environ. Sci. Technol., 45, 4862–4868, doi:10.1021/es200665d, 2011.

Maier-Reimer, E. and Hasselmann, K.: Transport and storage of CO_2 in the ocean—an inorganic ocean-circulation carbon cycle model, Clim. Dynam., 2, 63–90, doi:10.1007/BF01054491, 1987.

Matear, R. J. and Lenton, A.: Quantifying the impact of ocean acidification on our future climate, Biogeosciences, 11, 3965–3983, doi:10.5194/bg-11-3965-2014, 2014.

Mehrbach, C., Culberson, C. H., Hawley, J. E., and Pytkowicz, R. M.: Measurement of the apparent dissociation constants of carbonic acid in seawater at atmospheric pressure, Limnol. Oceanogr., 18, 897–907, doi:10.4319/lo.1973.18.6.0897, 1973.

Meincke, J. and Becker, G.: WOCE-NORD, Cruise No. 18, 2 September to 26 September 1991, Nordsee, cruise No. 19, 30 September to 12 October 1991, METEOR-Berichte 93-1, Universität Hamburg, Hamburg, 105 pp., 1993.

Mercier, H., Lherminier, P., Sarafanov, A., Gaillard, F., Daniault, N., Desbruyères, D., Falina, A., Ferron, B., Gourcuff, C., and Huck, T.: Variability of the meridional overturning circulation at the Greenland–Portugal OVIDE section from 1993 to 2010, Prog. Oceanogr., 132, 250–261, doi:10.1016/j.pocean.2013.11.001, 2015.

Millero, F. J., Zhang, J. Z., Lee, K., and Campbell, D. M.: Titration alkalinity of seawater, Mar. Chem., 44, 153–165, doi:10.1016/0304-4203(93)90200-8, 1993.

Mintrop, L., Pérez, F. F., González-Dávila, M., Santana-Casiano, J. M., and Körtzinger, A.: Alkalinity determination by potentiometry: Intercalibration using three different methods, Cienc. Mar., 26, 23–37, doi:10.7773/cm.v26i1.573, 2000.

Olafsson, J., Olafsdottir, S. R., Benoit-Cattin, A., Danielsen, M., Arnarson, T. S., and Takahashi, T.: Rate of Iceland Sea acidification from time series measurements, Biogeosciences, 6, 2661–2668, doi:10.5194/bg-6-2661-2009, 2009.

Olafsson, J., Olafsdottir, S. R., Benoit-Cattin, A., and Takahashi, T.: The Irminger Sea and the Iceland Sea time series measurements of sea water carbon and nutrient chemistry 1983–2008, Earth Syst. Sci. Data, 2, 99–104, doi:10.5194/essd-2-99-2010, 2010.

Olsen, A., Abdirahman, O. M., Bellerby, R. G., Johannessen, T., Ninnemann, U. S., Brown, K. R., Olsson, K. A., Olafsson, J., Nondal, G., Kivimäe, C., Kringstad, S., Neill, C., and Olafsdottir, S.: Magnitude and Origin of the Anthropogenic CO_2 Increase and the ^{13}C Suess Effect in the Nordic Seas since 1981, Global Biogeochem. Cy., 20, GB3027, doi:10.1029/2005GB002669, 2006.

Olsen, A., Key, R. M., van Heuven, S., Lauvset, S. K., Velo, A., Lin, X., Schirnick, C., Kozyr, A., Tanhua, T., Hoppema, M., Jutterström, S., Steinfeldt, R., Jeansson, E., Ishii, M., Pérez, F. F., and Suzuki, T.: An internally consistent data product for the world ocean: the Global Ocean Data Analysis Project, version 2 (GLODAPv2), Earth Syst. Sci. Data Discuss., doi:10.5194/essd-2015-42, in review, 2016.

Ono, T., Watanabe, S., Okuda, K., and Fukasawa, M.: Distribution of total carbonate and related properties in the North Pacific along 30° N, J. Geophys. Res.-Oceans, 103, 30873–30883, doi:10.1029/1998JC900018, 1998.

Orr, J. C.: Recent and future changes in ocean carbonate chemistry, in: Ocean Acidification, Vol. 1, edited by: Gattuso, J.-P. and Hansson, L., Oxford University Press, 41–66, 2011.

Paillet, J., Arhan, M., and McCartney, M. S.: Spreading of Labrador Sea Water in the eastern North Atlantic, J. Geophys. Res., 103, 10223–10239, doi:10.1029/98JC00262, 1998.

Pérez, F. F. and Fraga, F.: A precise and rapid analytical procedure for alkalinity determination, Mar. Chem., 21, 169–182, doi:10.1016/0304-4203(87)90037-5, 1987.

Pérez, F. F., Vázquez-Rodríguez, M., Louarn, E., Padín, X. A., Mercier, H., and Ríos, A. F.: Temporal variability of the anthropogenic CO_2 storage in the Irminger Sea, Biogeosciences, 5, 1669–1679, doi:10.5194/bg-5-1669-2008, 2008.

Pérez, F. F., Vázquez-Rodríguez, M., Mercier, H., Velo, A., Lherminier, P., and Ríos, A. F.: Trends of anthropogenic CO2 storage in North Atlantic water masses, Biogeosciences, 7, 1789–1807, doi:10.5194/bg-7-1789-2010, 2010.

Pérez, F. F., Mercier, H., Vázquez-Rodríguez, M., Lherminier, P., Velo, A., Pardo, P. C., Rosón, G., and Ríos, A. F.: Atlantic Ocean CO_2 uptake reduced by weakening of the meridional overturning circulation, Nat. Geosci., 6, 146–152, doi:10.1038/ngeo1680, 2013.

Pickart, R. S., Straneo, F., and Moore, G. K.: Is Labrador Sea Water formed in the Irminger basin?, Deep-Sea Res. Pt. I, 50, 23–52, doi:10.1016/S0967-0637(02)00134-6, 2003.

Piron, A., Thierry, V., Mercier, H., and Caniaux, G.: Argo float observations of basin-scale deep convection in the Irminger sea during winter 2011–2012, Deep-Sea Res. Pt. I, 109, 76–90, doi:10.1016/j.dsr.2015.12.012, 2016.

Pörtner, H. O., Langenbuch, M., and Reipschläger, A.: Biological Impact of Elevated Ocean CO_2 Concentrations: Lessons from Animal Physiology and Earth History, J. Oceanogr., 60, 705–718, doi:10.1007/s10872-004-5763-0, 2004.

Raven, J., Caldeira, K., Elderfield, H., Hoegh-Guldberg, O., Liss, P., Riebesell, U., Shepherd, J., Turley, C., and Watson, A.: Ocean acidification due to increasing atmospheric carbon dioxide, R. Soc. Lond. Document No. 12/05, The Royal Society, London, 2005.

Read, J. F.: CONVEX-91: water masses and circulation of the Northeast Atlantic subpolar gyre, Prog. Oceanogr., 48, 461–510, doi:10.1016/S0079-6611(01)00011-8, 2000.

Rhein, M., Fischer, J., Smethie, W. M., Smythe-Wright, D., Weiss, R. F., Mertens, C., Min, D.-H., Fleischmann, U., and Putzka, A.: Labrador Sea Water: Pathways, CFC inventory, and formation rates, J. Phys. Oceanogr., 32, 648–665, doi:10.1175/1520-0485(2002)032<0648:LSWPCI>2.0.CO;2, 2002.

Riebesell, U., Zondervan, I., Rost, B., Tortell, P. D., Zeebe, R. E., and Morel, F. M. M.: Reduced calcification of marine plankton in

response to increased atmospheric CO_2, Nature, 407, 364–367, doi:10.1038/35030078, 2000.

Ríos, A. F., Álvarez-Salgado, X. A., Pérez, F. F., Bingler, L. S., Arístegui, J., and Mémery, L.: Carbon dioxide along WOCE line A14: Water masses characterization and anthropogenic entry, J. Geophys. Res.-Oceans, 108, 3123, doi:10.1029/2000JC000366, 2003.

Ríos, A. F., Resplandy, L., García-Ibáñez, M. I., Fajar, N. M., Velo, A., Padin, X. A., Wanninkhof, R., Steinfeldt, R., Rosón, G., and Pérez, F. F.: Decadal acidification in the water masses of the Atlantic Ocean, P. Natl. Acad. Sci. USA, 112, 9950–9955, doi:10.1073/pnas.1504613112, 2015.

Sabine, C. L., Feely, R. A., Gruber, N., Key, R. M., Lee, K., Bullister, J. L., Wanninkhof, R., Wong, C. S., Wallace, D. W. R., Tilbrook, B., Millero, F. J., Peng, T.-H., Kozyr, A., Ono, T., and Rios, A. F.: The Oceanic Sink for Anthropogenic CO_2, Science, 305, 367–371, doi:10.1126/science.1097403, 2004.

Santana-Casiano, J. M., González-Dávila, M., Rueda, M.-J., Llinás, O., and González-Dávila, E.-F.: The interannual variability of oceanic CO_2 parameters in the northeast Atlantic subtropical gyre at the ESTOC site, Global Biogeochem. Cy., 21, GB1015, doi:10.1029/2006GB002788, 2007.

Sarafanov, A., Falina, A., Sokov, A., and Demidov, A.: Intense warming and salinification of intermediate waters of southern origin in the eastern subpolar North Atlantic in the 1990s to mid-2000s, J. Geophys. Res.-Oceans, 113, C12022, doi:10.1029/2008JC004975, 2008.

Sarafanov, A., Falina, A., Mercier, H., Sokov, A., Lherminier, P., Gourcuff, C., Gladyshev, S., Gaillard, F., and Daniault, N.: Mean full-depth summer circulation and transports at the northern periphery of the Atlantic Ocean in the 2000s, J. Geophys. Res., 117, C01014, doi:10.1029/2011JC007572, 2012.

Sarafanov, A., Mercier, H., Falina, A., Sokov, A., and Lherminier, P.: Cessation and partial reversal of deep water freshening in the northern North Atlantic: observation-based estimates and attribution, Tellus A, 62, 80–90, doi:10.1111/j.1600-0870.2009.00418.x, 2010.

Sarmiento, J. L., Orr, J. C., and Siegenthaler, U.: A perturbation simulation of CO_2 uptake in an ocean general circulation model, J. Geophys. Res.-Oceans, 97, 3621–3645, doi:10.1029/91JC02849, 1992.

Steinfeldt, R., Rhein, M., Bullister, J. L., and Tanhua, T.: Inventory changes in anthropogenic carbon from 1997–2003 in the Atlantic Ocean between 20° S and 65° N, Global Biogeochem. Cy., 23, GB3010, doi:10.1029/2008GB003311, 2009.

Stoll, M. H. C., van Aken, H. M., de Baar, H. J. W., and Kraak, M.: Carbon dioxide characteristics of water masses in the northern North Atlantic Ocean, Mar. Chem., 55, 217–232, doi:10.1016/S0304-4203(96)00058-8, 1996.

Thierry, V., de Boisséson, E., and Mercier, H.: Interannual variability of the Subpolar Mode Water properties over the Reykjanes Ridge during 1990–2006, J. Geophys. Res.-Oceans, 113, C04016, doi:10.1029/2007JC004443, 2008.

Uppström, L. R.: Boron/chlorinity ratio of deep-sea water from the Pacific Ocean, Deep-Sea Res., 21, 161–162, doi:10.1016/0011-7471(74)90074-6, 1974.

Vázquez-Rodríguez, M., Padin, X. A., Ríos, A. F., Bellerby, R. G. J., and Pérez, F. F.: An upgraded carbon-based method to estimate the anthropogenic fraction of dissolved CO_2 in the Atlantic Ocean, Biogeosciences Discuss., 6, 4527–4571, doi:10.5194/bgd-6-4527-2009, 2009a.

Vázquez-Rodríguez, M., Touratier, F., Lo Monaco, C., Waugh, D. W., Padin, X. A., Bellerby, R. G. J., Goyet, C., Metzl, N., Ríos, A. F., and Pérez, F. F.: Anthropogenic carbon distributions in the Atlantic Ocean: data-based estimates from the Arctic to the Antarctic, Biogeosciences, 6, 439–451, doi:10.5194/bg-6-439-2009, 2009b.

Vázquez-Rodríguez, M., Padin, X. A., Pardo, P. C., Ríos, A. F., and Pérez, F. F.: The subsurface layer reference to calculate preformed alkalinity and air–sea CO_2 disequilibrium in the Atlantic Ocean, J. Marine Syst., 94, 52–63, doi:10.1016/j.jmarsys.2011.10.008, 2012a.

Vázquez-Rodríguez, M., Pérez, F. F., Velo, A., Ríos, A. F., and Mercier, H.: Observed acidification trends in North Atlantic water masses, Biogeosciences, 9, 5217–5230, doi:10.5194/bg-9-5217-2012, 2012b.

Velo, A., Pérez, F. F., Tanhua, T., Gilcoto, M., Ríos, A. F., and Key, R. M.: Total alkalinity estimation using MLR and neural network techniques, J. Marine Syst., 111–112, 11–18, doi:10.1016/j.jmarsys.2012.09.002, 2013.

Wakita, M., Watanabe, S., Honda, M., Nagano, A., Kimoto, K., Matsumoto, K., Kitamura, M., Sasaki, K., Kawakami, H., Fujiki, T., Sasaoka, K., Nakano, Y., and Murata, A.: Ocean acidification from 1997 to 2011 in the subarctic western North Pacific Ocean, Biogeosciences, 10, 7817–7827, doi:10.5194/bg-10-7817-2013, 2013.

Wallace, W. R.: Storage and transport of excess CO_2 in the oceans: The JGOFS/WOCE global CO_2 survey, in: Ocean Circulation and Climate, edited by: Siedler, G., Church, J., and Gould J., Academic Press, 489–521, 2001.

Waugh, D. W., Hall, T. M., McNeil, B. I., Key, R., and Matear, R. J.: Anthropogenic CO_2 in the oceans estimated using transit time distributions, Tellus B, 58, 376–389, doi:10.1111/j.1600-0889.2006.00222.x, 2006.

Yashayaev, I.: Hydrographic changes in the Labrador Sea, 1960–2005, Prog. Oceanogr., 73, 242–276, doi:10.1016/j.pocean.2007.04.015, 2007.

Yashayaev, I. and Dickson, R.R.: Transformation and fate of overflows in the Northern North Atlantic, in: Arctic-Subarctic Ocean Fluxes: Defining the Role of the Northern Seas in Climate, edited by: Dickson, R. R., Jens, M., and Rhines, P., Springer, Science + Business Media B.V., Dordrecht, the Netherlands, 505–526, 2008.

Yashayaev, I., Bersch, M., and van Aken, H. M.: Spreading of the Labrador Sea Water to the Irminger and Iceland basins, Geophys. Res. Lett., 34, L10602, doi:10.1029/2006GL028999, 2007.

Yashayaev, I., Holliday, N. P., Bersch, M., and van Aken, H. M.: The History of the Labrador Sea Water: Production, Spreading, Transformation and Loss, in: Arctic–Subarctic Ocean Fluxes: Defining the Role of the Northern Seas in Climate, edited by: Dickson, R. R., Meincke, J., and Rhines, P., Springer, the Netherlands, 569–612, 2008.

Zunino, P., Pérez, F. F., Fajar, N. M., Guallart, E. F., Ríos, A. F., Pelegrí, J. L., and Hernández-Guerra, A.: Transports and budgets of anthropogenic CO_2 in the tropical North Atlantic in 1992–1993 and 2010–2011, Global Biogeochem. Cy., 29, 1075–1091, doi:10.1002/2014GB005075, 2015.